NEW INSIGHTS INTO APOPTOSIS-INDUCING FACTOR MEDIATED PRO-SURVIVAL ACTIVITY

A Dissertation
Submitted to the Graduate Faculty
of the
North Dakota State University
of Agriculture and Applied Science

By

Sujata Birua

In Partial Fulfillment of the Requirements
for the Degree of
DOCTOR OF PHILOSOPHY

Major Program:
Biochemistry

November 2022

Fargo, North Dakota

North Dakota State University
Graduate School

Title

NEW INSIGHTS INTO APOPTOSIS-INDUCING FACTOR MEDIATED PRO-SURVIVAL ACTVITY

By

Sujata Birua

The Supervisory Committee certifies that this ***disquisition*** complies with North Dakota State University's regulations and meets the accepted standards for the degree of

DOCTOR OF PHILOSOPHY

SUPERVISORY COMMITTEE:

John C. Wilkinson, Ph.D.
Chair

D.K. Srivastava, Ph.D.

Stuart J. Haring, Ph.D.

Estelle. Leclerc, Ph.D.

Approved:

November 18, 2022
Date

Gregory R. Cook, Ph.D.
Department Chair

ABSTRACT

Cancer is a group of diseases characterized by the uncontrolled growth of cells and is caused by the accumulation of genetic mutations that contribute to cell division, cell growth, and the DNA repair system. According to the American Cancer Society, more than 1.9 million new cancer cases will be diagnosed in 2022, hence there is a need to study new molecular mechanisms leading to tumorigenesis and develop novel treatment options.

While significant research has been done to understand the underlying mechanisms, cancer still poses challenges as it 1) resists cell death, 2) activates metastasis, 3) sustains proliferative signaling, and 4) deregulates cellular metabolism. The present work explores the cancer supporting role of apoptosis-inducing factor (AIF), a mitochondrial flavoprotein positioned at the convergence of the four hallmarks of cancer. AIF was initially characterized as an effector of caspase-independent death; however, increasing evidence has identified the physiological role of AIF in a variety of cancer including colorectal, prostate, and pancreatic cancer.

Expanding AIF activity studies in additional cancers, such as breast cancer, revealed the capability of AIF to modulate the consumption of biochemical substrates other than glucose, thus deregulating cellular metabolism. These alterations suggest the role of AIF in controlling a switch from metabolic flexibility to metabolic dependency, which can be exploited for therapeutic interventions. Moreover, AIF might be involved in mitochondrial biogenesis of breast cancer, unreported in cancer tested so far.

In addition to their metabolic function, AIF serves as a signaling molecule that promotes cadherin switching in a 3-dimensional cell culture model of pancreatic ductal adenocarcinoma, which is associated with tumor growth. Finally. When grown in 3-dimensional culture conditions, pancreatic cancer cells were sensitized to a metabolic inhibitor in an AIF-dependent manner.

Altogether, these AIF activities are functionally dissociable and demonstrate that AIF-mediated therapy has promise as a next-generations cancer treatment strategy.

ACKNOWLEDGMENTS

Without the unwavering support of so many people in my life, I would not have achieved my dream of attaining a doctorate degree.

First and foremost, I am deeply grateful to my advisor, Dr. John Wilkinson, for his years of mentoring, motivation, and guidance that helped me grow not only as a better scientist but also as a level-headed individual. His motto of "never getting discouraged by failure" gave me a new perspective on my research projects. His ability to be patient when I struggled in my work and personal life was a tool for my success as a graduate student.

I also thank my advisory committee, Dr. D.K. Srivastava, Dr. Stuart Haring, and Dr. Estelle. Leclerc, for their guidance, feedback, and support over the years. I am also glad to know and work with my colleagues in the lab. They assisted and inspired me in different aspects of my research- Sierra Giebel, Annie Schiro, Amanda Wilkinson, Andrew Scott, Sierra Walker, Kaitlyn Johnson, Joshua Krank, and Kaitlin Dailey. I am grateful to each of you for your friendship, support, and camaraderie.

Finally, I thank my parents, brother, and friends, who had complete confidence in me and were my pillar of encouragement throughout my time as a Ph.D. student. I will also extend my appreciation, especially to my mom and my boyfriend, William Christensen, who gave me calm and composure during stressful academic situations and provided me with life lessons about dealing with stress.

You all have my sincerest gratitude and appreciation; I couldn't have done it without you.

DEDICATION

To the memory of my Nani.

TABLE OF CONTENTS

LIST OF TABLES

LIST OF FIGURES

LIST OF ABBREVIATIONS

2D.....2-Dimensional

2DG.....2-Deoxyglucose

3D.....3-Dimensional

ADP.....Adenosine diphosphate

AIF .....Apoptosis-inducing factor

Apaf-1 .....Apoptotic protease activating factor 1

ATP .....Adenosine triphosphate

Bad .....Bcl-2 associated agonist of cell death

Bak .....Bcl-2 homologous antagonist/killer

Bax .....Bcl-2-like protein 4

Bcl-2.....B-cell lymphoma 2

Bcl-X_L .....B-cell lymphoma extra large

Bcl-Xs .....B-cell lymphoma extra small

Bid.....BH3 interacting-domain death agonist

Bik.....Bcl-2 interacting killer

Bim.....Bcl-2-interacting mediator of cell death

BIR.....Baculoviral IAP repeat

CA-JNK1 .....Constitutively active JNK1, MKK7β2-JNK1α1

CA-JNK2 .....Constitutively active JNK2, MKK7β2-JNK2α2

CHCHD4.....Coiled-coil-helix-coiled-coil-helix-domain containing protein 4

Cyt *c* .....Cytochrome *c*

DIABLO .....Direct IAP binding protein with low pI

DMEM .....Dulbecco's modified Eagle's medium

DNA ..... Deoxyribonucleic acid

Drp1 ..... Dynamin-related protein 1

ECM ..... Extracellular matrix

EGF ..... Epidermal growth factor

EGFR ..... Epidermal growth factor receptor

EMT ..... Epithelial-mesenchymal transition

ERK ..... Extracellular signal-regulated kinase

ETC ..... Electron transport chain

FAD/$FADH_2$ ..... Flavin adenine dinucleotide/Reduced FAD

FADD ..... Fas-associated protein with death domain

Fas ..... First apoptosis signal/Apoptosis stimulating fragment

FasL ..... First apoptosis signal ligand

FBS ..... Fetal bovine serum

G6P Glucose-6-phoshate

GFP ..... Green fluorescent protein

GTP ..... Guanosine triphosphate

H2AX ..... Histone 2A family member X

HGF ..... Hepatocyte growth factor

HIF ..... Hypoxia-inducible factor

HK ..... Hexokinase

HRP ..... Horseradish peroxidase

Hsp70 ..... 70 kilodalton heat shock protein

HtrA2 ..... High temperature requirement protein A2

IAP ..... Inhibitor of apoptosis

IMM ..... Inner mitochondrial membrane

IMS .....Intermembrane space

JNK .....c-Jun N-terminal kinase

JNK1 .....c-Jun N-terminal kinase 1

JNK2 .....c-Jun N-terminal kinase 2

KRAS.....Kirsten rat sarcoma viral oncogene homolog

LC3 .....Microtubule-associated protein 1A/1B light chain 3

LEF .....Lymphoid-enhancer binding factor

MAP2K.....Mitogen-activated protein kinase kinase

MAP3K.....Mitogen-activated protein kinase kinase kinase

MAPK.....Mitogen-activated protein kinase

MIF .....Migration inhibitory factor

MKK4 .....Mitogen-activated protein kinase kinase 4

MKP.....Mitogen-activated protein kinase phosphatase

MKP2.....Mitogen-activated protein kinase phosphatase 2

MLS .....Mitochondrial localization sequence

MMP .....Matrix metalloproteinase

MOMP .....Mitochondrial outer membrane permeabilization

MPT .....Membrane permeability transition

mRNA.....Messenger RNA

NAD^+/NADH.....Nicotinamide adenine dinucleotide/Reduced NAD

$NADP^+$/NADPH .....Nicotinamide adenine dinucleotide phosphate/Reduced $NADP^+$

NDI1 .....NADH dehydrogenase internal

NLS.....Nuclear localization sequence

NP-40 .....Nonidet P40

OMM.....Outer mitochondrial membrane

OXPHOS.....Oxidative phosphorylation

PA .....Polylactic acid

PARP.....Poly-ADP ribose polymerase

PBS .....Phosphate buffered saline

PCa.....Prostate cancer

PCR.....Polymerase chain reaction

PDAC.....Pancreatic ductal adenocarcinoma

PDGF .....Platelet-derived growth factor

PEG.....Polyethylene glycol

PGA.....Polyglycolic acid

PGAM.....Phosphoglycerate mutase

PGAM1 .....Phosphoglycerate mutase 1

PGAM5 .....Phosphoglycerate mutase family member 5

PI3K .....Phosphoinositide 3-kinase

PMSF .....Phenylmethylsulfonyl fluoride

PPP.....Pentose phosphate pathway

PTEN.....Phosphatase and tensin homolog

PVDF .....Polyvinylidene fluoride

Q.....Ubiquinone (coenzyme Q)

qPCR.....Quantitative PCR

RIPA .....Radioimmune precipitation assay buffer

RNA .....Ribonucleic acid

RNAi.....RNA interference

ROS.....Reactive oxygen species

RPMI 1640.....Roswell Park Memorial Institute 1640 medium

rRNA.....Ribosomal RNA

SDS .....Sodium dodecyl sulfate

SDS-PAGE .....Sodium dodecyl sulfate polyacrylamide gel electrophoresis

shRNA.....Short hairpin RNA

Smac.....Second mitochondria-derived activator of caspases

Smad4 .....Smad family member 4

SOD1.....Superoxide dismutase 1

SOD2.....Superoxide dismutase 2

tBHQ.....*tert*-butylhydroquinone

TCA.....Tricarboxylic acid

TGF-β1.....Transforming growth factor β1

TMRM .....Tetramethylrhodamine methyl ester

TNBC.....Triple negative breast cancer

TNF .....Tumor necrosis factor

TNFR .....TNF receptor

TNFα.....Tumor necrosis factor α

TRADD.....TNF receptor associated death domain

TRAIL.....TNF-related apoptosis-inducing ligand

TVA .....T263A/V300A mutation

VEGF .....Vascular endothelial growth factor

WB .....Western blot

WT .....Wild type

XIAP .....X-linked inhibitor of apoptosis

Zeb1 .....Zinc finger E-box binding homeobox 1 Zeb2

LIST OF SYMBOLS

α	Lowercase alpha, used to define intramolecular positions, protein subunits and isoforms
β	Lowercase beta, used to define intramolecular positions, protein subunits and isoforms
Δ	Uppercase delta, used to indicate a difference or describe protein deletions removing indicated amino acid residues
$\Delta\Psi_m$	Uppercase delta, uppercase Psi, m, indicates mitochondrial membrane potential
Δp	Uppercase delta, lowercase P, indicates electrochemical proton gradient or proton motive force.
ΔpH	Uppercase delta, lowercase P, uppercase H, indicates mitochondria pH gradient
μ	Lowercase mu, used to abbreviate the *micro-* prefix (10^{-6})
m	Lowercase m, used to abbreviate the *milli-* prefix (10^{-3})
n	Lowercase n, used to abbreviate the *nano-* prefix (10^{-9})
°C	Degree symbol, used to define degrees Celsius

I. INTRODUCTION

Mitochondria: ATP production, ROS signals, and cell death

Structure and function of Mitochondria

Mitochondria are membrane-bound organelles found in the cytoplasm of eukaryotic cells. They generate adenosine triphosphate (ATP), the primary source of cellular energy, and hence are referred to as "powerhouses of the cell". Mitochondria provide energy to perform fundamental cell functions such as muscle contraction, cell division, biosynthesis, folding and degradation of proteins, and the generation and maintenance of membrane potentials. Apart from ATP synthesis, mitochondria execute numerous functions, including the production of NADH and GTP in the citric acid cycle, the biosynthesis of amino acids, heme groups, and iron-sulfur clusters, and the synthesis of phospholipids for membrane biogenesis ([5]). They also act in calcium signaling ([6]), stress responses ([7]), and generally as cellular signaling hubs ([8]). Mitochondria may rapidly change from controlling normal cell function to promoting cell death as these organelles also play a central role in necrosis and apoptosis ([9]).

Mitochondria are approximately 0.5-3 micrometers in size and are characterized by a spherical or elongated ovoid shape ([10]). Unlike most organelles, mitochondria have two membranes that split the organelle into four distinct compartments: the outer membrane, the intermembrane space, the inner membrane, and the matrix. The outer membrane (OMM) consists of protein-based porins that allow the passage of ions and molecules as large as a small protein (e.g., H_2O, ATP, pyruvate). The intermembrane space (IMS) is the space between the outer and inner membranes that contains proteins (e.g., cytochrome *c*), which play major roles in mitochondrial energetics and apoptosis ([9]). The inner membrane (IMM) is also loaded with proteins involved in electron transport and ATP synthesis. In contrast to the outer membrane, the

inner membrane is highly impermeable, and most ions and molecules require transporters to cross. The inner membrane surrounds the mitochondrial matrix, which contains enzymes for the citric acid cycle, amino acid transamination, β-oxidation of fatty acids, and the initial stages of the urea cycle ([9]). The inner membrane is arranged into many folds called cristae. These folds increase the surface area, which is the seat of the electron transport chain (ETC).

The ETC produces energy via oxidative phosphorylation reactions as shown in Figure 1.1 and responds to fluctuating ATP/ADP levels ([11]). Mitochondrial oxidative phosphorylation is the final energy yielding pathway under aerobic conditions and the major provider of ATP. During glycolysis, β-oxidation, and the tricarboxylic acid cycle (TCA), substrates are oxidized, and their electrons are used to reduce NAD^+ to NADH or FAD to $FADH_2$. Electrons derived from NADH and $FADH_2$ pass through a series of protein electron carriers; final acceptor is the molecular oxygen. This pathway is called the electron transport chain. Electrons from NADH enter the electron transport chain in complex I and then are transferred from NADH to flavin mononucleotide and then, through iron-sulfur carriers, to coenzyme Q (also called ubiquinone). Electrons can also enter from complex II via $FADH_2$ and transfer directly to coenzyme Q. Coenzyme Q is a lipid-soluble molecule that carries electrons from complex I through the membrane to complex III. In complex III, electrons are transferred from cytochrome *b* to cytochrome *c.* Cytochrome *c*, a peripheral membrane protein bound to the outer face of the inner membrane, then carries electrons to complex IV (cytochrome oxidase), where they are finally transferred to molecular oxygen.

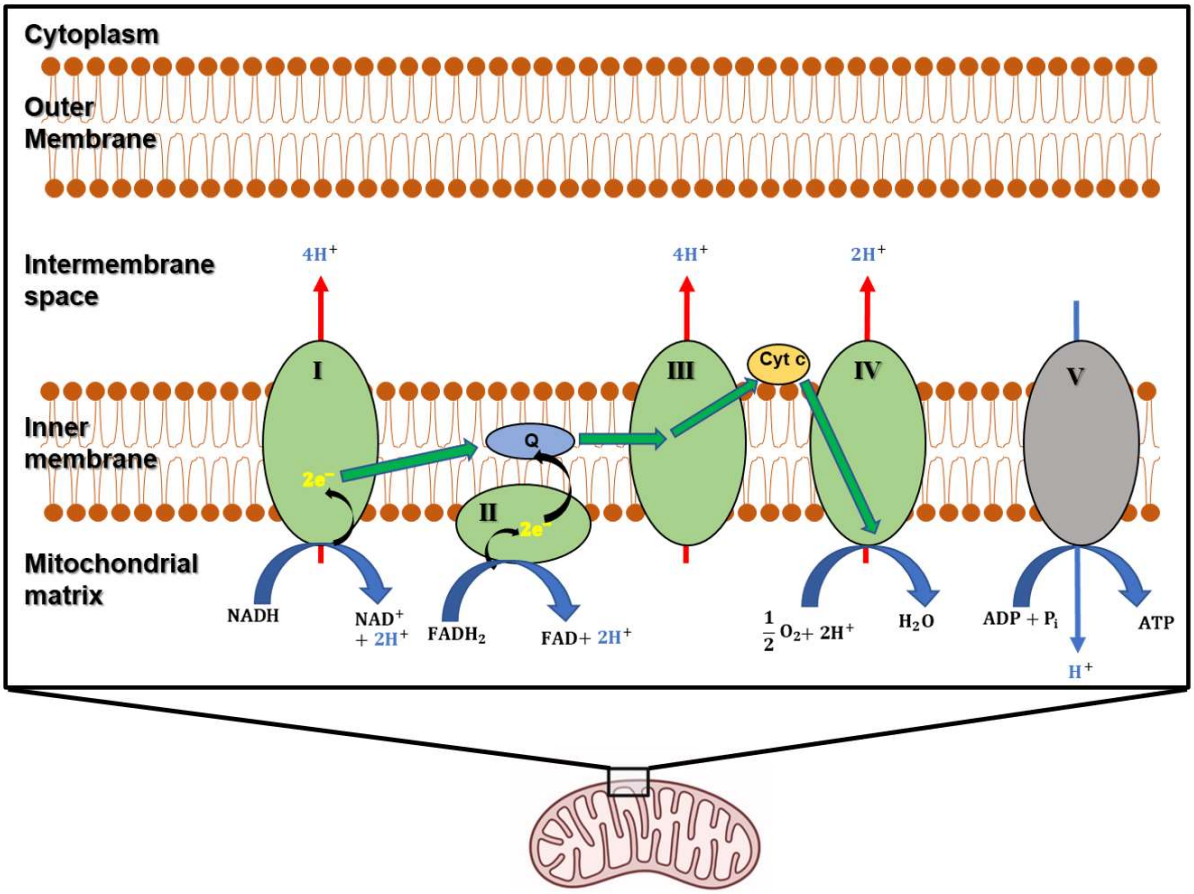

Figure 1.1: Oxidative phosphorylation in mitochondria.
Mitochondria consist of two membranes (OMM and IMM) separating the IMS and the matrix, with the IMM folded into cristae. Electrons enter the electron transfer chain at two primary sites: complex 1, where the electron donor is NADH, and complex 2, where the electron donor is $FADH_2$. Electrons are passed from complex I and II by coenzyme Q/ubiquinone (Q) to complex III. Cytochrome *c* (cyt *c*) is the mobile electron carrier from complex III to complex IV where electrons are passed to the terminal electron acceptor, O_2, which is then reduced to water in this step. Protons are pumped across the inner membrane at complex I, III and IV. ATP synthase, also known as complex V, uses the energy stored in the mitochondrial membrane potential to drive the phosphorylation of ADP to yield ATP, the energy currency in cells ([12]).

Electron transport through complexes I, III, and IV is coupled with the pumping of protons (H^+) from the matrix (low concentration of H^+) into the intermembrane space (high concentration of H^+). The pumping of the protons into the intermembrane space generates a pH gradient and a charge gradient across the inner mitochondrial membrane. The electrochemical potential energy generated by these gradients is called the proton motive force ([12]). When protons pass through the

inner mitochondrial membrane across electrochemical gradient, Complex V (ATP synthase complex) captures the proton-motive force for the production of ATP. This process is called chemiosmosis as shown in Figure 1.1 ([13]).

Aerobic metabolism occurs in mitochondria

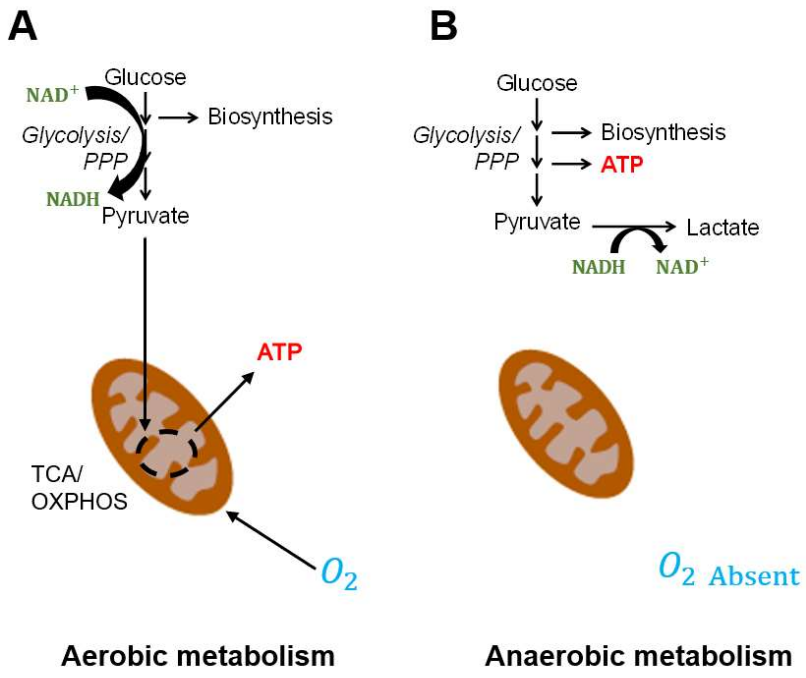

Figure 1.2: Glucose metabolism under aerobic and anaerobic conditions.
When oxygen is present, pyruvate is fully oxidized during the TCA cycle (Panel A). In absence of oxygen, pyruvate is converted to lactate to regenerate NAD+ for continued glycolysis-derived ATP production (Panel B)

In eukaryotes, the fate of the glycolysis's end product, pyruvate, depends on oxygen availability. Aerobic metabolism occurs in the presence of oxygen and involves two pathways- the citric acid cycle and electron transport chain (ETC), which take place in the matrix and the inner membrane of the mitochondria, respectively. During aerobic metabolism, pyruvate is converted into acetyl CoA by pyruvate dehydrogenase. Acetyl CoA is then completely oxidized to carbon dioxide by the citric acid cycle. The TCA cycle produces NADH (nicotinamide adenine dinucleotide), and $FADH_2$ (flavin adenine dinucleotide), which then fuels oxidative

phosphorylation to maximize ATP production, with minimal production of lactate. Under anaerobic conditions, when sufficient oxygen is unavailable in the cells, pyruvate undergoes a reduction reaction to produce lactate. This generation of lactate allows glycolysis to continue by cycling NADH back to NAD^+ but with less efficient ATP production compared with oxidative phosphorylation as shown in Figure 1.2.

Mitochondria and reactive oxygen species

Besides ATP synthesis, mitochondria generate 90% of reactive oxygen species (ROS) in mammalian cells as a byproduct of normal mitochondrial metabolism and homeostasis ([13]). During oxidative phosphorylation (OXPHOS), electrons can leak from complex I and III to generate superoxide anion radical ($O_2.^-$), caused by single-electron reduction of molecular oxygen (O_2). The O_2^- is rapidly converted into H_2O_2 by two dismutases: Cu/Zn superoxide dismutase (SOD 1) and manganese-dependent superoxide dismutase (SOD 2). Subsequently, H_2O_2 can be decomposed to water and oxygen by multiple enzymes such as peroxiredoxins, glutathione peroxidases, thioredoxins, and catalases ([14]) .

Under physiological conditions, both the generation of ROS and ROS scavenging are highly regulated. "Oxidative stress" occurs when the ROS production is beyond the normal or physiological threshold levels, and the existing endogenous antioxidants fail to regulate it. At the opposite end of the spectrum, if the reduced glutathione levels are too high in a cell, it will demonstrate a state of "reductive stress" ([13]). Mitochondria are well positioned to play a critical role as they can regulate the flux of metabolic regulators to fine-tune ROS levels depending on cellular demands.

Excessive production of ROS has been implicated in multiple conditions including asthma progression, cardiovascular diseases, cancer, digestive diseases, type II diabetes, aging, and

neurodegenerative disorders such as Alzheimer's, Huntington's, amyotrophic lateral sclerosis, and Parkinson's ([15],[16],[17],[18]). At the cellular level, ROS damages DNA by reacting with nitrogenous bases and deoxyribose, leading to mutations. Another main effect of ROS is lipid peroxidation, where the free radical oxidizes an unsaturated lipid chain, thus resulting in alterations of cell membrane structure ([19]). One of the critical aspects of oxidative stress is the oxidation of amino acid residues within proteins and the loss of catalytic activity of enzymes ([20]). Under normal cellular conditions, the levels of ROS account for ~2% of total oxygen consumed by mitochondria ([21]). Regulated oxidative stress or moderate levels of ROS are beneficial as these initiate diverse cellular responses ranging from signaling pathways involving cellular proliferation, differentiation, innate and adaptive immunity, and coordinated activation of mitochondrial fission and autophagy. Autophagy facilitates the clearance of abnormal mitochondria and cells by an orderly degradation and recycling of cellular components ([22],[23]). Furthermore, ROS has been shown to play a central role in regulating cell cycle progression, migration, and cell senescence ([24]). Interestingly, reductive stress is also detrimental to a cell as the ROS levels are too low to provide proper cellular functioning by regulating many biochemical reactions. As ROS serves as a signaling molecule, the principle "multet nocem" (excess is harmful) may become a key element in a switch operating between "pro-survival signaling" and “pro-death signaling” ([25]).

Significance of mitochondrial membrane potential

Mitochondrial membrane potential ($\Delta\Psi m$) is a key indicator of mitochondrial function ([26]). As mitochondria are the power plant of cells, mitochondria generate ATP utilizing proton electrochemical gradient potential, or electrochemical proton motive force (Δp). The electrochemical gradient potential (Δp) is the force driving protons into mitochondria; it is a

combination of both the mitochondrial membrane potential (ΔΨm, a charge or electrical gradient) and the mitochondrial pH gradient (ΔpH, an H^+ chemical or concentration gradient) ([27]).

While Δp helps regulate ATP production by providing the driving force, ΔΨm is not only related to energy production but also performs diverse non-energetic functions. It is suggested that mitochondrial membrane potential is necessary to transport metal cations and proteins carrying positively charged amino acids in the mitochondria, possibly providing retrograde signaling. These seem essential for maintaining mitochondrial structure and metabolism ([28]). Mitochondrial membrane potential also plays a crucial role in regulating the levels of ROS in the mitochondria. There is a threshold ΔΨm value above which a small increase in ΔΨm will result in a significant increase in ROS, thus displaying an exponential dependence of ROS on ΔΨm ([29]). Moreover, ΔΨm is also essential for eliminating damaged and dysfunctional mitochondria by a multistep process called mitophagy (mitochondrial autophagy). When the mitochondrial membrane potential is dissipated, PINK1 accumulates in the outer membrane, where it recruits the E3 ubiquitin ligase Parkin for ubiquitination and subsequent degradation of the impaired mitochondria ([28],[30]). Thus, to maintain a healthy population of mitochondria, the mitochondria membrane potential is a critical element in disposing of the dysfunctional mitochondria. Also, a controlled regulation of mitochondria abundance/population represents a crucial requirement for cell homeostasis.

Mitochondria are highly dynamic organelles that maintain homeostasis and morphology by undergoing continuous fission, fusion, and constant turnover through mitochondrial biogenesis and mitophagy ([31]). Mitochondria biogenesis might be enhanced through external stress stimuli such as cold exposure, energy deprivation, and physical exercise ([32],[33]). The imbalance of mitochondria abundance leads to various neurodegenerative diseases, including Alzheimer's

disease (AD), Parkinson's disease (PD), and amyotrophic lateral sclerosis (ALS), and myopathies ([34]).

The role of mitochondria in cell death

Mitochondria are "life-essential" organelles for producing ATP, but paradoxically, they also play a critical role in cell death ([35]). Cell death is an active and indispensable process to get rid of damaged cells in order to maintain homeostasis and regulate development in multicellular organisms. The existence of a tightly controlled and regulated signaling pathway that induces cell death is required for the normal functioning of cells and its deregulation can lead to catastrophic diseases such as cancer and autoimmunity (too little cell death) as well as degenerative diseases (too much cell death) ([36]). There are at least four significant types of morphologically distinct cell death: apoptosis, autophagy, necrosis, and entosis. Although they are executed distinctly, their signaling pathways might overlap in response to specific stimuli ([36],[37]). Mitochondria play a critical role in activating apoptosis in mammalian cells ([38]). The term "apoptosis" is derived from Greek, referring to the "falling off" leaves from trees in autumn. Apoptosis is a silent form of death that occurs in physiological and pathological conditions ([39]). In contrast to necrosis, damaged cells undergoing apoptosis fragment into smaller apoptotic bodies and are engulfed by neighboring cells or phagocytes, thus avoiding immune response without eliciting inflammation ([40]).

Apoptosis is characterized by morphological alterations such as chromatin condensation, nuclear fragmentation, blebbing, cell shrinkage, and chromosomal DNA fragmentation. The biochemical hallmarks of apoptosis are activation of caspases, flipping phosphatidylserine membrane lipids, permeabilization of the mitochondrial membrane, and activating pro-apoptotic Bcl-2 protein family members ([39]). Apoptosis can be triggered by two major signaling pathways: the extrinsic or death receptor pathway and the intrinsic or mitochondrial pathway. As the name

implies, the extrinsic (death receptor pathway) is triggered by a death ligand binding to a death receptor, such as TNF-α to TNFR1 or FasL to FasR. Upon ligand binding, recruitment of adapter proteins such as TRADD and/or FADD leads to dimerization of death effector domains followed by activation of initiator caspase 8. Caspases are cysteine proteases with specificity for aspartic acid residues in their substrates. The initiator caspase 8 triggers apoptosis by cleaving other downstream or executioner caspases ([39]). In contrast, the intrinsic or mitochondrial pathway is initiated within cells and is triggered by non-receptor mediated stimuli such as DNA damage, hypoxia, extremely high concentrations of cytosolic Ca^{2+}, and oxidative stress ([39]). All of these stimuli result in the opening of the mitochondrial permeability transition (MPT) pore and loss of mitochondrial membrane potential. The Bcl-2 family of proteins governs mitochondrial membrane permeability and can be either pro-apoptotic (e.g., Bax, Bak, Bad, Bid, Bik, and Bim) or anti-apoptotic (e.g., Bcl-2, Bcl-XL, and Bcl-W) ([39],[41]). While the anti-apoptotic proteins regulate apoptosis by blocking the mitochondrial release of the ETC molecule, cytochrome-*c*, the pro-apoptotic proteins promote its release. Cytochrome-*c* binds and activates Apaf-1 as well as procaspase-9, forming an "apoptosome." When the mitochondria membranes are permeabilized, other apoptotic factors are also released including apoptosis-inducing factor (AIF), the second mitochondria-derived activator of caspase (Smac). Upon apoptotic insult, Smac promotes apoptosis by inhibiting X-linked inhibitor of apoptosis proteins (XIAPs) activity ([41]). This subsequently results in activation of executioner caspases (caspase -3 or-7) to mediate cellular changes associated with apoptosis ([36]).

The mechanisms underlying cellular changes, cell death, cancer research, and drug discovery were studied on a 2-dimensional monolayer cell culture system ([42]). However, there has been an increasing trend to transit from 2D to 3D cell culture model system.

Three-dimensional cell culture: A potential bridge between traditional two-dimensional cell culture and animal models

Overview of 3D cell culture models

Mammalian cells have been cultured as two-dimensional (2D) monolayers for decades. However, the 2D monolayer fails to imitate the architecture and microenvironment found *in vivo*. They differ in terms of morphology, proliferation, cell-cell and cell-matrix interactions, signal transduction, differentiation, and other aspects as observed in the *in vivo* microenvironment ([43],[44]). Therefore, there has been a growing interest in the use of three-dimensional (3D) cell culture models in recent years. An ideal 3D cell culture system would recapitulate a tissue-specific physiological or pathophysiological disease-specific microenvironment where cells can proliferate, aggregate, and differentiate ([45]). Compared to 2D cell culture, the 3D cell culture model exhibits cell-to-cell, cell-to-ECM interactions, tissue-specific matrix stiffness, oxygen, nutrient, and metabolic waste gradients ([45]). In contrast to the 3D cell culture system, 2D lacks the interconnections between cells and the extracellular matrix (ECM). The extracellular matrix (ECM) is a highly complex fibrous mesh including matrix proteins (e.g., collagens), glycoproteins (e.g., fibronectin), glycosaminoglycans (e.g., hyaluronan), growth factors such as transforming growth factor-β (TGF-β), vascular endothelial growth factor (VEGF), platelet-derived growth factor (PDGF), hepatocyte growth factor (HGF) and other secreted proteins. The composition of ECM and its physical properties can influence cell proliferation, differentiation, migration, survival, adhesion, cytoplasmic structural organization, and cell signaling in normal physiology and development and many diseases such as fibrosis, cancer, and genetic disorders ([46]). The physical properties of the extracellular matrix, like stiffness and topography, contribute to drug resistance ([47]). Also, a multicellular 3D tissue model associated with stromal cells can stimulate

cell growth, induce angiogenesis, and promote inflammation in tumor cells, thus providing a better model platform for disease modeling, drug screening, and drug development ([48],[49],[50]).

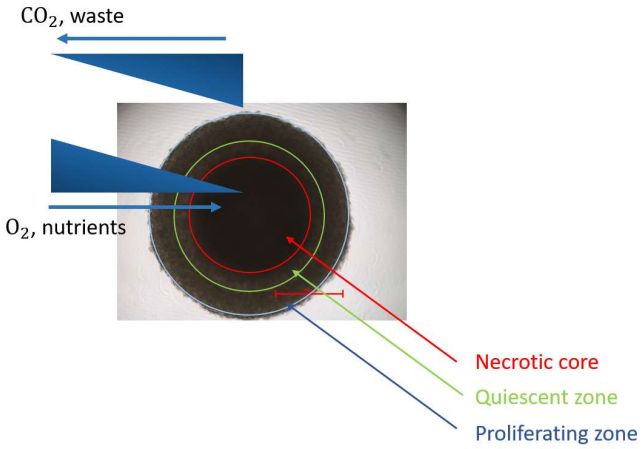

Figure 1.3: Schematic representation gradients in 3D spheroids.
3D spheroids are characterized by an external proliferating region and an internal quiescent zone (caused by the gradient of nutrient and oxygen diffusion), which surrounds a necrotic core, mimicking the cellular heterogeneity observed in solid tumors.

Figure 1.3 shows that concentration gradients for oxygen, pH, and nutrients exist in the 3D model, which are absent in a traditional monolayer. In *in-vivo* solid tumors, these natural gradients are influenced by the proximity to blood vessels, the diffusion of molecules through the ECM, and the extent of cellular metabolism that regulates oxygen and nutrient consumption and the production of cellular waste products. ([45]). Like a solid tumor, 3D has heterogeneous architecture, internal gradients of signaling factors, and pathophysiological gradients. The outer layer is the proliferating zone owing to the accessible access to oxygen and nutrient, the inner layer is the quiescent zone, and the necrotic zone in the core ([51]). The availability of oxygen and nutrients decreases, and the amount of carbon dioxide and waste products increases as we move from the outer layer to the core. Therefore, cells in the necrotic zone are either senescent or undergoing necrosis. Thus, 3D cultures, such as spheroids, give us insight into oxygen availability, growth

factor, and nutrient-mediated mechanisms leading to cell phenotype changes and drug response alterations ([45]).

Different types of 3D cell cultures

While 2D cell culture can be grown in a flat monolayer on a plate, 3D cell culture growth is often categorized into scaffold-based and scaffold-free 3D culture systems.

Scaffold-based 3D cell culture:

Scaffolds can be of biological origin or synthetically engineered to mimic key properties of ECM such as stiffness, charge, or adhesive moieties and provide physical support on which cells can aggregate, proliferate, and migrate. In scaffold-based cultures, cells are embedded into the matrix, and the chemical and physical properties of the scaffold material will influence cell characteristics ([52]). In scaffold-based techniques, scaffolds can either be natural hydrogels derived from sources such as collagen, chitosan, glycosaminoglycans, fibroin, agarose, alginate, and starch (mainly used as additives); or can be synthetic hydrogels such as polyethylene glycol (PEG), polylactic acid (PA), and polyglycolic acid (PGA) ([45]). Natural hydrogels are biocompatible, have lower toxicity, and sustain many physiological cell functions, while synthetic hydrogels are reproducible, versatile, and exhibit enhanced workability ([44]).

Scaffold-free 3D cell culture:

Scaffold-free 3D culture methods can culture cells on different media such as non-adherent plates, hanging drop plates, low adhesion plates with ultra-low attachment coating that promotes spheroid formation, and micropatterned plates that allow for microfluidic cell culture ([45]). This promotes the formation of spheroids by avoiding cell adhesion to surfaces and favoring cell-cell interactions and cell self-aggregation ([45]). The non-adherent plates are coated with a hydrophilic polymer such as agarose that inhibits cells from sticking to the surface and promotes cell clustering,

encouraging the formation of an extracellular matrix. This method is called a liquid-overlay technique. In a hanging-drop method, cells self-aggregate into spheroids at the bottom of the droplet when a surface is unavailable for cell attachment. Spheroids formed by the hanging-drop technique may represent tumor layers and gradients, as shown in Figure 1.3.

A 3D *in vitro* model to explore epithelial mesenchymal transition

Epithelial-to-mesenchymal transition (EMT) is a complex process occurring during embryogenesis (type 1 EMT) and wound healing (type 2 EMT) and is also highly implicated in cancer progression (type 3 EMT) ([53]). Type 3 EMT is associated with cancer progression and metastasis. An early event of EMT is the loss of epithelial phenotype and the down-regulation of E-cadherin, a well-characterized adhesive junction protein expressed in differentiated and polarized epithelial cells to assume a mesenchymal cell phenotype, which includes enhanced migratory capacity, invasiveness, elevated resistance to apoptosis, and significantly increased production of ECM components ([54]). The graded loss of E-cadherin correlates with the aggressiveness of numerous carcinomas, whereas the forced expression of E-cadherin suppresses tumor development in various *in vitro* and *in vivo* experimental tumor models ([55]).

EMT is regulated by multiple factors, including cell signaling, transcriptional control, epigenetic modification, and post-translational modifications ([56]). Epithelial cells receive EMT-inducing signals emanating from the tumor-associated stroma, such as HGF, EGF, PDGF, and TGF-β, which can induce or promote the EMT process ([54],[57]). These EMT-inducing signals upregulate specific transcription factors, notably Snail, Slug, zinc finger E-box binding homeobox 1 (ZEB1), and Twist ([54],[58]). The activated transcription factors can act pleiotropically to choreograph the complex EMT program through a series of intracellular signaling networks involving, among other signal-transducing proteins, ERK, MAPK, PI3K, Akt, Smads, β-catenin,

and lymphoid enhancer-binding factor (LEF) as well as cell surface proteins such as β4 integrins, α5β1 integrin, and αVβ6 integrin ([54],[59]). Though EMT has been largely studied, identifying a molecular target controlling invasion and metastasis events that lead to EMT still needs to be discovered due to the need for a proper cell culture model system. The traditional 2D models are not ideal for explaining the molecular mechanisms controlling EMT as they lack biological requirements such as nutrient and oxygen gradients and angiogenesis, unlike the 3D models that show heterogeneity and cell-matrix interactions that are better recreated by a complex aggregated cell population found in 3D ([57]). Therefore, 3D spheroids provide a pragmatic pathophysiological microenvironment and serves as a tool in better understanding changes, interactions, invasion, cellular and molecular signaling in cancer research.

However, traditional two-dimensional (2D) *in vitro* cell culture system has long been used in cancer research to delineate modes of regulated cell death as they play a critical role in organismal development, homeostasis, and pathogenesis. Of all the various types of regulated cell death, apoptosis is the best-understood and most relevant mode of cell death. Hence, it becomes imperative to employ a 3D cell culture model to study the critical importance of apoptosis in battling cancer.

Apoptosis-inducing factor: Dissociating the apoptotic role and physiological role of AIF

Overview of AIF architecture and activities

Apoptosis-inducing factor (AIF) is an evolutionary conserved, caspase-independent death effector ([60]). The *AIF* gene, also known as *PCDC8 and AIFM1*, was mapped within X chromosome region A6 in mice and the Xq25–26 region in humans respectively ([61]). Phylogenetic analysis revealed that AIF possesses significant homology with NADH ferredoxin reductases from eubacteria, archaebacteria and the yeast NDH-2 enzyme Ndi1 (designated as internal NADH

dehydrogenase) ([62]). Among eukaryotes, AIF has the strongest homology with dehydroascorbate reductase from Arabidopsis thaliana. AIF also shares substantial homology with four putative oxidoreductases from vertebrate (Xenopus laevis) and invertebrate (C. elegans, Drosophila melanogaster) animals, as well as S. pombe, nematodes, and fungi ([60]). Approximately 90% sequence identity was observed in AIF among mammals, thus implying that the AIF gene has been conserved throughout the eukaryotic kingdom ([61]). Transcription and translation of the nuclear-encoded AIFM1 gene (in humans) gives rise to a 67 kDa precursor molecule containing 613 amino acid residues (612 amino acid residues in mice), containing the N-terminal mitochondrial localization sequence (MLS), two nuclear-localization sequences (NLS), and the NAD- and FAD-binding motifs as shown in the Figure 1.4. The precursor AIF molecule can be imported into mitochondria and after the import, the N-terminal mitochondrial localization sequence (MLS) is cleaved at residue 54. This 62 kDa mature form of AIF (Δ1-54) is tethered to the intermembrane space of mitochondria by a stretch of hydrophobic amino acids with the soluble protein surfaces extending into the intermembrane space. Following import into mitochondria, AIF incorporates the flavin and adopts a glutathione reductase (GR) fold. Due to the incorporation of FAD, AIF was proposed to function *in vivo* as a superoxide producing NADH oxidase. Upon apoptotic insult followed by outer membrane permeabilization, membrane-bound mature AIF undergoes a second round of proteolytic cleavage at position 102 by cathepsins and/or calpains, forming the soluble apoptogenic 57 kDa fragment of AIF (Δ1-102). This apoptogenic AIF translocates to the nucleus, where it induces peripheral chromatin condensation and high-molecular-weight DNA fragmentation and eventually the demise of the cell ([63],[64]).

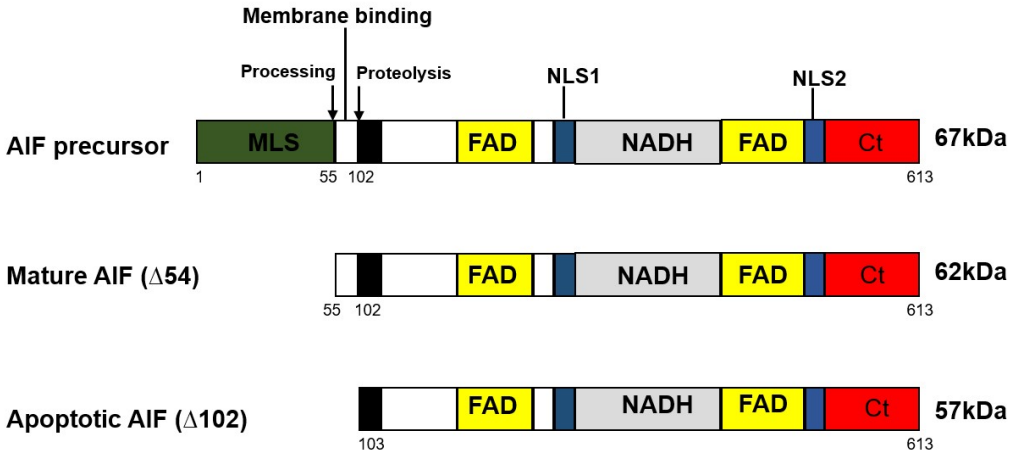

Figure 1.4: Domains of AIF.
AIF is translated into a precursor polypeptide containing a mitochondrial localization sequence (MLS), two FAD-binding domains, an NADH binding domain, two nuclear localization sequences (NLS), and a C-terminal (Ct) DNA-binding domain. AIF is cleaved at the indicated positions during processing and mitochondrial release.

The role of AIF in cell death

Kroemer and coworkers first demonstrated the role of AIF in cell death in 1996, when a soluble factor released from mouse mitochondria in a cell-free *in-vitro* system caused isolated nuclei to undergo apoptotic changes such as chromatin condensation and internucleosomal DNA fragmentation ([65]). Later, the soluble factor was identified as an apoptosis-inducing factor (AIF), as it could maintain the apoptogenic ability in the presence of a pan-caspase inhibitor benzyloxycarbonyl-Val-Ala-Asp (OMe) fluoromethylketone (z-vad.fmk) thus suggesting that AIF induces cell death in a caspase-independent manner ([66]).

When apoptosis is induced, the mitochondrial outer membrane is permeabilized, and AIF translocates to the nucleus. AIF interacts with DNA and recruits additional proteins, including histone H2AX, cyclophilin A (CypA), and endonuclease G (EndoG), to form DNA degrading complexes, degradosomes to induce peripheral chromatin condensation and a high-molecular-

weight (50kbp) DNA degradation ([67],[68],[69],[70]). The AIF-H2AX interaction is essential for AIF-mediated chromatin condensation and for initiation of DNA degradation; CypA assists cytonuclear translocation of apoptogenic AIF, whereas EndoG is a nonspecific nuclease that cleaves single- and double-stranded DNA and RNA in an Mg^{2+}/Mn^{2+}-dependent fashion ([71],[72],[73]).

AIF also participates in multiple death paradigms to facilitate the completion of apoptosis. Cell death signaling can be triggered by various stimuli, one such stimuli is excessive calcium influx that results in poly (ADP-ribose) polymerase (PARP) overactivation, which facilitates the translocation of AIF and initiates chromatin condensation ([74]). In response to p53 death signaling, the pro-apoptotic Bcl-2 family members, such as Bax and Bak, undergo conformational changes, forming pores in the OMM that induces the release of AIF ([69],[75]). In recent findings, it was demonstrated that AIF may bind to macrophage migration inhibitory factor (MIF), a previously unrecognized nuclease, and translocate to the nucleus, where it directly degrades chromosomal DNA and causes cell death ([76]).

Our lab also identified an additional AIF-associated factor, a mitochondrial phosphoglycerate mutase, PGAM5 that triggers a novel death pathway leading to mitophagic cell death. AIF and PGAM5 can both be ubiquitinated and inhibited by XIAP. X-linked inhibitor of apoptosis protein (XIAP) belongs to the family of IAPs and possess E3 ubiquitin ligase activity ([77]). This AIF/PGAM5/XIAP axis could regulate mitophagy, indicating AIF is likely to play a role in atypical death mechanisms associated with XIAP and PGAM5. Additionally, this death triad also regulates antioxidant response which are crucial for cell survival. Therefore, further exploration on this triad axis is required to determine how non-canonical ubiquitination influences decisions of cell fate.

Heat shock protein 70 (Hsp70) is not only the first cytoplasmic partner of AIF but also the pro-survival partner of AIF. Hsp70 interacts with the exogenous and endogenous AIF and retains AIF in the cytoplasm, preventing the initiation of nuclear apoptosis ([78]). XIAP is also another pro-life partner of AIF. AIF can inhibit the interaction of XIAP with Smac/DIABLO, another death-signaling protein released from mitochondria that prevent XIAP from binding to caspases. XIAP in cooperation with AIF, decreases ROS levels and removes both initiator and executioner caspases from the cell via ubiquitination and proteasome degradation, thus promoting cell survival ([77],[79]). Therefore, apoptogenic AIF can exert diverse effects depending upon the interactions with the cytoplasmic proteins acting as pro-survival or pro-death effectors.

Altogether, AIF has a crucial role as a death effector in various cell demise paradigms. However, pro-death functions of AIF contribute to pathological conditions limited to a narrow range of cell types, primarily neurons and cardiomyocytes ([80],[81],[82]). The death activity of AIF is also limited to certain stimuli such as hypoxia, glucose deprivation, formation of free radicals, and DNA damage implying that whether AIF is essential for cell death depends on the cell type, apoptotic stimuli, and interactions with cytoplasmic proteins ([64],[83],[84]). Therefore, contrary to its name and initial characterization, AIF does not function as a universal effector of cell death.

Role of AIF in cell survival and homeostasis

For decades, the role of AIF as an evolutionarily conserved death executioner grabbed attention of researchers. However, over the past few years, compelling evidence has emerged that AIF has additional functions beyond apoptogenic activity. AIF is a flavoprotein and belongs to the electron-transferase class of NADH reductases. AIF can catalyze the oxidation of both NADH and NADPH while reacting rapidly with oxygen to form superoxide (O_2^-) *in vitro* ([85]). Still, the NADH oxidase activity *in vivo* and how it contributes to cellular homeostasis remains unclear.

The physiological significance of AIF was first reported in a homozygous AIF knockout in mice, where genetic inactivation of Aifm1 resulted in cell death during early embryogenesis ([86]). Next, progressive neurodegeneration, ataxia, and blindness were observed in Harlequin mutant mice. The Harlequin mutation was derived from a proviral insertion in the X-linked Aifm1 locus, causing an 80% reduction in Aifm1 mRNA expression, thus bolstering the significance of AIF ([87]). Moreover, gene silencing of AIF by small interfering RNA (siRNA) in HeLa cells and genetic deletion of Aifm1 in mouse ES cells led to diminished oxygen consumption rate (OCR) and enhanced lactate production ([88]). Further tissue and cell-specific AIF knockout studies demonstrated defects in mitochondrial respiration, dilated cardiomyopathy, skeletal atrophy, aberrant mitochondrial morphology, and loss of cristae organization ([88],[89],[90]). Together, these studies suggest that AIF regulates mitochondrial bioenergetics. It was proposed that AIF might regulate mitochondrial function by participating in the respiratory complex assembly and/or stabilization. This was further supported by the discovery that AIF interacts with the coiled-coil-helix-coiled-coil-helix domain containing 4 (CHCHD4), a crucial component of the mitochondrial import machinery. AIF deficiency enhances intermembrane space degradation of CHCHD4 and eventually results in a loss of OXPHOS subunits. These findings support that AIF indirectly assists the assembly of the OXPHOS system since it contributes to the proper folding of OXPHOS subunits and other factors in a CHCHD4-dependent fashion ([91],[92],[93]). On the other hand, AIF may influence the cellular process by associating with eukaryotic translation initiation factor 3 subunit g (eIF3g) to inhibit protein synthesis during apoptosis ([94]). Similarly, AIF maintains the reduced state of PTEN, a tumor suppressor, and regulates the Akt signaling pathway ([95]). Several clinical reports have described mutations in the *AIFM1* gene that are causally linked to mitochondrial diseases that lead to respiratory chain malfunction with a spectrum of clinical manifestations,

including mitochondrial encephalomyopathy, familial and sporadic auditory neuropathy, Cowchock syndrome and early-onset severe infantile motor neuron dysfunction ([96],[97],[98],[99]).

Together, these findings establish the widespread view of AIF as a death effector with a critical role in maintaining mitochondrial function and confirm AIF as a significant mediator of cell survival and homeostasis.

AIF functions as a pro-tumor molecule

Cancer cell metabolism and redox homeostasis

Cancer is a large group of diseases that occurs when cells accumulate genetic mutations, resulting in uncontrolled cell division and eventually forming tumors that can spread to other tissues and organs. In order to fuel their rapid proliferation rate and tumor progression, cancer cells alter their cell metabolism. Otto Warburg discovered that cancer cells exhibit high glucose uptake rates and lactic acid production, even in the presence of oxygen, often referred to as “aerobic glycolysis. ([100]). This so-called "Warburg effect" hypothesized that cancer cells prefer aerobic glycolysis to OXPHOS due to functional defects in mitochondria ([101]). It was later confirmed that cancer cells upregulate aerobic glycolysis while retaining mitochondrial respiration, contradicting Warburg's claim for mitochondrial defects ([102]). In cancer cells, a switch in metabolism towards glycolysis over respiration despite their functional oxidative phosphorylation machinery constitutes metabolic reprogramming. However, the Warburg effect is generally thought to confer growth advantages to tumor cells by enhancing glycolysis to supply carbon for anabolic processes and biomass needed to favor the growth of rapidly proliferating cells ([103]). This excess carbon is used for the *de novo* synthesis-up of nucleotides, lipids, and proteins and can be redirected into several pathways that arise from glycolysis ([104]). This suggests that targeting Warburg Effect mediators is an emerging and promising strategy for cancer treatment.

Racker, Jeffrey Flier, and Morris Birnbaum proposed the Warburg Effect confers growth factor signaling function to tumor cells ([104],[105],[106],[107]). The signaling function of tumors is attributed to the generation and modulation of reactive oxygen species (ROS) ([108]). A threshold exists for increased ROS and maintaining an appropriate balance of ROS is essential since excessive ROS has other deleterious effects ([14],[109]). Insufficient ROS disturbs signaling processes beneficial for cell proliferation, such as inactivating phosphatase tensin homolog (PTEN), and tyrosine phosphatases ([109]). ROS-dependent signaling regulated by the mitogen-activated protein kinase (MAPK) family of proteins is a significant example of how ROS levels impact cell fate. MAPK cascades consisting of the extracellular signal-related kinases (ERK1/2), the c-Jun N-terminal kinases (JNK), and the p38 kinase (p38) are major intracellular signal transduction pathways that play an essential role in cell growth, differentiation, development, cell cycle, survival, and cell death ([110]). ERK and JNK pathways can be activated through phosphorylation by upstream kinases (MAPKKK) and relief of MAPK phosphatase (MKP)-mediated inhibition ([108],[111]).

The ERK signaling pathway plays an important role in proliferation, tumor invasion, and metastasis. Thus, inhibiting the ERK signaling pathway will prevent tumor cell proliferation and promote cell apoptosis ([112]). Similarly, transient activation of JNK activity promotes cell survival, whereas prolonged JNK activity induces apoptosis ([113]). Cancer cells elevate ROS levels that drive both pro-survival and proliferative activities through ERK and JNK signaling pathways. Therefore, therapeutic targeting of redox-mediated signaling could lead to cancer cells exhibiting an increased sensitivity to oxidative stress-induced toxicity relative to normal cells.

Tumorigenic activities of AIF

The NADH oxidoreductase activity of AIF in normal cells is well positioned to be exploited by cancer cells for cell survival and mitochondrial homeostasis ([63],[64],[85]). An increased expression of AIF was observed in diverse cancer cell types, including esophageal, skin, colorectal, gastric, pancreatic, and prostate, indicating that AIF might support tumor development contrary to its tumor-suppressive capabilities ([114],[115],[116],[117],[118],[119]).

How might an overexpression of AIF in cancer benefit cancer growth? Firstly, the death function of AIF contributes to pathological conditions but is limited to a narrow range of cell types, primarily neurons and cardiomyocytes, and responds to limited stimuli such as hypoxia, glucose deprivation, formation of free radicals, and DNA damage ([79],[80],[81]). Secondly, the expressions of pro-survival partners of AIF (Hsp70, XIAP) are also elevated in cancer, and together, they could prevent the initiation of nuclear apoptosis or ubiquitination of caspases, thus promoting cell survival ([78],[120]). Therefore, contrary to its name and initial characterization, the pro-survival activities of AIF would serve to mediate tumor permissive metabolic and oxidative states.

A potential explanation of the supportive role of AIF in cancer might be due to its ability to regulate the biogenesis of the electron transport chain and eventually play a role in mitochondrial bioenergetics ([121]). Studies have shown that an impairment of the mitochondrial respiratory chain in cancer cells promotes cancer progression to a chemoresistance or invasive phenotype ([122]). AIF might also support tumor progression through elevated levels of ROS, which would serve as signaling molecules in the MAPK pathway to promote proliferation and survival ([14],[108],[123]).

Knockout studies conducted in two human colon carcinoma cell lines first demonstrated a pro-tumor role for AIF. In these cells, knockout of AIF resulted in lower mitochondrial complex I oxidoreductase activity and decreased production of ROS but increased sensitivity to peroxide- or

drug-induced apoptosis ([124]). This signifies for the first time that AIF could function in a tumor-permissive manner rather than as a tumor suppressor of tumor, likely through control of cellular metabolism and/or ROS-mediated survival signaling.

AIF enzymatic activity supports advanced prostate cancer

Our group has extended the investigation of the tumorigenic role of AIF in the context of advanced prostate cancer ([117]). Loss of PTEN, a tumor suppressor, in prostate cancer (PCa) promotes tumor progression and metastasis ([125],[126]). In a mouse model of prostate cancer, deletion of PTEN substantially increased AIF expression compared to the wild-type prostate tissues, indicating a potential role of AIF in prostate tumorigenesis. The bioinformatics and immunohistochemical analysis in prostate cancer patients further demonstrated an increased AIF expression at both the RNA and protein levels in patient's tumors relative to normal tissue. These data suggest that elevated AIF is a signature of prostate tumorigenesis in humans and mice.

To test the involvement of AIF in cancer progression, AIF was stably suppressed in various PCa cell lines: androgen-sensitive (LNCaP) and androgen-insensitive (PC3 and DU145). Under nutrient-rich conditions *in vitro,* the proliferation rate of AIF ablated prostate cancer was unaffected. However, PC3 and DU145, the advanced prostate cancer cell lines, require AIF for invasion, migration, and growth in the Matrigel™ substrate. Xenograft studies of AIF-mediated tumorigenesis in mice were then conducted using PC3 cells, demonstrating that AIF is critical for tumor growth *in vivo*. Also, AIF-deficient advanced prostate cancer cell lines exhibited decreased levels of complex I but were unaffected in LNCaP cells. Interestingly, this was the first report of a context in which AIF does not regulate complex I. The knockdown of AIF in advanced prostate cancer cells also exhibited metabolic changes, including increased glucose consumption, lactate secretion, and decreased oxygen consumption. These metabolic studies suggests that the increased

glucose consumption results from the impairment of OXPHOS, confirming that a metabolic switch occurs in DU145 and PC3 cells following AIF ablation. To determine the significance of altered glucose metabolism, cells were treated with the glycolysis inhibitor, 2-deoxyglucose. Following 2-deoxyglucose treatment, only AIF-deficient PC3 and DU145 cells demonstrated reduced viability, while LNCaP cells (androgen-sensitive) were unaffected. Together, these data suggested that AIF plays a critical role in advanced prostate cancer cell lines surviving under conditions of growth stress both *in vitro* and *in vivo*.

To determine if the NADH-oxidase activity of AIF is necessary for the support of prostate cancer cell growth, cells were restored with either wild-type (WT) AIF or AIF with T263A/V300A mutations (TVA), which impairs catalytic activity. AIF-deficient PC3 cells restored with WT-AIF restored the metabolic and growth effects of AIF deficiency to control levels, but not TVA AIF, demonstrating that the NADH-oxidase activity of AIF supports normal glucose consumption, aggressive growth, and survival under growth stress in advanced prostate cancer cells. While WT-AIF can restore growth and metabolism, both WT-AIF and TVA-AIF can restore complex I. This suggests that the enzymatic activity of AIF is not significant to the complex I level but is required for cellular metabolism. Altogether these experiments demonstrate the essential role of AIF enzymatic activity in support of prostate cancer cells that is restricted to cells that have achieved a more advanced status, suggesting that AIF acts at a later stage in tumor development.

The impact of enzymatic activity of AIF in the activation of JNK, a redox-sensitive MAPK, was explored in PC3 cells ([127]). AIF-deficient (shAIF) and AIF-proficient (shLacZ) PC3 cells were restored with either empty vector, WT-AIF, or TVA-AIF and were induced oxidative stress ([128]). Restoration of AIF-deficient PC3 cells with WT-AIF, but not TVA-AIF, resulted in activation of JNK following ROS stimulation and demonstrated that the enzymatic activity of AIF

is required for oxidant induced JNK phosphorylation. The JNK subfamily consists of three isoforms: JNK1, JNK2, and JNK3. JNK1 and JNK2 are ubiquitously expressed, whereas JNK3 is expressed primarily in the brain and, to a lesser extent, in the heart and testis ([129]). In order to identify the isoform of JNK that has been activated by ROS stimulation, we used isoform-specific antibodies for JNK1 and JNK2. Only JNK1 was phosphorylated in response to acute oxidant stimulation, suggesting JNK1 is the target of tBHQ. It was also worth noting that under basal conditions, AIF-dependent changes in JNK phosphorylation were observed in PC3 (prostate cancer); HPAC (pancreatic cancer); MRC-5 (normal lung); HCT 116 (colorectal cancer); and MIA PaCa-2 (pancreatic cancer), thus indicating that AIF-dependent JNK phosphorylation is widespread among cell types.

To determine the downstream effects of AIF-mediated JNK signaling, alteration in protein expression of cadherin levels in AIF-deficient PC3 cells were assessed. JNK contributes to various cellular programs regulating death, survival, proliferation, and differentiation ([130]). One important cellular activity influenced by JNK in cancer is the epithelial-to-mesenchymal transition (EMT) ([131]). A key event of EMT is the cadherin switch, whereby cells reduce the expression of E-cadherin and elevate N-cadherin, thus leading to metastasis ([132]). Immunoblot analysis revealed that AIF ablation resulted in the upregulation of E-cadherin and downregulation of N-cadherin, thus demonstrating that AIF promotes cadherin switch in PC3. To further assess the involvement of JNK in the cadherin switch in PC3 cells in an AIF-dependent manner, JNK activity was suppressed either by a pan-JNK inhibitor, SP600125, or by genetic knockdown in AIF-deficient (shAIF)/ AIF-proficient (shLacZ) PC3. Inhibition of JNK activity triggered an elevation in E-cadherin and a reduction in N-cadherin levels in AIF-deficient PC3. Moreover, JNK1 activity in AIF-deficient PC3 was restored using constitutively active forms of JNK (CA-JNK1) fused with

the JNK activator MKK7 and tagged with a FLAG epitope. When CA-JNK1 was introduced in AIF-deficient PC3, E-cadherin expression levels were similar to AIF-proficient cells, confirming that AIF regulates the cadherin switch by activating JNK1 and not by JNK2.

Since AIF regulates E-cadherin expression by activating JNK1, effects of reverting E-cadherin were assessed in AIF-deficient cells. Stable knockdown of E-cadherin in AIF-deficient PC3 cells (PC3–shAIF/shE-cadherin) increased levels of N-cadherin, suggesting N-cadherin levels can be altered by E-cadherin in an AIF-dependent manner. Taken together, these data suggest that AIF is an upstream effector of JNK1, and AIF/JNK1/E-cadherin/N-cadherin axis likely exists.

AIF supports the growth and survival of metabolically defined pancreatic cancer cells

Additional publications from our group also demonstrated AIF as a major contributor to the growth-promoting metabolic state of pancreatic tumor cells ([118]). Pancreatic ductal adenocarcinoma (PDAC), the most common form of pancreatic cancer, is not only one of the most bioenergetically sensitive and metabolically diverse, but also considered an aggressive tumor ([133],[134]). Since pancreatic cancer is notoriously aggressive and are particularly evasive and resilient, it becomes difficult to treat. Therefore, we further evaluated the role of AIF in pancreatic cancer tumorigenesis.

Oncomine data analysis indicated that elevated AIF expression is not a global trend in pancreatic cancer, but there exists a subtype of pancreatic tumors (approximately one-third of the population) in which AIF expression is significantly elevated. To test the involvement of AIF in pancreatic tumorigenesis, AIF was suppressed in a panel of pancreatic cancer cell lines (PANC-1, BxPC-3, HPAC, HPAF-II, and MIA PaCa-2). According to gene expression analysis, sensitivity to metabolic inhibitors, and metabolite profiling, PANC-1 and BxPC-3 cells derived most of their energy from OXPHOS. In contrast, HPAC cells rely on lipogenic pathways, whereas HPAF-II and

MIA PaCa-2 are more reliant on glycolysis. AIF ablation did not impact cell death in pancreatic cancer cells in response to toxic chemical triggers such as actinomycin D and gemcitabine, indicating that AIF does not play a significant regulatory role in death induction. Further, AIF contributes to growth rate and migration in AIF ablated pancreatic cancer cells (PANC-1, BxPC-3, HPAC) under nutrient-rich conditions *in vitro* through a mechanism that appears different from that shown in prostate cancer. Also, AIF-deficient pancreatic cancer cell lines (PANC-1, BxPC-3, HPAC) exhibited decreased levels of complex I activity and increased glucose consumption rate that were correlated with both metabolic phenotype and changes in growth. To further define the significance of AIF-mediated glucose metabolism in cell survival, glycolysis was inhibited in our panel of cell lines by treatment with 2-deoxyglucose. Following 2-deoxyglucose treatment, OXPHOS-dependent cell lines PANC1 and BxPC-3 were sensitized to glycolytic disruption in an AIF-dependent manner. However, due to their metabolic flexibility, AIF-deficient HPAC cells were not sensitized to 2-deoxyglucose treatment. Moreover, minimal or no changes in either growth or glucose metabolism were identified in HPAF-II and MIA PaCa-2 cells as they exhibit a greater dependence on glycolysis that could not be further exacerbated by AIF ablation. Altogether, these experiments demonstrate the essential role of AIF in support of some pancreatic cancer cells by facilitating a metabolic balance, and this metabolic function is most beneficial to cell populations that display a metabolic phenotype not solely reliant on glycolysis for survival.

Open questions and research objectives

Optimizing a 3D cell culture model of PDAC to evaluate AIF-mediated tumorigenesis

Pancreatic ductal adenocarcinoma (PDAC) is one of the most aggressive and lethal diseases, and most PDAC tumors exhibit higher drug resistance ([138],[137]). Therefore, there is an urgent need for new strategies to treat pancreatic cancer and improve therapeutic efficacy and clinical outcomes.

Previous work from our lab has demonstrated that in a 2D cell culture system, AIF supports the growth of metabolically defined pancreatic cancer cell lines, that do not rely entirely on glycolysis for survival ([118]). Still, the underlying mechanism of how AIF promotes growth and whether AIF holds relevance to pancreatic cancer in a more complex environment, such as a 3D cell culture system, needs further investigation. 2D cultures do not necessarily reflect the complex microenvironment cells encounter in cancer. One of the physiological limitations of 2D cultures is the lack of interconnections between cells and the extracellular matrix, which contributes to drug resistance ([45]). Also, an additional publication from our lab has assessed the role of AIF in promoting the EMT pathway in PC3, prostate cancer. However, the assessment was limited to only one type of cancer and was conducted in a conventional 2D cell culture system. Therefore, it is imperative to include more types of cancer cells and perform it in a 3D cell culture system that closely mimics the tumor microenvironment.

Expanding studies of AIF metabolic activity to breast cancer

Urbano *et al*. demonstrated that AIF promotes increased chemoresistance in colon cancer, suggesting that AIF represents a novel drug target ([124]). Our lab demonstrated that AIF supports the growth and survival of advanced prostate cancer (androgen-irresponsive). Also, in pancreatic cancer, the selectivity of AIF dependence in tumorigenesis is more critical as cells become aggressive, requiring a crucial balance between mitochondrial energy metabolism and glycolysis.

Altogether, AIF expression and metabolic contribution increases with disease progression and are associated with the aggressive phenotype. Is the pro-tumor function limited to cancer progression in the prostate, pancreatic and colorectal cancer? Consequently, we want to expand the pro-survival activity in additional cancer cells such as breast cancer. Breast cancer is a heterogeneous disease driven by genetic, epigenetic, and metabolic phenotypes ([135]).

Breast cancer is one of the most common malignancies among women worldwide. Breast cancer can be classified into different subtypes depending upon several clinical biomarkers, such as estrogen (ER) and progesterone (PR) receptors and the human epidermal growth factor receptor 2 (HER2) gene amplification ([3]). Triple-negative breast cancer (TNBC) accounts for about 15% of all breast cancers and is considered the most aggressive. TNBC is characterized by a lack of ER, PR, and HER2 receptors and is regarded as aggressive as they are unresponsive to endocrine therapy and HER2-targeted treatment. Also, one of the molecular features of TNBC is metabolic reprogramming. TNBCs reprogram their metabolic phenotype and that of stromal cells in the microenvironment to survive under nutrient-deprived conditions ([136]). Hence, it can be hypothesized that AIF in breast cancer might be well-positioned to influence aggressive breast cancer that critically rely on metabolic reprogramming for growth and survival. Therefore, AIF might contribute to metabolic vulnerabilities and thus could be implicated as a potential therapeutic target.

Summary of research

The present study explores the role of AIF in cellular energetics and metastasis in a more complex environment than observed in 2D monolayer, such as a 3D cell culture system. Analyses of 3D pancreatic cancer cell lines implicated AIF's role in their growth and metabolism. AIF was revealed to promote metastatic events known as the cadherin switching in a 3D model of pancreatic cancer. This was in contrast to our previous studies where AIF influencing metastasis was limited

to a 2D model of PC3, thus indicating that 3D is a better model to study AIF-mediated cadherin switching due to the presence of stronger cell-to-cell interactions in the 3D cell culture system. Studies conducted in breast cancer cell lines of clinically and metabolically diverse phenotypes revealed that AIF supports the growth and survival in triple-negative breast cancer cell lines. The critical role of AIF in regulating mitochondrial biogenesis might be restricted to triple-negative breast cancer and has been undocumented in other cancer cell lines examined so far. The metabolic function of AIF highlights the ability of AIF to alter the consumption of biochemical substrates other than glucose, thus deregulating cellular metabolism to produce energy required for growth, and survival in triple-negative breast cancer cell lines. Finally, AIF activity can be maximally exploited in aggressive breast cancer as it switches from metabolic plasticity to metabolic dependencies and provides a framework for AIF-mediated therapies.

II. 3D CELL CULTURE REVEALS THE ROLE OF AIF AS A DRIVER OF EMT IN PDAC TUMORIGENESIS

Abstract

Apoptosis-inducing factor (AIF) is a flavoprotein that resides in the intermembrane space of mitochondria. Contrary to its death activity, AIF functions as a survival factor via NADH oxidoreductase activity *in vitro*. Our previous publications demonstrated how AIF supports the growth of metabolically defined pancreatic cancer and advanced prostate cancer cell lines. These studies showed that AIF-deficient cancer cells display increased sensitivity to metabolic-mediated cell death, further suggesting that targeting AIF is a novel approach in cancer therapy. Recently, three-dimensional (3D) cell cultures have gained popularity due to their complex tissue architecture closely mimicking the *in vivo* cancer environment, thus making these culture systems better models for drug screening. In our current studies, we used 3D tumor spheroids of PDAC to investigate the role of AIF in promoting cancer progression and metastasis. A modified hanging drop technique was employed to generate cohesive, compact, robust, and manageable 3D spheroids of AIF-deficient PDAC cells. AIF-deficient 3D spheroids of PDACs were smaller than the control spheroids. Also, the size of 3D spheroids was greater than 400μm in diameter size, suggesting the presence of hypoxia core as observed in *in-vivo* tumors. We observed that the protein expression of examined EMT markers such as E-cadherin and N-cadherin was more evident in the 3D arrangement than in the 2D monolayer, suggesting a stronger cell adhesion in the 3D model. Also, the AIF-deficient 3D PDAC cells displayed increased expression of E-cadherin and reduced expression of N- cadherin, which inversely might affect the tumor cells' motility and impede invasion to distant sites. The present study also highlights the metabolic significance of AIF by demonstrating an increased sensitivity of AIF-deficient 3D spheroids to 2-

deoxyglucose. Future work will define how cadherin switching driven by AIF expression affects intracellular signal transduction cascades.

Introduction

Pancreatic ductal adenocarcinoma (PDAC) is projected to be the second most frequent cause of cancer-related deaths worldwide by 2040, with a 5-year overall survival of less than 10%, due to the high incidence of recurrence and metastasis ([140]). The current challenges in treating pancreatic cancer arise due to difficulties in detecting at an early stage, increased metastatic potential to distinct sites, and poor prognosis ([137]). Unfortunately, most PDAC patients die after cancer has metastasized to other body parts; this emphasizes the urgent need to develop novel therapeutics that target not just the primary tumor but also the biological vulnerabilities of metastatic PDAC cells.

"Epithelial-to-mesenchymal transition" (EMT) plays a pivotal role in PDAC tumorigenesis and is characterized by the loss of epithelial features, including their cell polarity and cell-cell adhesion, to become the mesenchymal cells that have enhanced migratory capacity, invasiveness, elevated resistance to apoptosis, and significantly increased production of ECM components ([141],[56]). A key event of EMT is the cadherin switch, whereby cells reduce the expression of the tumor suppressor E-cadherin and elevate N-cadherin, rendering tumor cells invasive and able to metastasize distant organs ([54]). The graded loss of E-cadherin correlates with the aggressiveness of numerous carcinomas, whereas the forced expression of E-cadherin suppresses tumor development in various *in vitro* and *in vivo* experimental tumor models ([55]).

Previous work has demonstrated the significance of apoptosis-inducing factor (AIF) in promoting the cadherin switch in PC3, a prostate cancer cell line ([127]). AIF is a mitochondrial oxidoreductase that contributes to caspase-independent cell death but also possesses an intrinsic

NADH-oxidase activity that was demonstrated to be critical to the growth and survival of pancreatic ([118]), prostate ([127],[117]), and colorectal ([115]) cancers. The ability of AIF to act as a redox-signaling molecule and control the JNK1-mediated cadherin switch in PC3 was indeed a novel finding ([127]). However, the assessment was limited to only one type of cancer and was conducted in a conventional 2D cell culture system.

2D monolayer cell cultures grown on glass or plastic substrates are often not representative of the *in vivo* cellular environment, and sometimes signaling pathways such as Wnt or Notch are regulated differently in polarized structures ([56],[142]). 3D spheroid formation is one of the best-characterized models to reflect the *in vivo* behavior of cells in tumor tissues as they display nutrient and oxygen gradients, complex cell–cell and cell–extracellular matrix (ECM) contact interactions ([142],[44],[143]). The growth of 3D spheroids was obtained by a modified hanging drop method utilizing methylcellulose, as described ([144]). Methylcellulose is a good thickening agent, cell-impermeable, non-ionic, non-toxic, and protects suspended cells from shear stress ([145],[146]).

The present study aimed to generate and characterize homogenous 3D spheroids of AIF-deficient/proficient PDACs and to investigate the role of AIF in cadherin switch in PANC1 and HPAC cell lines grown as 3D spheroids. Our goal was to employ 3D spheroids to bridge the gap between traditional two-dimensional cell culture and animal models. Here, we not only explored the ability of AIF to induce a cadherin switch in a 3D cell culture system but also revealed a metabolic function of AIF in a 3D model that might pave a new pathway to AIF-mediated therapy.

Materials and methods

Materials

DMEM, DMEM/F-12, GlutaMax, insulin, transferrin, epidermal growth factor, trypsin, 4-12% bis-tris polyacrylamide gels, nitrocellulose membranes, fetal bovine serum (FBS), phosphate

buffer saline (PBS), and Pierce ECL 2 Western blotting substrate were from Thermo-Fisher Scientific; protease inhibitor tablets were from Roche Applied Science; all other materials were from Sigma. Antibodies were obtained as follows: anti-AIF (Santa Cruz Biotechnology, sc-13116); anti-E-cadherin (Cell Signaling**,** 4065); anti-N-Cadherin (Cell Signaling, 4061); anti-Vimentin (Cell Signaling, 5741); anti-Snail (Cell Signaling, 3879) and anti-β-actin (Sigma, A5316).

Cell culture

Cells were cultured in an atmosphere of 95% air and 5% CO2 at 37°C. All media formulations were supplemented with 2mM GlutaMAX. HEK293T and PANC-1 cells were cultured in DMEM supplemented with 10% FBS and HPAC cells in a 1:1 mixture of DMEM and Ham's F-12 medium were supplemented with 5% FBS, 2µg/ml insulin, 5µg/ml transferrin, 40ng/ml hydrocortisone, and 10ng/ml EGF.

NOTE: Cell cultures were not used for more than 90 days after thawing of stock cultures.

Plasmids

Lentiviral plasmids FG12-shLacZ-puro and FG12-shAIF-puro have been assessed and used as described ([127],[118],[117]). The 64-bp oligonucleotide containing the LacZ and AIF targeting sequence were sequenced. FG12-shAIF-puro, a lentiviral plasmid for RNA suppression (RNAi) of AIF that contains the targeting sequence GATCCTGAGCTGCCGTACA, was generated as described ([147]). Lentiviral packaging plasmids pRRE, pRSV-rev, and pHCMV-G are as described ([148]).

Lentiviral pLKO.1 plasmids were obtained as follows: psPAX2 and pMD2.G-vsv-G from Dr. Didier Trono (Addgene plasmids 12260 and 12259); pLKO.1–puro-scramble ([149]) from Dr. David Sabatini (Addgene plasmid 1864); pLKO.1–puro-shE-cadherin ([150]) from Dr. Robert

Weinberg (Addgene plasmid 18801). All shRNA sequences have been rigorously assessed for off-target effects and used as described previously ([127],[118],[117],[148],[149],[150]).

Lentiviral production and stable infection of cell lines

To establish cell lines stably suppressing AIF, RNAi plasmids and equal amounts of lentiviral packaging plasmids were transfected into HEK293T cells using the calcium phosphate precipitation method ([147]). Virus containing supernatants of transfected HEK293T cultures were then collected and filtered through 0.45-μm PVDF Millex-HV filters (Millipore), and concentrated by centrifugation at 20,000 × g for 90 min at 4°C. Viral pellets were resuspended in PBS and then incubated overnight at 4°C prior to use. Cell lines were then infected as described ([117]). PANC-1 and HPAC cells were infected with lentiviruses carrying shLacZ-puro or shAIF-puro and then selected using 2 μg/mL puromycin.

For the establishment of cell lines stably suppressing E-cadherin, pLKO.1-based lentiviruses were generated by transfecting HEK293T cells with pMD.2, psPAX2, and pLKO.1 shRNA using the calcium phosphate method. Viral supernatant was collected at 72 h post-transfection and then filtered using 0.45-μm pore size Millex HV PVDF filter units. Target cells were incubated with viral supernatant and 8 μg/ml Polybrene for 24h. Stably infected cells were selected using 2 μg/ml puromycin.

NOTE: After establishing and verifying the stable cell lines, cells were frozen in multiple vials. Cells were not used more than 90 days after the thawing of stock cultures.

Formation of 3D spheroids by hanging-drop method

For spheroid formation media, cell media specific to the cell line was supplemented with a 20% methylcellulose stock solution. For the preparation of methylcellulose stock solution: 6 g of autoclaved methylcellulose powder (Sigma, M0512) was dissolved in preheated 250 mL basal

medium (60°C) for 20 min. Thereafter, 250 mL of medium (room temperature) containing supplements specific to the cell line and double the amount of FBS was added to a final volume of 500 mL, and the whole solution was mixed overnight at 4°C. The final stock solution was aliquoted and cleared by centrifugation (4000 rpm for 90 minutes at room temperature). Only the clear, highly viscous supernatant was used for the spheroid formation, which was approximately 90–95% of the stock solution ([144]). We used 20% of the stock solution and 80% culture medium for a spheroid generation, corresponding to the final 0.24% methylcellulose. Twenty microliters drop of the 0.24% methylcellulose-culture medium solution containing 20,000 cells were pipetted onto the lid of 100 mm dishes and were inverted over dishes containing 10 mL phosphate buffer solution as a humidity source. Hanging drop cultures were incubated under standard culture conditions (5% CO_2, at 37°C) for 7 days, and the images were captured by phase contrast microscopy using the 4× objective of a Nikon TS100F microscope equipped with a Nikon DS-Fi1 digital camera detection system and NIS elements 4.0 software and analyzed by ImageJ software ([151]).

Formation of 3D spheroids by liquid overlay method

Each well of a 96-well plate was coated with 100µl of 1% agarose and was left to dry for 20-30 minutes in laminar hood. After drying, 100µl of media containing 20,000 cells was seeded and incubated at (5% CO_2, at 37°C) for 7 days.

Cell lysis and Immunoblot analysis

For 2D cell lysates, cells were harvested by trypsinization, washed, and resuspended in radioimmune precipitation assay lysis buffer (PBS containing 1% Nonidet P-40, 0.5% sodium deoxycholate, 0.2 % sodium dodecyl sulfate, 1 mM dithiothreitol, 1 mM phenylmethanesulfonyl fluoride, and 1 protease inhibitor mixture tablet per 10 mL). For 3D cell lysates, fifty spheroids

were suspended in 2ml of media and centrifuged at 400rpm for 5 mins; the resultant pellet was washed and resuspended in Laemmli buffer (62.5 mM Tris-HCl, pH 6.8, 2% SDS, 10% glycerol, and 5% β-mercaptoethanol), followed by sonication. Lysates obtained from 2D, and 3D cells were then normalized for protein content using Bradford. 30 ug protein sample were loaded on 4-12% gradient SDS-polyacrylamide followed by electrotansfer to nitrocellulose membranes. Membranes were blocked with 5% milk or BSA in TBS containing 0.1% Tween 20 and then incubated with the indicated primary antibodies. Membranes were washed three times and incubated with HRP-conjugated anti-mouse or anti-rabbit, followed by visualization using enhanced chemiluminescence with a MyECL imaging system (Thermo Scientific).

Viability assay

The 3D spheroids were grown by hanging-drop method in a 100mm dish for 6 days. Spheroids were removed and placed separately in single wells of a 96-well opaque culture plate (BD falcon, 353948). Cell Titer-Glo® 3D reagent was added to each well and the luminescence signal was read after 30 minutes with the Agilent BioTek Gen 5 microplate reader.

Glucose consumption measurements

The 3D spheroids were grown on 1% Agarose overlay in a 96-well plate for 6 days. After 6 days, 3D spheroids were collected for glucose consumption assay. Each spheroid was harvested and disrupted using trypsin. 0.4% Trypan blue solution (Sigma, Milan, Italy) was used to stain the dead cells. Viable cells were then counted manually with a hemocytometer. Media was collected from each well, and total glucose was measured using the QuantiChrom^{TM} Glucose Assay Kit (BioAssay Systems). In order to assess glucose consumed per cell, total glucose consumption per sample was divided by its corresponding cell count. Fold change in glucose consumption was determined by dividing populations of AIF-deficient cells by corresponding control populations.

Scratch assay

The cells were harvested by trypsinization, washed, resuspended in fresh media, and seeded in replicate 35mm dishes. The cells were incubated for 12–36 h, and a single scratch was made through the middle of each well using a p-200 pipette tip (*[152]*). Cells were immediately washed, fresh media was added, and each scratch was imaged. Cells were then incubated for 24–48 h before the final assessment of scratch width. All images were captured by phase contrast microscopy using the 10× objective of a Nikon TS100F microscope equipped with a Nikon DS-Fi1 digital camera detection system and NIS Elements 4.0 software.

Drug treatment

The 3D spheroids were grown using the hanging drop method for 72 h. After 72 h, spheroids were left untreated or treated with 200 mM 2-deoxyglucose and were observed for additional 7 days. The untreated and treated spheroids were transferred to a glass slide using a p-200 pipette tip to evaluate their robustness or integrity. They were imaged using phase contrast microscopy using the 4× objective of a Nikon TS100F microscope equipped with a Nikon DS-Fi1 digital camera detection system and NIS Elements 4.0 software.

Statistics

Statistical analyses were performed using two-tailed, Student's t tests for unpaired samples A minimum of three independent biological replicates (unless otherwise stated) were assessed for all experiments. Statistical significance is represented as: $^{*}P < 0.05$; $^{**}P < 0.01$; $^{***}P < 0.001$.

Results

Generation of 3D pancreatic cancer cell cultures

We have previously shown that AIF mediates the cadherin switch in 2D-monolayer cultures of PC3 cancer cells, an androgen-independent line of prostate cancer cells commonly used

as a model for advanced prostate cancer ([127],[153]). However, that study was limited to PC3 cells and could not be replicated in other monolayer cultures of various cancer types. Thus, to assess whether the AIF-mediated cadherin switch mechanism translates in different cancer cells, we used a 3D cell culture model. As *in vitro*, 3D cell culture mimics better cell-cell and cell-matrix interactions of tumor microenvironment compared to monolayer; thus, spheroids were regarded as the potential model to study cadherin-mediated cell signaling ([144],[143],[154],[155]). To determine whether cadherin-associated cell signaling is AIF-dependent, we suppressed AIF in PANC1 and HPAC cells using the lentiviral RNAi approach, as described ([118],[147],[148]). Figure 2.1 shows the stable suppression of AIF was successful and was assessed by immunoblot analysis.

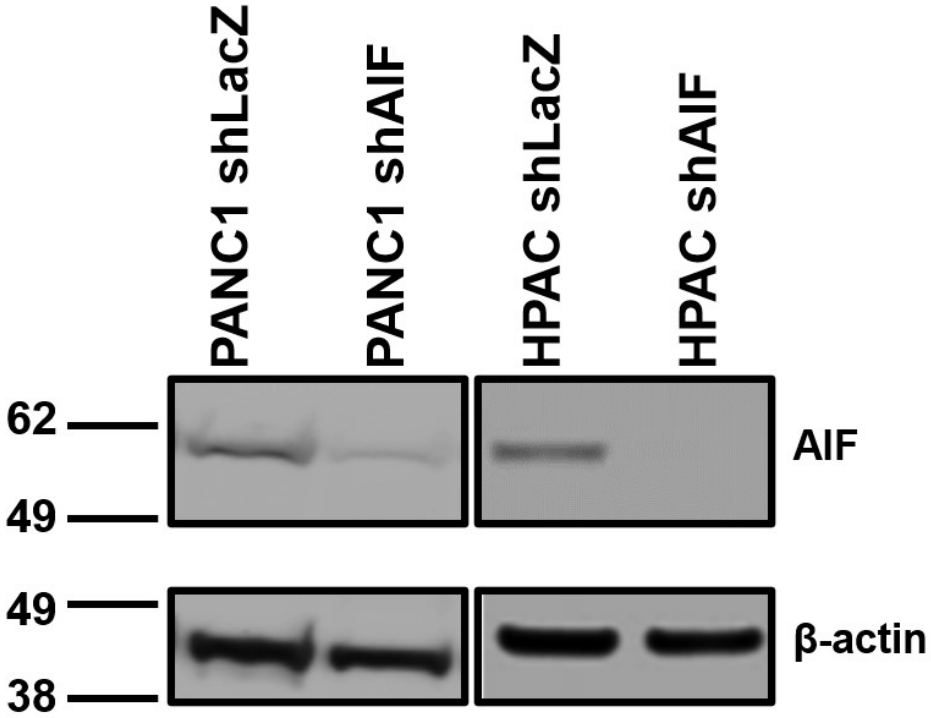

Figure 2.1: Establishment of AIF-deficient pancreatic cancer cell lines.
PANC1 and HPAC were stably infected with shRNA hairpins targeting LacZ or AIF with Puromycin as a selectable marker via lentiviral delivery. Immunoblot was performed to verify the suppression of AIF protein expression. Representative blot image is shown and actin was used as the loading control Actin was used as the loading control.

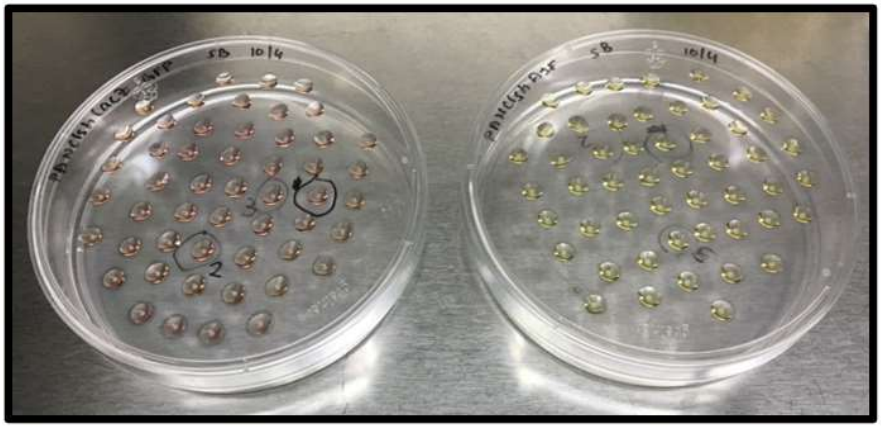

Figure 2.2: Generation of 3D spheroids using modified hanging drop method.
Representative image of AIF-deficient/proficient PDAC (PANC1 and HPAC) grown as 3D spheroids by hanging drop method using methylcellulose as an additive.

To delineate the role of AIF in regulating any morphological difference in spheroid formation in PDAC cells, spheroids were grown by the hanging drop method. Previously it was reported that pancreatic cancer cells are weak in self-aggregating to form spheroids using conventional approaches such as traditional hanging drop or liquid overlay methods ([144],[156]); therefore, a modified hanging drop method was employed by adding methylcellulose to the hanging drop ([156]). Spheroids were grown in media containing 0.24% methylcellulose and were imaged at different time points using phase contrast microscopy. The spheroids of PANC1 were circular, but in the case of HPAC, only a few spheroids were circular (4 out of 50 spheroids), while the rest were irregular in shape. The diameter of AIF-proficient PANC1 spheroids was larger than that of AIF-deficient PANC1 spheroids as shown in Figure 2.3A, and their diameter was measured using ImageJ software (https://imagej.nih.gov). The diameter of the AIF-deficient PANC1 spheroids was significantly less than the AIF-proficient PANC1 as shown in Figure 2.3B. The size of the 3D-spheroids was approximately in a range of 500-1600 μm.

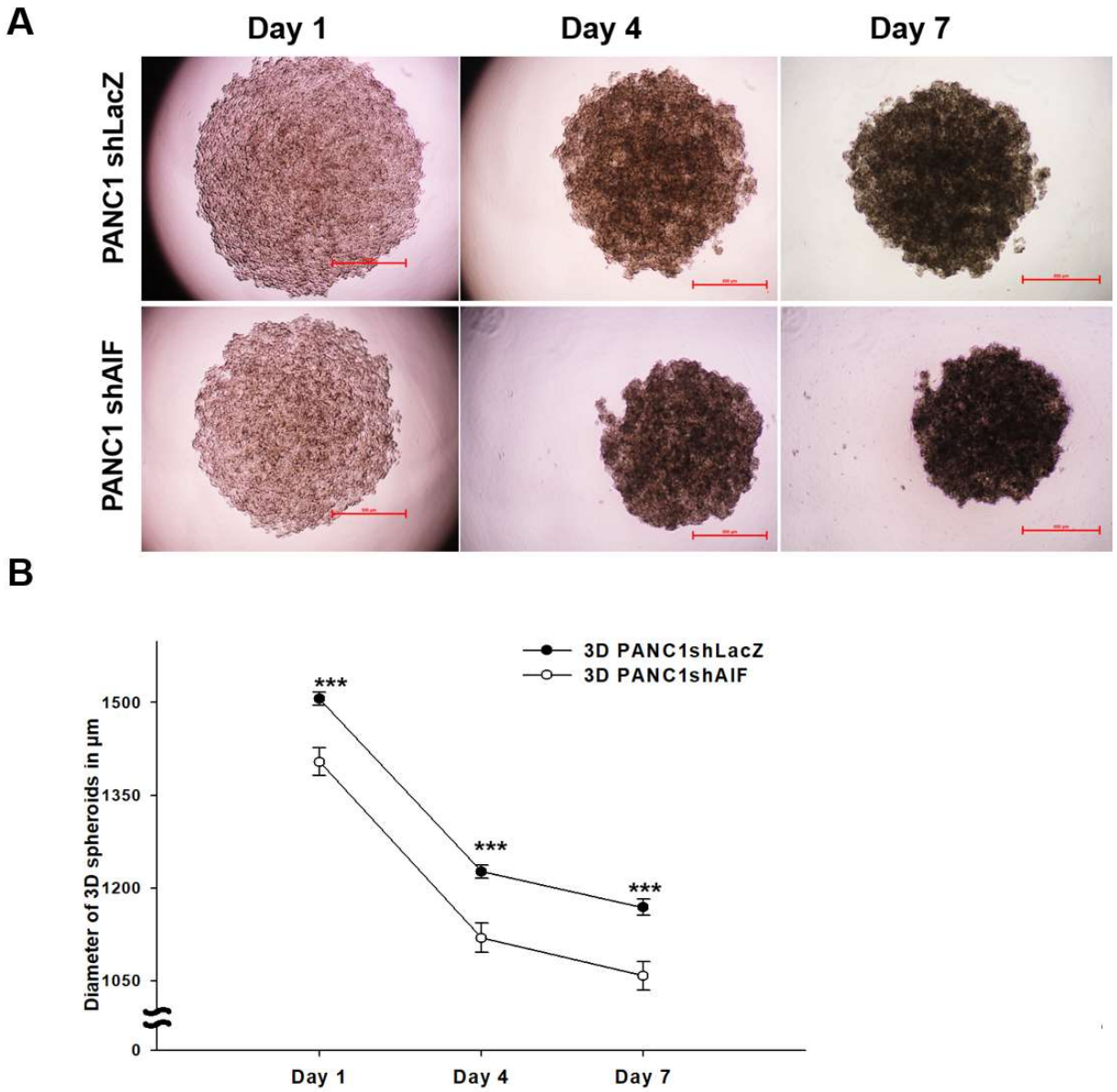

Figure 2.3: Effect of AIF ablation on the 3D PANC1s spheroid formation.
Spheroids of AIF deficient/proficient PANC1 were grown in hanging drop seeded with 20,000 cells per 20 µL drop and cultivated in DMEM and 0.24% methylcellulose at 37°C. All images were captured by phase contrast microscopy using the 4× objective of a Nikon TS100F microscope equipped with a Nikon DS-Fi1 digital camera detection system and NIS Elements 4.0 software. Images were analyzed using the open-source software ImageJ (Panel A). Diameter and all shape parameters were classified according to the image analysis function of ImageJ. Data are shown as average ± s.e.m (Panel B) The statistical significance was determined by Student's t-test. (*, $p < 0.05$; **, $p < 0.01$; ***, $p < 0.001$; ns, $p > 0.05$) N=20. Scale bar: 500µm

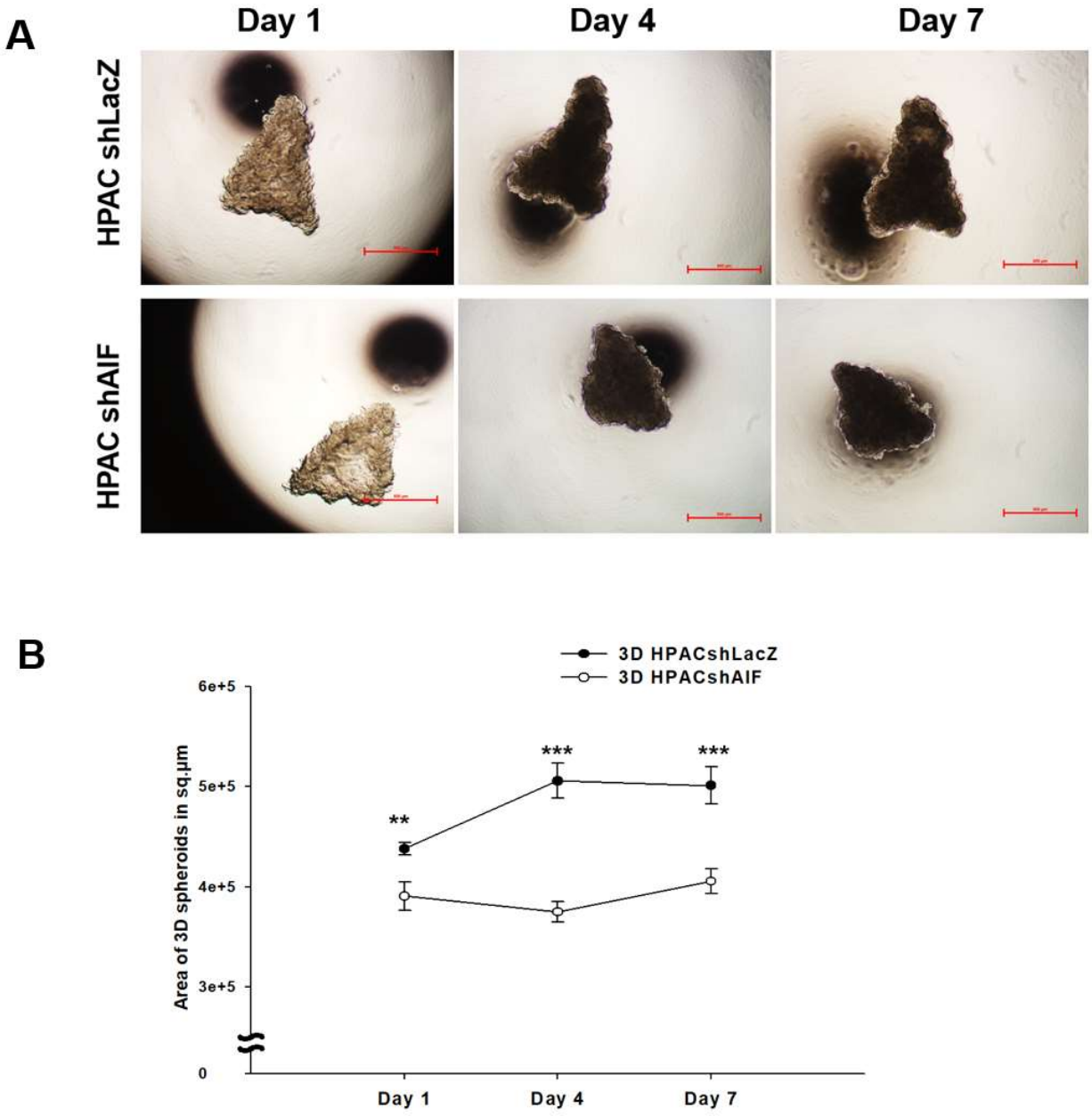

Figure 2.4: Effect of AIF ablation on the 3D HPACs spheroid formation.
Spheroids of AIF deficient/proficient HPAC were grown in hanging drop seeded with 20,000 cells per 20 µL drop and cultivated in DMEM/F-12 and 0.24% methylcellulose at 37°C. All images were captured by phase contrast microscopy using the 4× objective of a Nikon TS100F microscope equipped with a Nikon DS-Fi1 digital camera detection system and NIS Elements 4.0 software. Images were analyzed using the open-source software ImageJ (Panel A). Diameter and surface area parameters were classified according to the image analysis function of ImageJ. Data are shown as average ± s.e.m (Panel B). The statistical significance was determined by Student's t-test. (*, $p < 0.05$; **, $p < 0.01$; ***, $p < 0.001$; ns, $p > 0.05$) N=20. Scale bar: 500µm

Interestingly, there were no evident differences in the size of both AIF-proficient/deficient PANC1 spheroids after 7 days. As 3D spheroids of HPACs possess irregularity, the surface area was selected as a parameter to characterize the spheroids instead of diameter. The assessment was done by Image J software. The surface area of AIF-deficient HPACs was less than its control cells as shown in Figure 2.4B. However, the growth of AIF-proficient/deficient PDAC 3D spheroids plateaued after 7 days. The data after 7 days not shown.

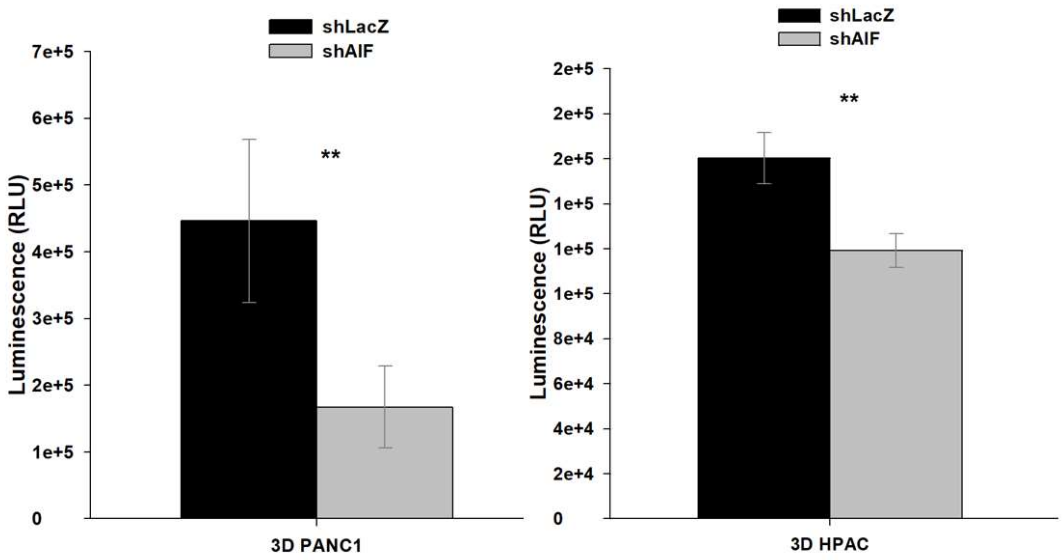

Figure 2.5: Viability assay using ATP based cell viability kit method.
3D spheroids were grown for 6 days and were treated with Cell Titer-Glo 3D reagent, shaken for 5 minutes to mix the contents and luminescence was recorded 30 minutes after reagent addition. It is a homogeneous method to determine the number of viable cells in 3D cell culture based on quantitation of the ATP present, which is a marker for the presence of metabolically active cells. Data are presented as average ± standard deviation. The statistical significance was determined by Student's t-test. (*, $p < 0.05$; **, $p < 0.01$; ***, $p < 0.001$; ns, $p > 0.05$) N=4

Next, an ATP viability assay was conducted using Cell Titer-Glo® 3D Cell Viability Assay to determine if the viability of 3D spheroids was affected when AIF was ablated. The spheroids were grown in hanging drop for 6 days, and then an equal number of spheroids were collected in 96-well plates and mixed with equal volume of Cell Titer-Glo® 3D Reagent; the plate luminescence was measured by Agilent BioTek Gen 5 microplate reader and recorded. Figure 2.5

shows luminescence intensity (in relative intensity units) for PANC1 and HPAC cells, it can be observed that the AIF-deficient PDAC demonstrated lower viability (lower luminescence) than the control PDAC cells (higher luminescence) which was statistically significant. This implies that AIF supports the growth and affects the size and surface area of PDACs under a 3D environment.

AIF regulates cadherin switching in 3D PDAC

The 3D AIF-deficient PDAC cells were less viable than AIF-proficient PDACs, suggesting that AIF has a role in controlling the growth of three-dimensional PANC1s and HPACs. PANC1 and HPACs are characterized as being aggressive and invasive ([157],[158]). Literature suggests that the loss of E-cadherin expression and overexpression of N-cadherin, inducers of epithelial-to-mesenchymal transition (EMT), is correlated to the histological grade and invasive phenotype of pancreatic adenocarcinoma tissue ([159]).

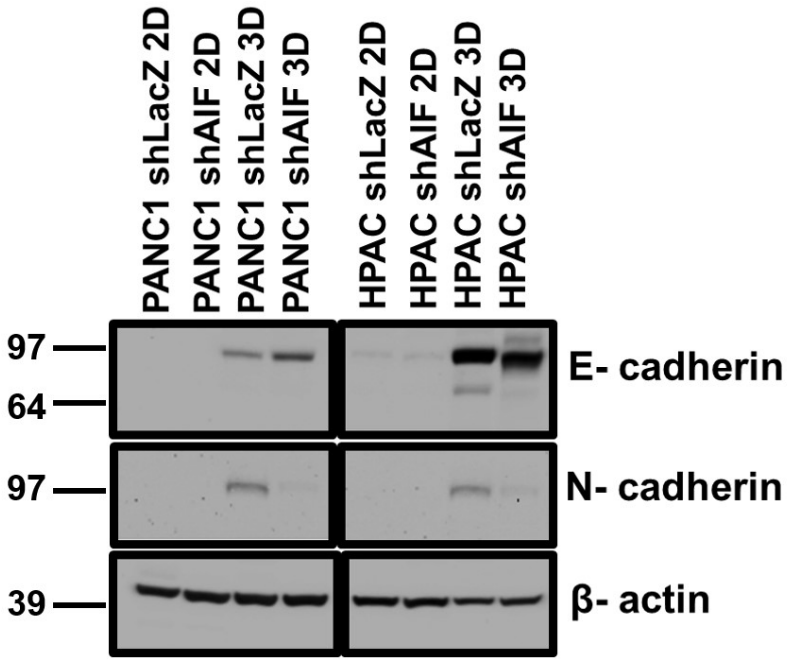

Figure 2.6: AIF suppresses E-cadherin and elevates N-cadherin in 3D PDAC.
AIF-proficient/deficient pancreatic cancer cells were grown as 2D monolayer and 3D spheroids and were lysed and probed with the indicated antibodies by immunoblot analysis. Representative blot image is shown and actin was used as the loading control.

EMT is a highly dynamic process in which epithelial cells convert into a mesenchymal phenotype and plays a fundamental role during the early steps of invasion and metastasis of carcinomas ([160],[131]). Therefore, we sought to evaluate the role of AIF in EMT.

In our previous studies, the ability of AIF to promote the cadherin switch was only observed in monolayer prostate cancer cell line (PC3), and cadherin expression were observed in PDAC cells when grown in 2D ([127]). In the search for an EMT profile, there is increasing evidence that 3D spheroids are superior to a 2D monolayer; therefore, we changed our model from a 2D monolayer to a 3D spheroid to study the cadherin switch ([161],[56]). When 2D monolayer cultures are compared with 3D spheroids, 3D spheroids mimic *in vivo* tumor microenvironments more accurately, such as their spatial architecture, cell morphology, and cell-cell interactions, and the process of EMT involves changes in cell-cell adhesion or cell-matrix adhesion, proving 3D spheroids as a better alternative ([143],[42]). To determine whether AIF is responsible for a cadherin switch in PDAC cells, we grew AIF-deficient PDAC in the hanging drop method for 7 days to generate 3D spheroids and then were harvested, and their lysates were probed for E-cadherin and N-cadherin. Figure 2.6 shows that the examined EMT markers were undetectable in 2D cells, but PANC1s exhibited a cadherin switch by expressing high levels of E-cadherin and low levels of N-cadherin after AIF knockdown, thus suggesting that AIF is required for cadherin switch in PANC1s when grown in 3D. However, in 3D HPACs, the E-cadherin protein expression was modestly affected, but the N-cadherin protein expression was suppressed when AIF was ablated. This behavior of HPAC may reflect its metabolic flexibility derived from its lipogenic phenotype and is consistent with our previous observations that HPAC only partially relies on AIF or mitochondria for survival and growth and therefore HPAC cells are moderately sensitized to AIF ablation ([162]).

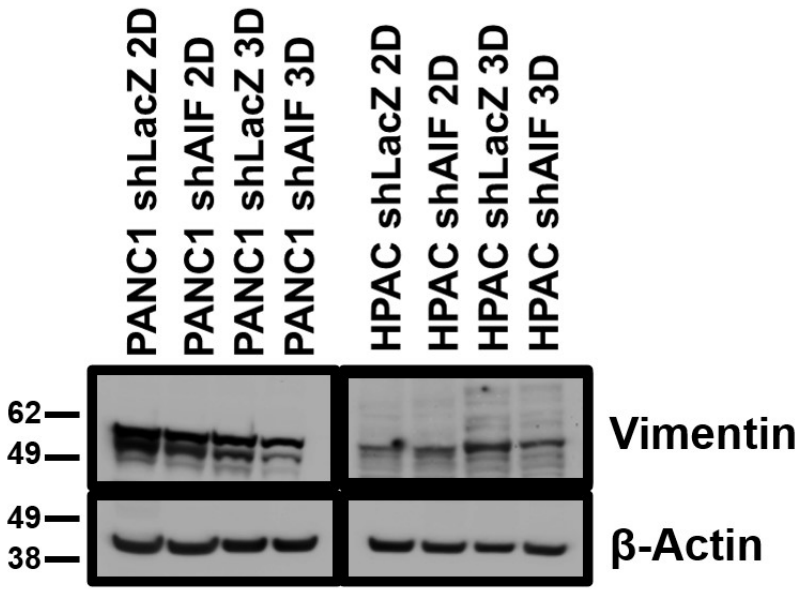

Figure 2.7: AIF alters the protein expression of Vimentin in 3D PDAC.
AIF-proficient/deficient pancreatic cancer cells were grown as 2D monolayer and 3D spheroids and were lysed and probed with the indicated antibodies by immunoblot analysis. Representative blot image is shown and actin was used as the loading control Actin was used as the loading control.

Figure 2.7 shows a concomitant downregulation of Vimentin, a mesenchymal marker, in AIF-ablated PDAC cells thus supporting the hypothesis that PDACs cells require AIF for cadherin switching and 3D spheroids are better models to study EMT as most EMT markers are undetected in 2D monolayers. Also, different isoforms of Vimentin (57kDa and 49kDa) were observed in PANC1 cells but the expression levels of isoforms were at low levels particularly in HPAC cells.

Metabolic function of AIF in 3D PDACs

Previously we have defined the metabolic role of AIF in 2D pancreatic cancer cells by assessing alteration in glucose consumption ([118]). Increased glucose consumption is associated with AIF ablation due to impairment of the mitochondrial respiratory complex. PANC1 and HPAC cells display a metabolic phenotype that is not solely reliant upon glycolysis, followed by AIF

ablation exhibiting elevated glucose consumption in 2D monolayer. Hence, we performed a glucose consumption assay on PDAC grown as 3D spheroids to assess whether AIF's metabolic function depends on the cell culture system.

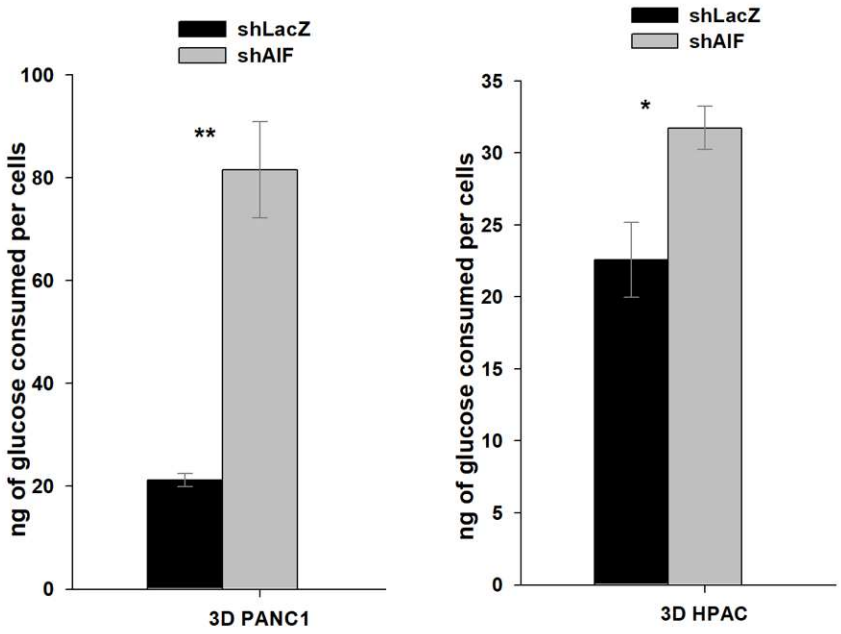

Figure 2.8: Metabolic function of AIF via glucose consumption assay.
The 3D spheroids were grown on 1% Agarose overlay in 96 well plate and after 6 days, glucose consumption assay was carried out using BioAssay systems QuantiChromTM glucose assay kit. The total cell number was assessed using both hemocytometer and ATP-based Cell Titer-Glo 3D kit. Data are shown as average ± standard deviation. *, $p < 0.05$. **, $p < 0.01$. N=3

3D spheroids of AIF-deficient/proficient PDAC were grown by liquid overlay for 6 days. AIF-deficient PANC1s consumed ~4-fold more glucose whereas AIF-deficient HPACs consumed only ~1.5 fold more glucose than their controls when grown in a 3D cell culture system as shown in Figure 2.8. This corroborated the relevance of AIF in glucose metabolism when grown under 3D. Next, to determine the benefit of AIF-mediated glucose metabolism, we inhibited glycolysis with 2-deoxyglucose only in PANC1 (relies on oxidative phosphorylation as a source of energy) and not in HPAC cells.

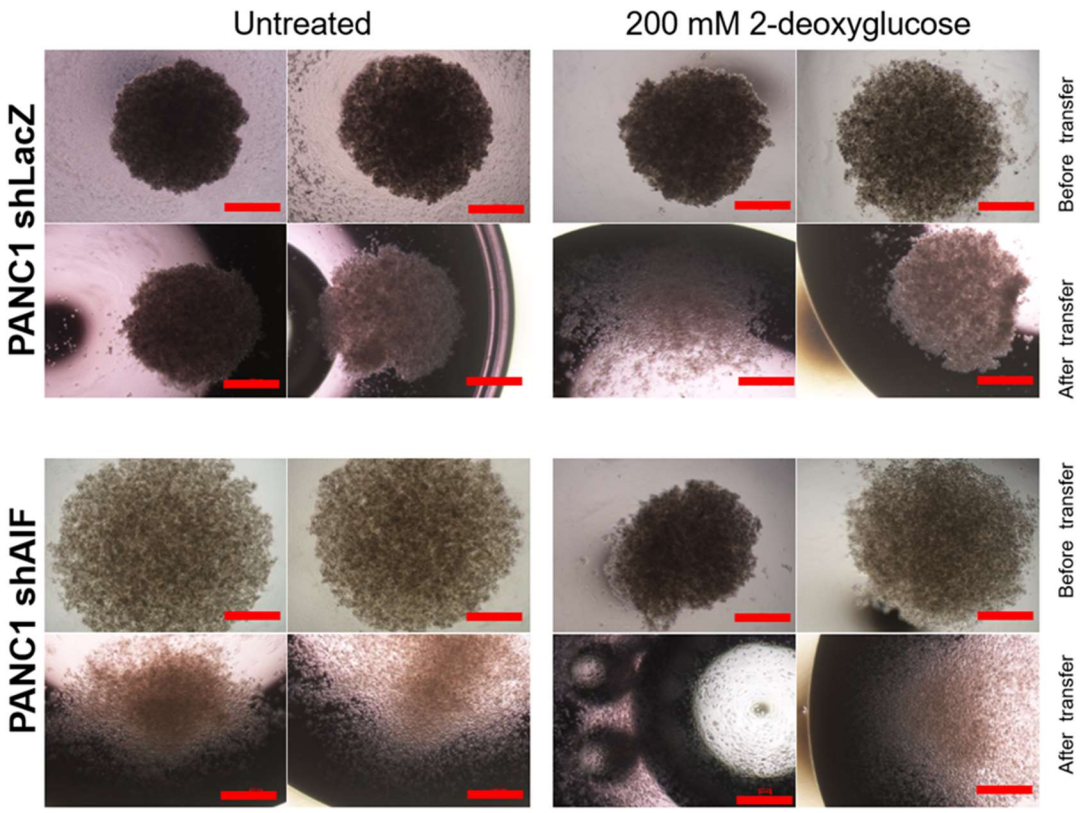

Figure 2.9: AIF ablation sensitizes pancreatic cells to a glycolytic inhibitor.
The 3D spheroids were grown in hanging drops and treated with 200mM 2-deoxyglucose after 72 hours, and then it was observed for additional 7 days. On day 7, the spheroids were transferred on to slide for imaging. All images were captured by phase contrast microscopy using the 4× objective of a Nikon TS100F microscope equipped with a Nikon DS-Fi1 digital camera detection system and NIS Elements 4.0 software. Representative blot images are shown Scale bar = 500µm

In our previous publication, 2D AIF-deficient PANC1 demonstrated increased sensitivity to glycolytic disruption; however, 2D AIF-deficient HPAC consumed modest levels of glucose and were not sensitized to 2-deoxyglucose (glycolysis inhibitor) as HPAC display metabolic flexibility and has the capacity to derive energy from lipid metabolism and thus circumvent the metabolic blockage. Therefore, 3D HPAC cells were not assessed for the sensitivity to 2-deoxyglucose (glycolytic inhibitor).

To assess sensitivity in PANC1s, 3D spheroids were grown by hanging drop for 72 h and then treated with 200 mM 2-deoxyglucose for additional 7 days. On 10^{th} day, the 3D spheroids

were transferred onto the microscopic slide to determine if the 3D spheroids maintain their spherical shape or integrity The robustness of 3D spheroids meant that spheroids avoid disassembly or disintegration after gentle agitation or undergoing several experimental steps. The integrity and robustness of untreated and treated 3D spheroids revealed that AIF-proficient PANC1 cells were capable of maintaining their integrity after 2-deoxyglucose treatment i.e., both the replicates of spheroids were mostly spherical and did not disintegrate completely when they were transferred onto the microscopic slide. However, the spheroids of AIF-deficient PANC1 cells were treated with 2-deoxyglucose, the spheroids disintegrated and failed to maintain their sphericity after they were transferred onto a slide as shown in Figure 2.9. These data and our previous publication support the hypothesis that sensitivity of AIF-deficient PANC1 to glycolytic inhibitors increases as the glycolysis pathway becomes critical due to suppression of AIF.

Suppression of E-cadherin in AIF-deficient cells promotes migration

We observed that AIF ablation leads to overexpression of E-cadherin and how AIF facilitates migration in PANC1 ([118]); therefore, we then explored the effects of reverting E-cadherin in AIF-deficient cells in controlling the aggressiveness of pancreatic tumor cells. To test this concept, PANC1 shLacZ and PANC1 shAIF cells were subjected to a second round of lentiviral infection in which E-cadherin levels were suppressed. Lentiviral vectors, derived from the human immunodeficiency virus, have been extensively used due to their ability to transduce stably and with high efficiency ([163]).

Lentiviruses harboring either control scramble shRNA or shRNA against E-cadherin ([127]) were generated and then used to infect PANC1–shLacZ and PANC1–shAIF cells. And the shRNA sequences were rigorously assessed for off-target effects and used as described previously ([127],[148],[150]).

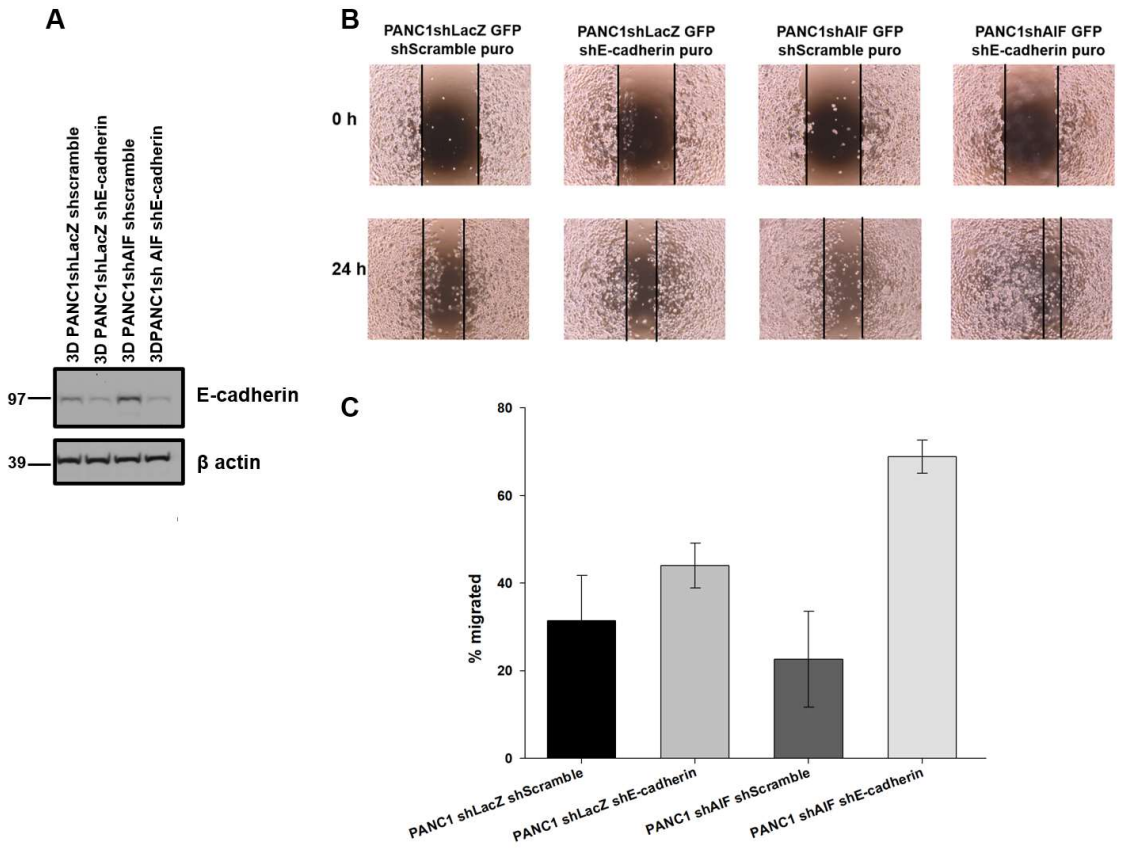

Figure 2.10: Suppression of E-cadherin in AIF-deficient PDACs promotes migration. AIF-deficient/proficient PANC1s were stably infected with lentiviruses harboring either control scramble shRNA or shE-cadherin followed by immunoblot for E-cadherin. Actin was used as the loading control (Panel A). The cells were seeded at 1,000,000 cells/35-mm dish and allowed to attach for 16h. A p-200 pipette tip was used to scratch a region from the center of each plate, the plates were immediately washed, and fresh medium was added. Gap size was then measured as time 0 hr. The cells were incubated for an additional 24 h, and percentage of distance migrated for each cell line was then determined (Panel B-C). All quantitative data are presented as average ± standard deviation. N=4.

Stable knockdown of E-cadherin in AIF-deficient PANC1 cells (PANC1–shAIF/shE-cadherin) and AIF-proficient PANC1 cells (PANC1-shLacZ/shE-cadherin) were generated and verified by immunoblot as shown in Figure 2.10A.

To define the role of E-cadherin in mediating migration in an AIF-dependent manner, the scratch assay was performed. High densities of cells were plated in replicate and allowed to attach for 12–24 h; a scratch was made across the middle of each well with a p-200 pipette tip, the plates

were immediately washed, and fresh medium was added. Gap size was assessed immediately following cell displacement at 0 h and incubated for an additional 12–24 h later, and the width of the closed gap was measured. PANC1-shAIF/shE-cadherin exhibited increased migration compared to cells harboring control scramble shRNA. However, for PANC1-shLacZ/shE-cadherin, E-cadherin is ablated, and suppression of E-cadherin results in elevation of N-cadherin (as observed in EMT) that has migratory properties and thus a modest increase in migration was observed.

Discussion

Several studies have reported the advantages of the 3D tumor spheroids when compared to traditional 2D cultures as they mimic better *in vivo* tumor morphology ([142],[164]). 3D Spheroids display heterogeneity in tumor cell proliferation, metabolic activity, and DNA damage repair (DDR) signaling ([165]). Our long-term objective is to elucidate the cellular signaling mechanisms and metabolic significance of AIF in a 3D culture system that mimics the tumor microenvironment and apply that knowledge to AIF-mediated therapy. A previous publication demonstrated that the suppression of AIF in prostate tumors substantially affected tumor growth *in vivo* ([117]). And the present study assessed the diameter size and surface area of AIF-deficient/proficient 3D pancreatic spheroids. AIF-deficient PDACs were significantly smaller than the AIF-proficient PDACs, thus confirming that AIF directly contributes to the growth of aggressive pancreatic cancer. As shown in Figure 2.3 and 2.4, spheroids displayed a formation pattern: cell sedimentation, an increase in density and compactness, and a plateau phase in growth. The plateau phase during the growth of spheroids after 7 days can be attributed to the degradation of nutrients, growth factors, vitamins, and amino acids and increased osmolarity due to evaporation ([144]). Alternatively, the 3D spheroids could be replenished with fresh media solution after 7 days or the spheroids can be harvested

before the onset of hypoxia or necrosis. The diameter of AIF-deficient/proficient PDAC 3D spheroids was larger than 500 μm, suggesting the presence of a hypoxia center as spheroids exceeding 400 μm in diameter do pack tightly, develop a hypoxic core and activate known survival signaling pathways to maintain cell viability ([166],[167]). The ATP-based viability data suggests that AIF is an essential factor for pancreatic cancer progression in a 3D environment. Altogether, this corroborates using a modified hanging drop to generate 3D spheroids of PDAC to study AIF-mediated signaling. Also, from the Figure 2.2, it can be observed that AIF-deficient PANC1s spheroids turned yellow after 5 days; this can be attributed to the fact that AIF-deficient cells secrete more lactic acid, as observed in 2D prostate cancer ([117]).

Epithelial-mesenchymal transition (EMT) is a biological process by which epithelial cells lose their cell polarity and cell-cell adhesion to become the mesenchymal cell that has enhanced migratory capacity, invasiveness, elevated resistance to apoptosis, and significantly increased production of ECM components ([160]). An early essential event of EMT is the downregulation of E-cadherin, a well-characterized adhesive junction protein expressed in differentiated and polarized epithelial cells. Various *in vitro* and *in vivo* literature revealed that the graded loss of E-cadherin is correlated with the aggressiveness of numerous carcinomas. In contrast, the forced expression of E-cadherin suppresses tumor development ([55]). Other publications have shown that primary tumors of pancreatic cancers display a reduced expression of E-cadherin and an increased expression of N-cadherin, which are significantly related to histological grade and the invasive/undifferentiated phenotype. Figure 2.6 showed protein expression of E-cadherin and N-cadherin in 3D; conversely, the cadherin proteins were undetectable in 2D as 3D-spheroids have stronger cell adhesion. Immunoblot analysis demonstrated a reversal of the cadherin switch by expressing high levels of E-cadherin and low N-cadherin following AIF ablation in both types of

pancreatic cancer. In HPAC, E-cadherin degradation fragments were observed, which can be explained by posttranslational modifications such as ubiquitination ([168]) or glycation ([169]). Figure 2.7 showed a decrease in another mesenchymal marker, Vimentin when AIF was suppressed. Figure 2.11 also reveals an inverse correlation between Snail and E-cadherin at the protein level in PANC1, while protein expression of Slug and Twist (not shown) was undetectable. We have already shown how AIF deficiency in prostate cancer results in a substantially reduced ability to form aggressive tumors *in vivo* in mice. ([117]), and others have shown that overexpression of E-cadherin is inversely proportional to tumor growth ([55]).

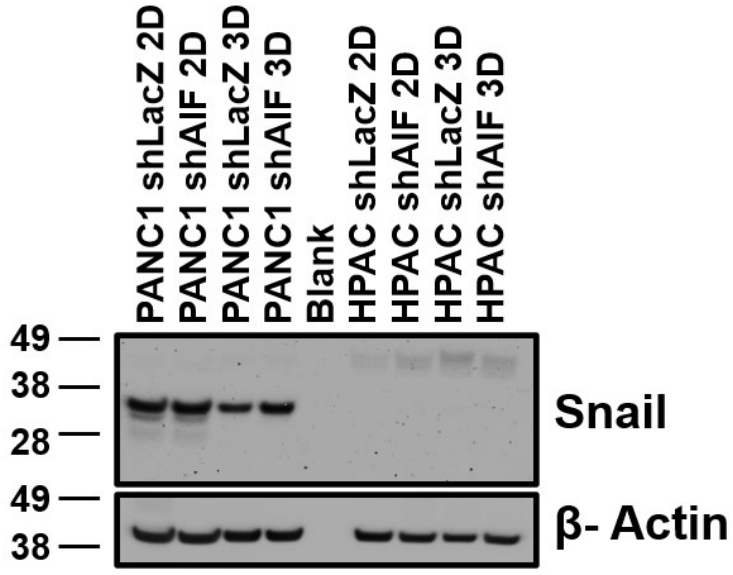

Figure 2.11: AIF alters the protein expression of Snail in 3D PANC1s.
AIF-proficient/deficient pancreatic cancer cells were grown as 2D monolayer and 3D spheroids and were lysed and probed with the indicated antibodies by immunoblot analysis. Representative blot image is shown and actin was used as the loading control

The current study demonstrates a likely axis of suppression of AIF/ upregulation of E-cadherin/downregulation of N-cadherin/ decrease in spheroid size. Thus, AIF is possibly well-positioned to regulate tumor progression via E-cadherin. The contribution of AIF in E-cadherin-

mediated migration, as shown in Figure 2.10, also underscores the emphasis on AIF mediating the aggressiveness of pancreatic cancer. In the previous study, we established a pro-tumorigenic role for AIF in 2D pancreatic cancer derives from its basal metabolic state ([118]). 3D spheroids of PANC-1, and HPAC cells, possess a metabolic phenotype that is not solely reliant upon glycolysis and thus exhibited reduced viability and elevated glucose consumption levels in the range of (~1.5-4-fold) following AIF ablation. Figure 2.9 suggests that AIF-deficient PANC1 was sensitized to glycolytic disruption as AIF-deficient spheroids lost their integrity and robustness after 2-deoxyglucose treatment. The elevated AIF expression is not a universal feature in pancreatic cancer; however, there is a subtype of pancreatic cancer population (~33%) in which AIF is significantly elevated. Nevertheless, the study presented here highlights the metabolic significance of AIF and cadherin switch by AIF to PDAC in a 3D environment and suggests a strong possibility of AIF representing as a novel therapeutic target.

III. RELIANCE ON AIF IN TRIPLE-NEGATIVE BREAST CANCER INCREASES METABOLIC DEPENDENCIES

Abstract

Apoptosis-inducing factor (AIF) is a phylogenetically conserved mitochondrial flavoprotein that induces cell death but also possesses a 'life' function by participating in the assembly of respiratory chain complexes. Early studies on colorectal cancer revealed that an elevation of AIF protects tumor cells from chemotherapy. More recently we demonstrated that advanced prostate cancer cells exhibit reduced growth and survival following AIF ablation. Further studies revealed that AIF-deficient pancreatic cancer cells display increased sensitivity to metabolic and chemical stress-mediated cell death, further suggesting that targeting AIF is a novel approach in cancer therapy. Presently, AIF's role as a tumor promotor in breast cancer is undefined. Breast cancer is the second most common cancer in women, and new target molecules for developing advanced therapeutics are sorely needed. The implication of the potential role of AIF in subsets of breast cancer specimens was revealed by a modest elevation of AIF transcript levels using the Oncomine database. Knockdown of AIF in breast cancer cell lines such as MDA-MB-231 and MDA-MB-468 resulted in changes in growth rate, alteration in glucose consumption, and decreased expression of mitochondrial complex I subunits changes that were not observed in MCF-7, a non-invasive breast cancer cell line. These data suggests that the activity of AIF in support of breast cancer cells is restricted to triple-negative breast cancer cells that have achieved a more aggressive state. AIF ablation dissipated the mitochondrial electrochemical gradient and decreased mitochondrial abundance in AIF-deficient MDA-MB-231 and MDA-MB-468, undocumented in other cancer types tested so far. Moreover, suppression of AIF in MDA-MB-231 and MDA-MB-468 results in modulation in consumption of glycolytic substrates and TCA cycle substrates in

favor of tumor cell growth but not in MCF-7. Altogether these data provide a promising framework for AIF-mediated therapy by indicating that AIF can be exploited to initiate a metabolic switch that can be manipulated to limit substrate flexibility in triple-negative breast cancer cells.

Introduction

The Warburg effect is a hallmark of cancer cells that refers to the preference of cancer cells to rely on glycolysis regardless of the availability of oxygen, and hence this metabolism is often referred to as "aerobic glycolysis." Warburg initially hypothesized that dysfunctional mitochondria are the root of aerobic glycolysis in cancer cells. ([101],[100]). However, increasing evidence shows that cancer cells generate the most energy through mitochondrial functions despite their high glycolytic rates, suggesting that targeting both aerobic glycolysis and mitochondrial metabolism may be required ([102],[170]). Mitochondria are not only "life-essential" organelles for providing cellular energy via the electron transport chain (ETC) and oxidative phosphorylation (OXPHOS), but they also play a critical role in activating apoptosis.

Apoptosis-inducing factor (AIF) is a mitochondrial flavoprotein initially identified for its role in caspase-independent cell death. However, the pro-death function of AIF is limited to a narrow range of cell types, primarily neurons and cardiomyocytes ([80],[81],[82]), and is also limited to certain stimuli such as hypoxia, glucose deprivation, DNA damage, or the formation of free radicals ([64],[83],[86]). In contrast to its role in cell death, AIF also possesses an intrinsic NADH-oxidase activity that can be linked to mitochondrial homeostasis, regulation of metabolism, and oxidative stress ([87],[117],[118],[127]).

The biological implications of AIF in mitochondrial homeostasis have been demonstrated in studies of genetic deletion of AIF in mouse embryonic stem cells ([88]) and tissue and cell-specific AIF knockout studies ([89],[90]). Together these studies suggested that AIF regulates mitochondrial

bioenergetics by participating in the complex respiratory assembly and stabilization as AIF interacts with a crucial component of mitochondrial import machinery (CHCHD4) that contributes to the proper folding of OXPHOS subunits ([91],[92],[93]). Also, studies conducted in mice with AIF deficiency displayed adaptive mechanisms such as increased glycolysis, mild acidosis, and mitochondrial biogenesis, thus supporting the widespread role of AIF in cell metabolism and survival ([121]).

The pro-survival activity of AIF in normal cells is well-positioned to be exploited by cancer cells in promoting their growth. Moreover, various publications have reported increased expression of AIF in diverse cancer cell types, including esophageal, skin, colorectal, gastric, pancreatic, and prostate, indicating that AIF might support tumor development contrary to its tumor-suppressive capabilities ([117],[118],[113],[114],[115],[116]). Increased AIF levels in colorectal cancer protect cells from chemoresistance ([115]). Furthermore, our published data demonstrated the significance of AIF in the growth and survival of advanced prostate cancer cells (androgen-insensitive) ([117]), and in pancreatic cancer, where the selectivity of AIF dependence in tumorigenesis correlates with cellular metabolic preferences ([118]). Based on our finding that AIF is essential for the aggressiveness of advanced-stage prostate cancer cells (as discussed in chapter 1) and pancreatic ductal adenocarcinoma (PDAC) (as shown in chapter 2), a disease that almost always reaches an advanced stage before diagnosis. Consequently, we questioned whether the pro-survival activity of AIF contributes to breast cancer tumorigenesis.

Breast cancer is a heterogeneous disease and one of the most common malignancies found in women. Breast cancer can be classified into different subtypes depending upon several clinical biomarkers, such as estrogen (ER) and progesterone (PR) receptors and the human epidermal growth factor receptor 2 (HER2) gene amplification ([3]). Triple-negative breast cancer (TNBC) is

characterized by a lack of receptors and is regarded as aggressive as they are resistant to endocrine therapy and HER2-targeted treatment. Also, one of the molecular features of TNBC is metabolic reprogramming ([136]). Hence, it can be hypothesized that AIF in breast cancer might be well-positioned to influence aggressive breast cancer that critically rely on metabolic reprogramming for growth and survival. Therefore, AIF might contribute to metabolic vulnerabilities and thus can be implicated as a potential therapeutic target.

In the present study, we propose that AIF could maximally be exploited in triple-negative breast cancer by revealing a metabolic vulnerability as it switches from metabolic plasticity to metabolic dependencies. Previously, cells that relied only upon glycolysis could not benefit from AIF's metabolic activity in pancreatic cancer cell lines. Therefore, our efforts are to identify different substrates other than glucose that could be manipulated to increase the sensitivity and selectivity of hormone-independent breast tumors and can be exploited for neoadjuvant or adjuvant chemotherapy.

Materials and methods

Materials

RPMI 1640, GlutaMAX, trypsin, 4–12 % bis-tris polyacrylamide gels, and nitrocellulose membranes were obtained from Life Technologies; fetal bovine serum, phosphate-buffered saline, and Pierce ECL 2 Western Blotting Substrate were from Thermo-Fisher Scientific; QuantiChrom™ Glucose Assay Kit was from BioAssay Systems, protease inhibitor tablets were from Roche Applied Science; all other materials were from Sigma. Antibodies were obtained as follows: anti-AIF (Santa Cruz Biotechnology, sc-13116); anti-complex I 39 kDa (Life Technologies, 459100); anti-complex I 20 kDa (Life Technologies, 459210); anti-complex I 17 kDa (Life Technologies, A21359); anti-phospho-ERK Thr-202/Tyr-204 (Cell Signaling, 4377);

anti-ERK1/2 (Cell Signaling, 9107); anti-JNK (Cell Signaling, 9252); anti- β-actin (Sigma, A5316); peroxidase-conjugated anti-mouse (Amersham Biosciences, NA931V); and peroxidase-conjugated anti-rabbit (Amersham Biosciences, NA934B).

Oncomine data analysis

Data sets examining AIF mRNA expression in breast tumors versus normal breast tissue from 11 studies were analyzed using Oncomine ([4],[171]). Statistical calculations and normalization techniques are given by the Oncomine website (http://www.oncomine.org).

NOTE: Oncomine is no longer available since January 17th, 2022

Cell culture

MDA-MB-231, MCF-7, and MDA-MB-468 cells were from ATCC. HEK293T cells were as described ([117]). Cells were grown in an atmosphere of 95 % air and 5 % CO2 at 37°C. All media was supplemented with 2 mM Gluta-MAX. Cell lines were grown and cultured with the following media formulations: HEK293T cells in DMEM supplemented with 10 % FBS and breast cancer cell lines in RPMI 1640 supplemented with 10 % FBS.

Lentivirus production and infection

Lentivirus harboring FG12-derived plasmids that target AIF and LacZ by RNA interference (RNAi) has been assessed and used as described ([117]). Lentiviral packaging plasmids pRRE, pRSV-rev, and pHCMV-G are as described ([172]). RNAi plasmids and equal amounts of lentiviral packaging plasmids were transfected into HEK293T cells using the calcium phosphate precipitation method ([147]). Supernatants of transfected HEK293T cultures were then filtered through 0.45-μm PVDF Millex-HV filters (Millipore) and concentrated by centrifugation at 20,000 × g for 90 min at 4°C. Viral pellets were resuspended in PBS and then incubated overnight at 4°C prior to use. Cell lines were then infected as described ([173],[174]). MDA-MB-231, MCF-7, and MDA-

MB-468 cells were infected with lentiviruses carrying shLacZ-puro or shAIF-puro and then selected using 2 μg/mL puromycin.

NOTE: After establishing and verifying the stable cell lines, cells were frozen in multiple vials. Cells were not used more than 90 days after the thawing of stock cultures.

Drug treatment

Equal density of cells was seeded and then subjected to (tert-Butylhydroquinone) tBHQ treatment at 0-4mM for 30 minutes to stimulate ROS. Following treatment, cells were harvested and assessed in assays as described below.

SDS-PAGE and immunoblotting

For western blotting, the whole protein was extracted by (RIPA) radioimmune precipitation assay lysis buffer (PBS containing 1 % Nonidet P-40, 0.5 % sodium deoxycholate, 0.1 % sodium dodecyl sulfate, 1 mM dithiothreitol, 1 mM phenylmethanesulfonyl fluoride, and 1 protease inhibitor mixture tablet per 10 mL). Lysates were then normalized for protein content, separated by SDS-PAGE, and transferred to nitrocellulose membranes. Membranes were blocked with 5 % milk in Tris-buffered saline with 0.1 % Tween-20 and incubated with primary antibodies for overnight at 4°C under shaking conditions. Membranes were then washed and incubated with peroxidase-conjugated anti-mouse or anti-rabbit IgG secondary antibody for 45 min at room temperature, followed by washing and visualization using enhanced chemiluminescence with a MyECL imaging system (Thermo Scientific).

Cell growth rate measurements

Cells were harvested by trypsinization, washed, resuspended in fresh medium, and seeded at 30,000 cells/well, and replicate wells of 6-well plates were prepared. Three wells from each cell

type were harvested by trypsinization at 24 h intervals for a total of 96 h, and the total number of cells in each replicate was determined by CellDrop™ Automated Cell Counters – DeNovix.

Immunofluorescence

Cells were grown to at least 80% confluence. The cells were washed three times with PBS for 5 minutes, followed by fixing with 4% paraformaldehyde for 15 minutes at room temperature. The cells were then permeabilized with 0.1% Triton-X-100 in PBS for 15 minutes and then blocked with 5% BSA in PBS for 1 hour. The cells were subsequently incubated with an anti-AIF antibody (dilution 1:50) for 1 hour or overnight at 4°C. Following washing with PBS, the cells were incubated with a secondary antibody (goat anti-rabbit Alexa-Fluor 488; dilution 1:50) for 1 hour. After the final wash, the nuclei of the cells were stained with DAPI. Images were acquired on a Zeiss Axio Scope A1 (Carl Zeiss, Jena, Germany) with an AxioCam ICc1 camera under a × 20 objective. The images were photographed using Zen 2.6 lite software and analyzed by ImageJ software ([151]). Equivalent exposure conditions and scaling were used between controls and test cells and adjusted with only contrast and brightness adjustment

Glucose consumption measurements

The cells were harvested by trypsinization, washed, resuspended in fresh medium, and seeded at equal densities in 6-well plates. Cells were grown at 37°C for 72 h. Media was then collected from each well, and total glucose was measured using the QuantiChrom™ Glucose Assay Kit (BioAssay Systems). The total cell number in each sample was determined by Coulter™ counting. In order to assess glucose consumed per cell, total glucose consumption per sample was divided by its corresponding cell count. Fold change in glucose consumption was determined by dividing populations of AIF-deficient cells by corresponding control populations.

Measurements of mitochondrial ΔΨm and abundance

The membrane potential was monitored using the dye Tetramethyl Rhodamine Methyl ester (TMRM) and was carried out as described previously ([175]). Equal density of cells was seeded and allowed to attach for overnight at 37°C. The cells were harvested and resuspended in PBS containing 200 nM TMRM and incubated at 37°C for 15 minutes, followed by a flow cytometer. Staining for mitochondrial abundance was carried out by incubating cells with 100 nM MitoTracker™ Red at 37°C for 15 minutes, followed by an assessment of stain intensity using an Accuri C6 flow cytometer

Modified MitoPlate assay

A Mitoplate assay was employed with a slight modification to assess the mitochondrial function of cells as described previously ([176]). The assay used a standard half-area 96-well plate with Biolog Mitochondrial Assay Solution (BMAS, catalog# 72303) together with dye mixture MC (tetrazolium-based dye, catalog# 74353) provided by Biolog, Inc. Dye mixture MC uses a modified version of tetrazolium dye that acts as a terminal electron acceptor in the electron transport chain, resulting in the formation of water-soluble formazan upon reduction. The formation of purple-colored formazan directly correlates with cellular ETC activities and can be measured at an absorbance of 590nm (OD_{590}). An assay mixture consisted of 2x BMAS, MC, 2.4 mg/ml saponin, and 100 mM substrate solution in the ratio of 6:4:1:1. Twenty-three substrates used comprised from glycolysis, the pentose phosphate pathway, TCA cycle anaplerosis, fatty acid transport/oxidation, one-carbon metabolism and amino acid metabolism. All the substrates were acquired from Sigma. Thirty microliters of the assay mixture were distributed to each well of the 96-well plate. AIF deficient/proficient cells were collected in a 15-ml centrifuge tube and centrifuged at 400 × g for 5 min. The supernatant was removed, and the cell pellet was washed

with PBS and centrifuged. Finally, the cell pellet was resuspended in 1x BMAS to achieve a final cell density of 2×10^6 cells per ml. Thirty microliters of the cell suspension was pipetted into each well of the microarray containing the assay mixture. The final assay mixture was composed of 6×10^4 cells per well. After inoculation, the OD_{590} was measured every 10 min with an Agilent BioTek Gen 5 microplate reader for total of 3 hours and 30 minutes. These data were then normalized by subtracting the absorbance readings of control (no substrate) wells containing 2x BMAS, MC, saponin, and water at a 6:4:1:1 ratio. 30 µL of the assay mixture (no substrate) was transferred to each well of the plate and 30 µL of the cell suspension in 1x BMAS was added to each well, and OD_{590} measurements were performed similarly.

Furthermore, to test whether chemotherapeutic drug such as lonidamine (a complex II inhibitor) or lithium chloride (phosphoglucomutase inhibitor) reverses the consumption of the substrates as the control cells was assessed by the use of modified Mitoplate assay. In this assay, cells were permeabilized and added to the assay mixture with or without the chemotherapeutic drug. The final concentration of the inhibitors in the well were 100 µM of lonidamine or 10 mM lithium chloride. The data was then normalized by subtracting the absorbance readings of control (no substrate) wells.

MTT assay

Cells were seeded with 30,000- 50,000 cells per well in 24-well plates and allowed to attach overnight. Cells were left untreated or treated with 100 µM lonidamine or 10 mM lithium chloride for 48-72h. Cells treated with DMSO were the solvent control. The media was removed, followed by adding a fresh medium of 100 µl containing 10 µl of the MTT stock [3-(4,5-dimethylthiazol-2-yl)-2,5-diphenyltetrazolium bromide (MTT, catalog # 97,062–376, VWR) (5 mg/ml)] and incubating it at 370C for 3 hours. After incubation all but 25 µl of the medium was removed, and

50 µl of DMSO was added and incubated at 37°C for 10 minutes in order to solubilize the formazan. The solubilized formazan was then transferred to a 96-well plate, and the absorbance was measured at 540 nm using a microplate reader. The absorbance was adjusted by subtracting the absorbance of the media control.

Statistical analysis

Statistical analyses were performed using two-tailed, Student's t tests for unpaired or paired samples A minimum of three independent biological replicates (unless otherwise stated) were assessed for all experiments. Statistical significance is represented as: $^{*}P < 0.05$; $^{**}P < 0.01$; $^{***}P < 0.001$.

Results

Elevation of AIF mRNA transcripts in breast cancer

To evaluate the potential role of AIF in breast cancer, we analyzed the catalogued microarray database available at Oncomine (oncomine.com), a web-based data mining platform. Archival data from a total of 11 data sets comparing AIF expression in breast carcinoma to normal breast tissue were assessed ([1],[177],[2]). While comparing the average AIF expression between cancer vs. normal groups, AIF mRNA transcript was significantly overexpressed in six data sets ($p < 0.001$) from a total of 11 data sets (fold change ranging from 1.543-1.639). Representative data sets as shown in Figure 3.1 were shown that were statistically significant, with p values in the range from 0.013-0.043.

To further explore AIF expression changes in these cohorts of cancer vs. normal tissues, we compared individual expression data from each sample within each cohort (Figure 3.1.D-F). Interestingly, in 6 of the 11 data sets, a subtype within each cancer group displays elevated AIF expression significantly beyond the 90% confidence interval defined for normal tissues ([1],[2]).

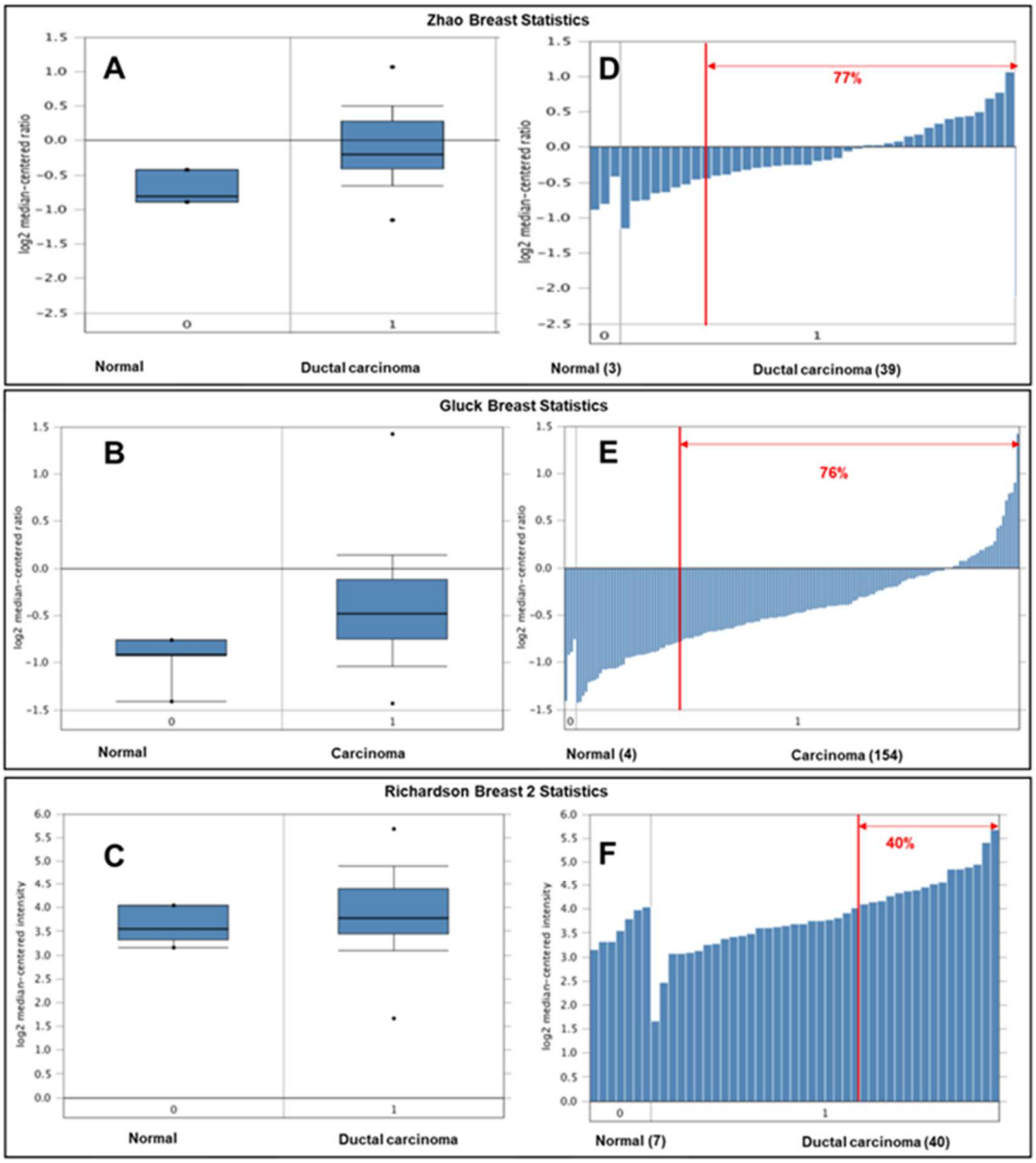

Figure 3.1: AIF expression in breast cancer.
Data comparing AIF mRNA transcript expression in breast tumors compared to normal breast tissue was retrieved from the Oncomine database. Panels A-C: Average relative AIF mRNA expression in breast tumors vs. normal breast tissue. Panels D-F: Relative AIF mRNA levels among individual samples within each cohort. Fractions of tumor specimens within each cohort exhibiting statistically significant AIF expression changes relative to normal tissue are (p-value in range from 0.013-0.043) indicated in red. The number of samples in each class is given in parentheses. Each gene was assessed for differential expression with t-statistics using Total Access Statistics 2002 (FMS Inc., Vienna, VA). t-Tests were conducted both as two-sided for differential expression analysis and one-sided for specific overexpression analysis.

This subtype represents ~33 % of the total among these six cohorts, and while elevated AIF is observed, the magnitude of this elevation remains modest (less than 3-fold relative to control tissue). These data are in accordance with similar analyses examining AIF mRNA and protein expression in prostate cancer and pancreatic cancer tissues ([118],[117]). These data collectively suggest that while elevated AIF expression is not a universal feature of breast cancer, there exists a subtype of breast tumors (approximately one-third of the total samples assessed) in which AIF expression is significantly elevated. Earlier studies revealed that overexpression of AIF induces cell death; however, the expression of AIF in breast cancer is modestly elevated, indicating that elevated AIF expression in breast cancer cells is insufficient to trigger cell death. This suggests that the range of overexpression over which the increased AIF is of benefit is narrow and that greater levels of AIF may become toxic. Thus, there exists a benefit of AIF expression in breast cancer that is worth exploring ([67]).

Establishment of AIF-deficient breast cancer cell lines

The Oncomine analysis of AIF gene expression microarray data from clinically derived breast cancer tissues implied a connection between elevated AIF expression and breast tumors. In one of our studies, AIF supports the growth of advanced prostate cancer which was androgen-insensitive, and in other studies, AIF supports the growth of metabolically defined pancreatic cancer, thus demonstrating the role of AIF in tumor development ([117],[118]). Therefore, to determine the potential role of AIF in breast cancer, a panel of breast cancer cells was selected to reflect diversity both in metabolic requirements and hormonal status. Thus, we targeted AIF in a panel of three breast cancer cell lines (MDA-MB-231, MDA-MB-468, and MCF-7) that displayed diverse metabolic characteristics. A comprehensive systems biology analysis of metabolic profiling,

metabolic inhibitor responses, siRNA screening, and tyrosine kinase inhibitor analysis has revealed metabolic heterogeneity in breast cancer and its subtypes ([178]).

Table 1: Molecular classification and metabolic phenotype of breast carcinoma

	Glycolysis	OXPHOS	Metabolic flexibility	Classification	Histology grade	Type
MDA-MB-231	Moderate	Low	Low	Basal B	ER–, PR–, HER2–	highly aggressive, invasive and poorly differentiated triple-negative breast cancer
MCF-7	Moderate	Moderate (Glutamine as the substrate)	High	Luminal A	ER+, PR+/–, HER2–	poorly-aggressive and non-invasive cell line
MDA-MB-468	Moderate	High	High	Basal A	ER–, PR–, HER2–	moderately aggressive, invasive and poorly differentiated triple-negative breast cancer

ER: estrogen receptor
HER2: human epidermal growth factor receptor 2
PR: progesterone receptor

Together these analyses indicated that MDA-MB-231 relies on glycolytic metabolism while MDA-MB-468 depends on oxidative metabolism in the basal state ([178]). However, MCF-7 does not display a consensus regarding its metabolic phenotype. Some reports suggest that MCF-7 can show stronger glycolytic dependence ([3]), while other studies suggest that MCF-7 are more dependent on mitochondrial respiration ([179]). Therefore, there is a likelihood of MCF-7 exhibiting metabolic flexibility by balancing the energy requirements derived from glycolysis and oxidative metabolism. There is additional literature suggesting that glutamine, but not pyruvate, confers additional oxidative capacity in MCF-7 cells ([180]).

Among these breast cancer cell lines, MDA-MB-231 (mesenchymal-like subtype) and MDA-MB-468 (basal-like subtype) cells are triple-negative breast cancer cells (TNBC) that are considered as aggressive and invasive, display poor prognosis, and are poorly differentiated. In

contrast, MCF-7 (luminal-like subtype) cells is human epidermal growth factor receptor 2 (HER2) negative, and weakly invasive ([181],[182],[183],[184]). Knockdown of AIF was achieved by infecting with lentiviruses harboring short-hairpin RNA (shRNA) sequences targeting either AIF (shAIF) or LacZ (shLacZ) as control via RNA interference. Breast cancer cell lines were infected with lentiviruses carrying the puromycin N-acetyl transferase gene as a selectable marker, and stably infected cells were derived by treatment with 2ug/ml of puromycin. To determine if AIF was successfully suppressed in our panel of breast cancer cell lines, immunoblot analysis was employed, which demonstrated AIF knockdown levels greater than 95 % in all cases when compared to either parental cells or shLacZ negative controls as shown in Figure 3.2A. Immunoblot data was further confirmed by immunofluorescence analysis of the endogenous expression of AIF in our panel of breast cancer cell lines. In agreement with our previous immunoblotting experiments, shLacZ cells were positive for shAIF cells were negative for AIF as shown in Figure 3.2B

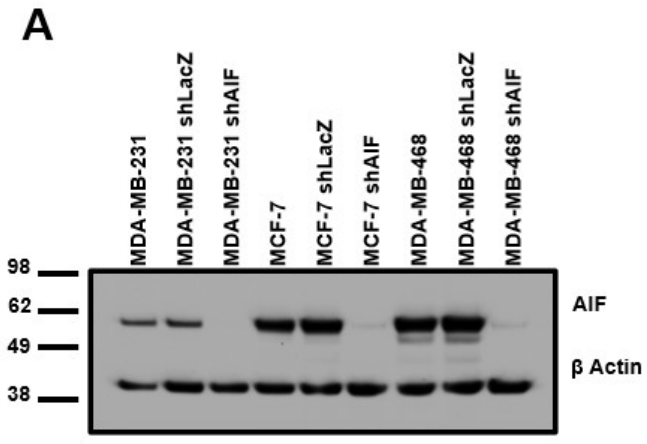

Figure 3.2: Establishment of AIF-deficient breast cancer cell lines.
MDA-MB-231, MCF-7, and MDA-MB-468 were stably infected with shRNA hairpins targeting LacZ or AIF with Puromycin as a selectable marker via lentiviral delivery. (Panel A) Suppression of AIF protein expression was verified by immunoblot analysis. Representative blot image is shown and actin was used as the loading control. (Panel B) Suppression of AIF protein expression was verified by immunofluorescence analysis. Images were taken at 20X magnification. Scale bar = 200μm.

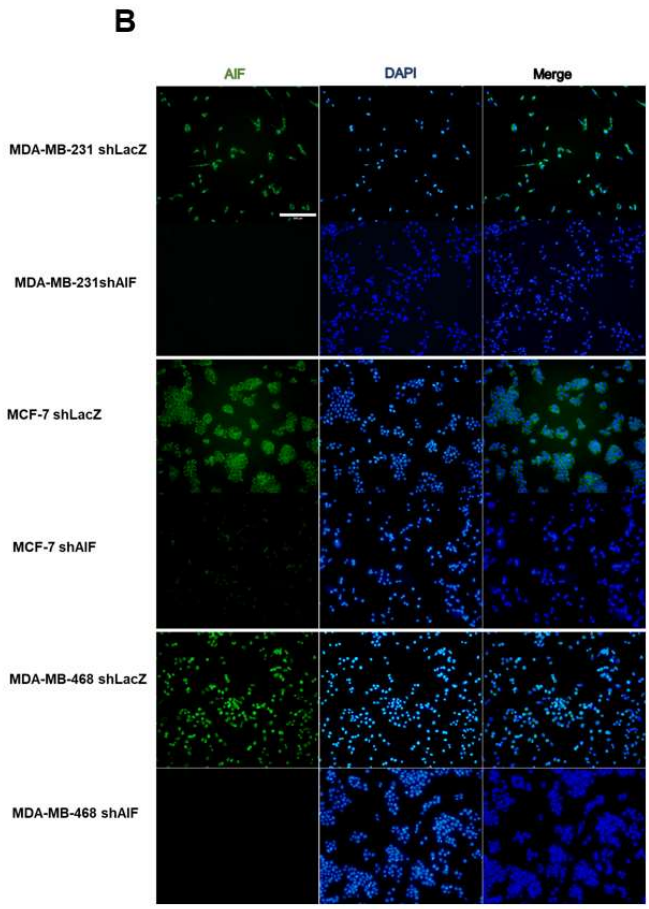

Figure 3.2: Establishment of AIF-deficient breast cancer cell lines (continued).
MDA-MB-231, MCF-7, and MDA-MB-468 were stably infected with shRNA hairpins targeting LacZ or AIF with Puromycin as a selectable marker via lentiviral delivery. (Panel A) Suppression of AIF protein expression was verified by immunoblot analysis. Representative blot image is shown and actin was used as the loading control. (Panel B) Suppression of AIF protein expression was verified by immunofluorescence analysis. Images were taken at 20X magnification. Scale bar = 200μm.

AIF-mediated signaling is uncoupled from AIF-dependent metabolism

The role of AIF in maintaining cell homeostasis and survival and growth of cells has been extensively studied ([127]). However, AIF dependent redox-mediated signaling pathways that regulate tumorigenesis need more exploration. We have shown previously that AIF is required for oxidant-induced JNK phosphorylation in PC3 (prostate cancer), HPAC, and MIA PaCa-2 (pancreatic cancer) ([127]). Therefore, we further explored whether AIF -dependent phosphorylation of JNK is true in breast cancer.

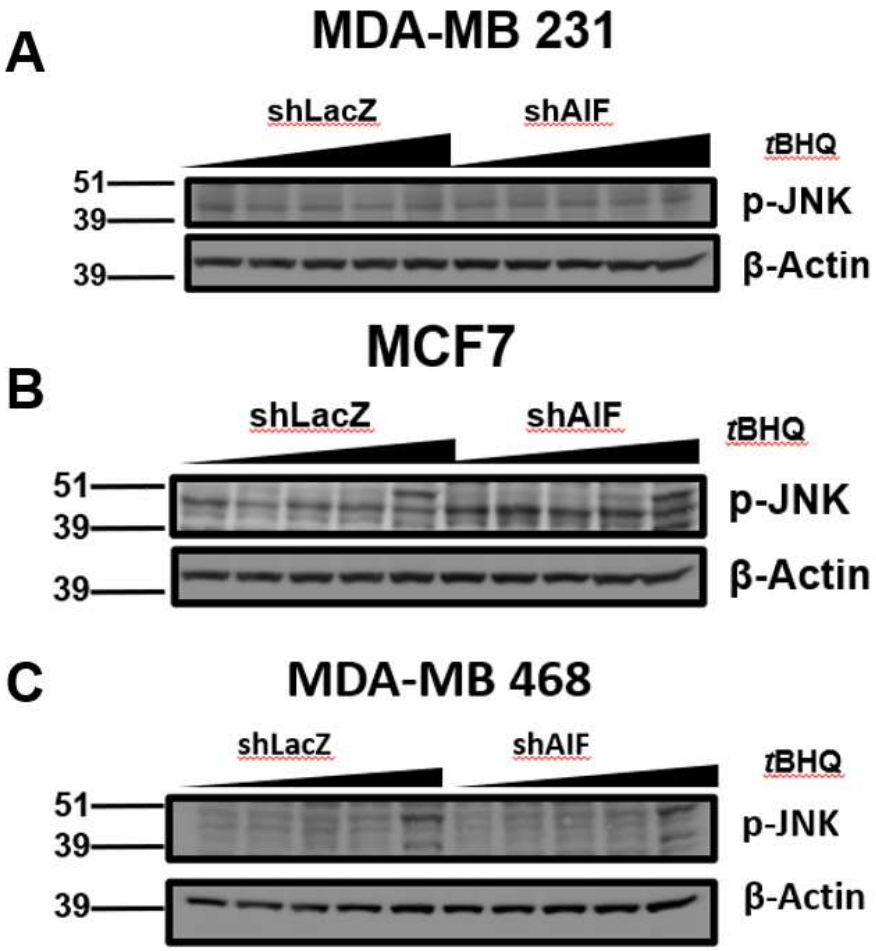

Figure 3.3: Effect of tBHQ on JNK phosphorylation in AIF-deficient breast cancer cell lines. MDA-MB-231-derived **(A)**, MCF-7-derived **(B)**, and MDA-MB-468-derived were treated with increasing concentrations of *t*BHQ as follows: 0, 0.1, 0.25, 0.5, and 1mM.Following treatment, immunoblots were performed with the indicated antibodies. Representative blot image is shown and actin was used as the loading control.

Figure 3.3 suggests that AIF is not required for JNK activation in our panel of breast cancer cells, thus implying that ROS-mediated AIF-dependent JNK signaling is not a global trend. However, ROS is also believed to act as a stimulus to another mitogen-activated protein kinase pathway (MAPK) related protein such as extracellular signal-regulated kinase (ERK); ROS-responsive signaling molecules whose activation by phosphorylation can control a spectrum of cellular activities ranging from cell death to survival ([123],[14]).

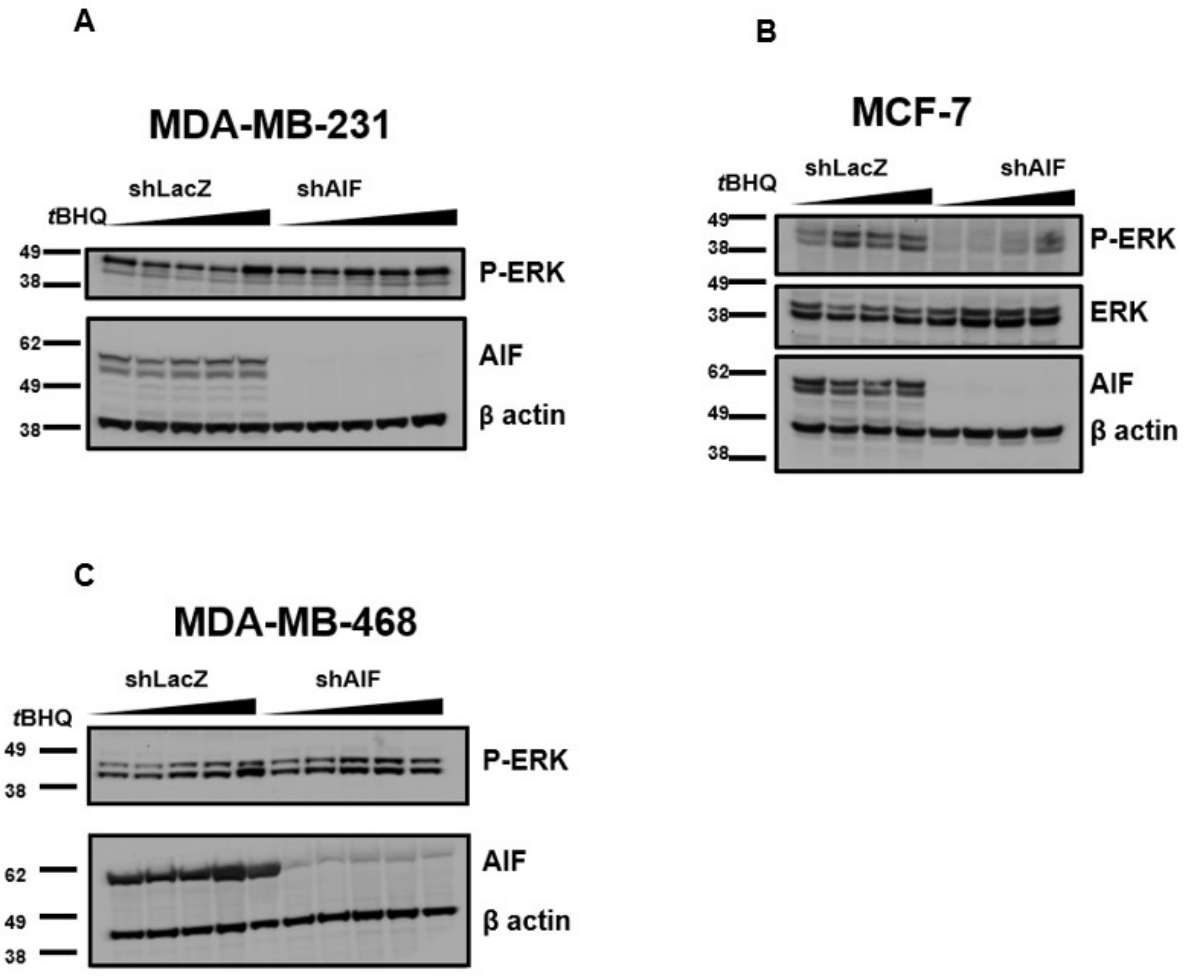

Figure 3.4: Effect of tBHQ on ERK phosphorylation in AIF-deficient breast cancer cell lines. MDA-MB-231-derived **(A)**, MCF-7-derived **(B)**, and MDA-MB-468-derived **(C)** cell lines were treated with increasing concentrations of *t*BHQ as follows: 0, 1, 2, and 3mM (MCF-7); 0, 1, 2, 3, and 4mM (MDA-MB-231, and MDA-MB-468) for 30 minutes. Following treatment, immunoblots were performed with the indicated antibodies. Representative blot image is shown and actin was used as the loading control.

Thus, we then questioned whether AIF acts as secondary messenger in cellular signaling in the ERK pathway and if it is coupled to the stabilization of the mitochondrial respiratory chain. We treated our panel of breast cancer cell lines with an increasing concentration of tert-butylhydroquinone (tBHQ) to stimulate ROS; we then assessed protein levels of activated ERK, a phosphorylated form of ERK. Only in MCF-7 cells was AIF dependency apparent in ERK phosphorylation but not in MDA-MB-231 or MDA-MB-468. It was interesting to note that in

aggressive breast cancer cell lines, AIF-dependent redox-signaling was not apparent but was observed in non-invasive breast cancer cell lines as shown in Figure 3.4. These suggests that AIF does not regulate the aggressiveness of breast cancer cell lines via ROS dependent ERK or JNK activity but must be vital in modulating cellular metabolism.

Triple-negative breast cancer cells require AIF for *in vitro* growth, membrane potential ΔΨm and mitochondrial abundance.

A growth assay was performed to determine whether AIF ablation in breast cancer affects its ability to grow under nutrient-rich conditions. AIF-deficient MDA-MB-231 and MDA-MB-468 cells grew more slowly than AIF-proficient cells, but no spontaneous death was observed. However, suppression of AIF did not affect the growth of MCF-7. Combined with the observation that AIF ablation alters the growth of MDA-MB-231 and MDA-MB-468 cells but not for MCF-7, these data suggested that AIF might contribute to the growth of triple-negative breast cancer cells but not for less aggressive breast cancer cells, under nutrient-rich conditions. Moreover, these results are distinct from our previous publications: in prostate cancer, the growth rate is unaffected in AIF ablated advanced prostate cancer cells, under nutrient-rich conditions whereas, in pancreatic cancer, the selectivity of AIF support for growth rate relies on the cellular energy preferences. The current data is inconsistent with previous data that the growth rate of AIF ablated breast cancer is correlated to the aggressiveness of breast cancer and not to its metabolic preferences.

We evaluated the mitochondrial status in our panel of breast cancer cell lines to determine whether mitochondrial function and/or biogenesis was impaired when AIF was ablated. Mitochondria are responsible for maintaining oxidative phosphorylation, and they do so by

creating a membrane potential that supports the correct functioning of the electron transport chain ([26,28,31]).

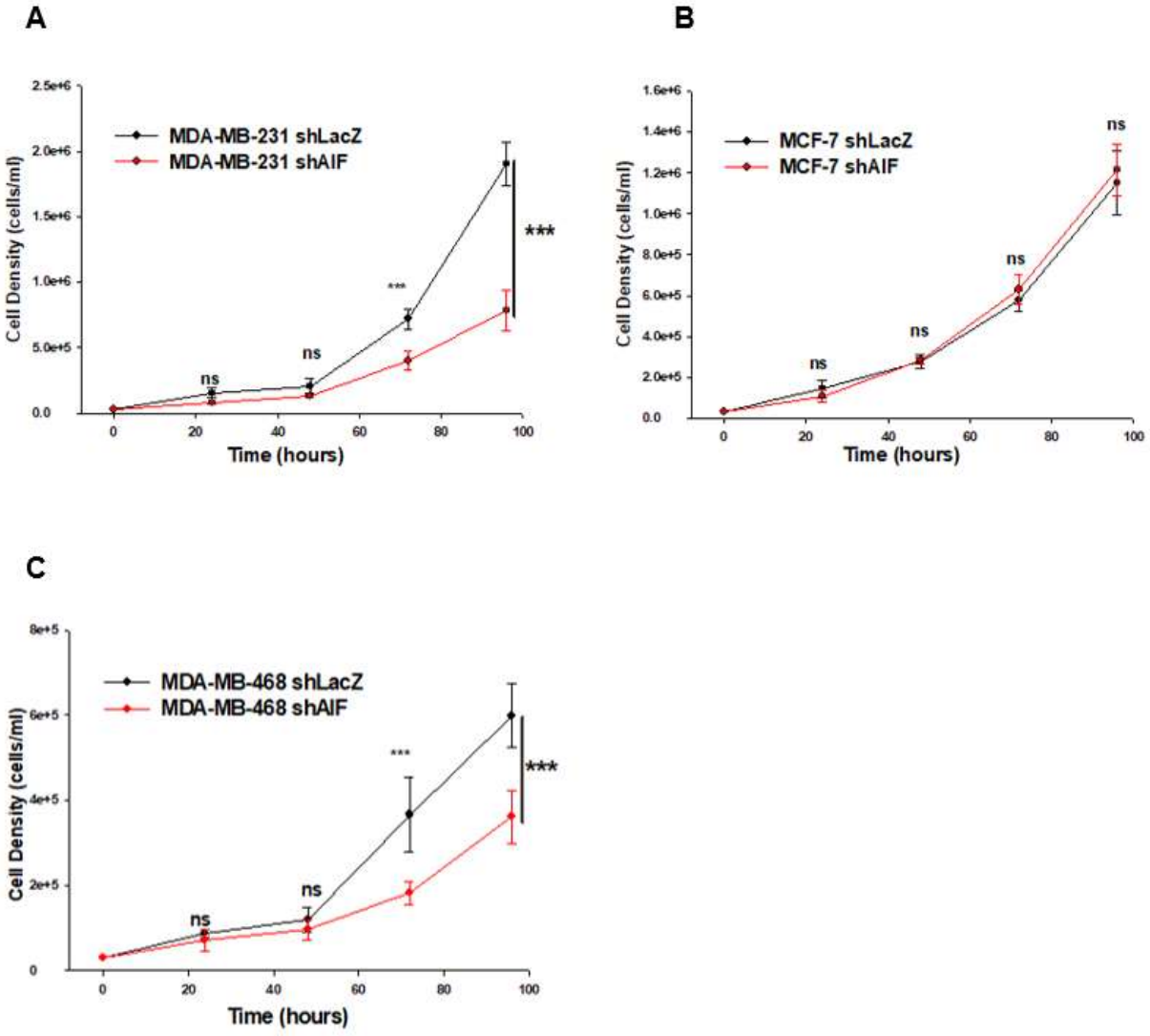

Figure 3.5: Growth of triple-negative breast cancer cells in nutrient-rich medium is affected by AIF ablation.
MDA-MB-231-derived **(A)**, MCF-7-derived **(B)**, and MDA-MB-468-derived **(C)** cell lines were plated at 30,000 cells/well in replicate plates. The cells were then harvested every 24 h (for a total of 96 h), and the total number of cells in each well was assessed by CellDrop™ Automated Cell Counters – DeNovix (n=3). The averages ± standard deviation of triplicate samples is shown for each data point. The statistical significance of end point values was determined by Student's t test. *, $p < 0.05$; **, $p < 0.01$; ***, $p < 0.001$; ns, $p > 0.05$

Thus, we investigated whether the membrane potential was altered after AIF was ablated. For evaluating membrane potential, cells were stained with TMRM, and then stain intensity was assessed by flow cytometry. It was observed that AIF ablation dissipated mitochondrial electrochemical gradient in invasive breast cancer lines such as MDA-MB-231, and MDA-MB-468 but was minimally decreased in non-invasive MCF-7. Thus far, it seems that AIF is more important in invasive breast cancer than non-invasive breast cancer. Next, we extended to study the impact of AIF ablation on mitochondrial abundance and whether any changes are selectively observed in invasive breast cancer cell lines. We then focused on another aspect of mitochondrial status: mitochondria abundance and whether AIF deficiency results into a similar trend as observed in membrane potential. Mitotracker^{TM} Red staining was performed as an indicator of mitochondrial abundance; surprisingly, AIF ablation resulted in decreased mitochondria in our panel of breast cancer cell lines. Intriguingly, this AIF-dependent mitochondrial status change was not reported in other AIF-ablated cancer cells tested so far suggesting that mitochondrial response to AIF is distinct in different cancer cell lines and AIF might be more critical for mitochondrial biogenesis and fitness in triple-negative breast cancer cell lines.

The ability of AIF to alter glucose consumption in aggressive breast cancer cells is dependent on complex I activity but not metabolic phenotype

Mutation in the AIFM1 locus on the X chromosome leads to a disease that is phenotypically similar to those caused by the mutation in the mitochondrial components. These defects are presumably due to the role of AIFM1 in the biogenesis of complex I or its involvement in the transport of electrons from NADH (or NADPH) to ubiquinone ([88]). This demonstrates the significance of AIF in regulating oxidative phosphorylation by controlling the expression of proteins subunits in the respiratory chain, especially of complex I ([88],[90]).

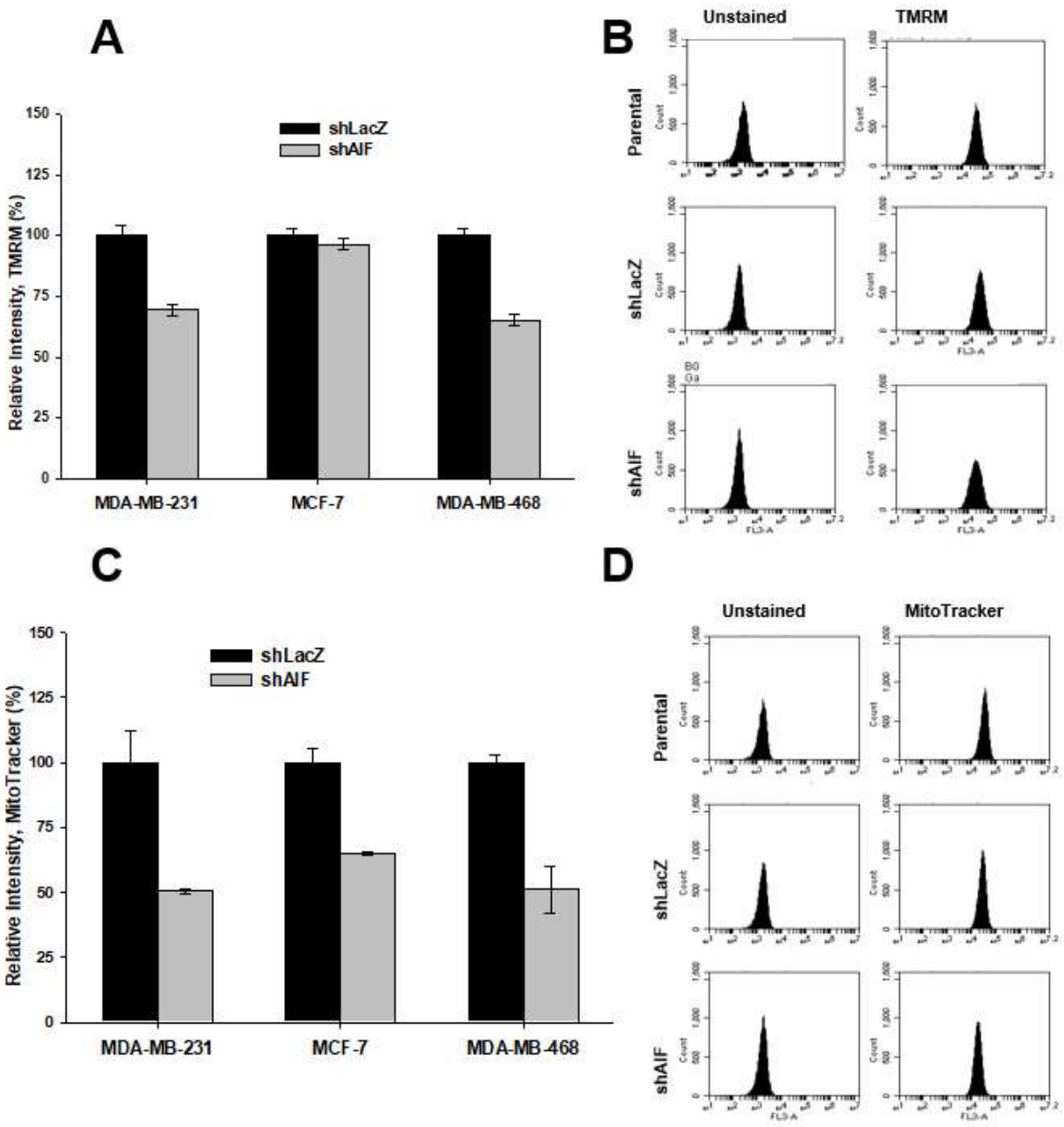

Figure 3.6: AIF is required for the mitochondrial $\Delta\Psi_m$ and abundance.
The indicated cell lines were stained with either TMRM (Panel A-B) or Mitotracker™ Red (Panel C-D) was used to determine membrane potential and the abundance of mitochondria, respectively, in cells proficient (shLacZ) and deficient in AIF (shAIF). (Panel A and C) are representative images from AIF proficient/deficient breast cancer cells stained with TMRM or Mitotracker™ Red and measured by flow cytometer. Changes following AIF ablation compared with control cells are shown.

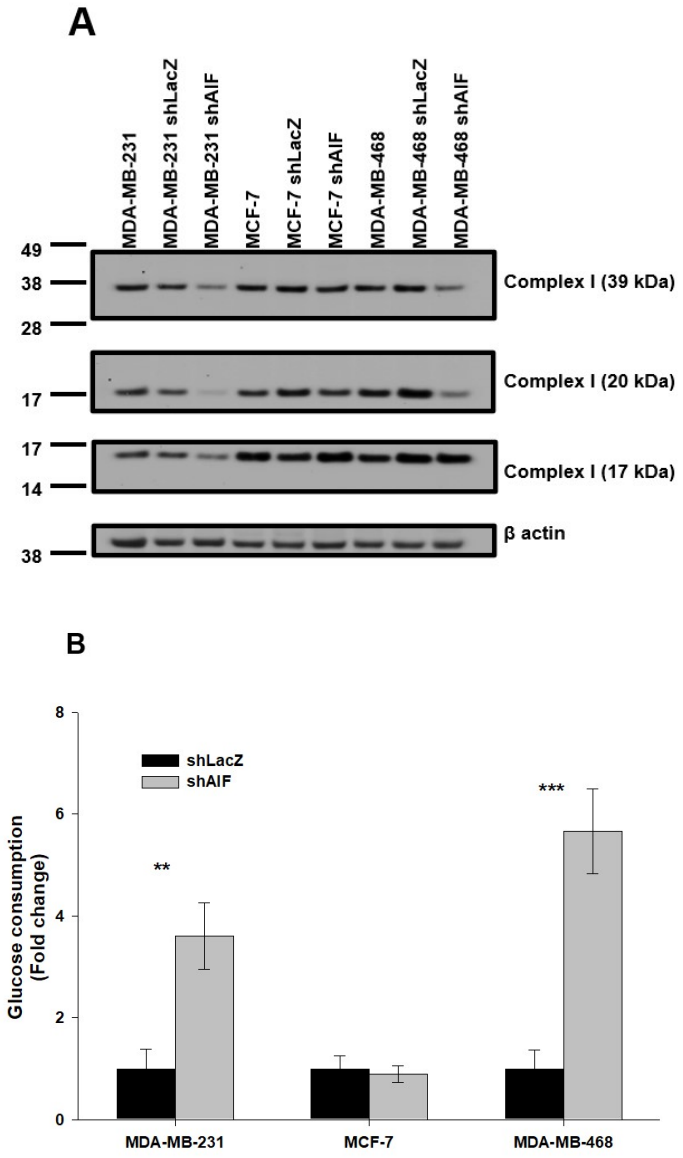

Figure 3.7: AIF-deficient TNBC cells exhibit reduced complex I expression and increased glucose consumption.

AIF selectively controls respiratory chain protein expression in breast cancer cell (Panel A). Following suppression of AIF, respiratory chain status was assessed by immunoblot analysis of complex I (39-, 20-, and 17-kDa subunits) and actin was used as the loading control. Glycolytic dependence is reflected by the metabolic phenotype of AIF-deficient breast cancer (Panel B). The indicated cell lines were harvested, washed, and seeded at equal densities in fresh medium. 48 h after plating, medium was collected, and the total glucose was assessed using the BioAssay systems QuantiChrom^{TM} glucose assay kit. The total number of cells in each well was assessed by Coulter counting and used to determine glucose consumption per cell (N=3). The data shown are pooled from three independent experiments. Data are shown as average ± s.e.m. *****, $p < 0.05$. ******, $p < 0.01$, p *******< 0.001

Immunoblot analysis was used to determine whether knockdown of AIF affects the expression levels of complex I in the panel of breast cancer cell lines. In MCF-7, none of the complex I subunits was reduced after AIF ablation; however, reductions in 39-kDa, 20-kDa, and 17-kDa complex I subunits was observed in MDA-MB-231; whereas suppression of only 39-kDa, and 20-kDa were altered in MDA-MB-468 as shown in Figure 3.7A. These data suggest that the loss of complex I in breast cancer is dependent on the aggressive phenotype of breast cancer in agreement to our previous publication where AIF supports the advanced prostate cancer or aggressive pancreatic cancer cell lines.

Mitochondria are essential for cellular energetics and metabolism ([185, 186],[186]). Since the loss of complex I impairs oxidative phosphorylation, any alterations in the respiratory subunits of complex I will likely switch reliance on energy production from oxidative phosphorylation to glycolysis ([187]). Thus, to determine whether the ablation of AIF affects the glucose consumption in our panel of AIF-ablated breast cancer cell lines, glucose consumption was measured. MCF-7 displayed slight alteration in glucose consumption when compared to control. These data are in concurrence with AIF ablation having a negligible effect on its complex I subunits. The AIF-deficient MDA-MB-231, and MDA-MB-468 consumed 4-fold and 6-fold, respectively, more glucose than their corresponding controls as shown in figure 3.7B. Moreover, MDA-MB-231 likely displays an addiction to glycolysis (Table 1), revealing an upregulated glucose consumption when AIF was ablated. These findings were not identified in MIA PaCa-2, a pancreatic cancer cell line, which displayed a severe pre-existing addiction to glycolysis, and thus no changes in glucose metabolism were observed when AIF was ablated. Thus, AIF-ablated breast cancer studies are different from our previous publication, where the basal metabolic phenotype of pancreatic cancer

cell lines dictated the AIF activity in cancer ([118]). This evidence indicates a weak association between metabolic phenotype and sensitivity to AIF ablation in breast cancer.

Differences in substrate utilization in AIF-deficient breast cancer cell lines

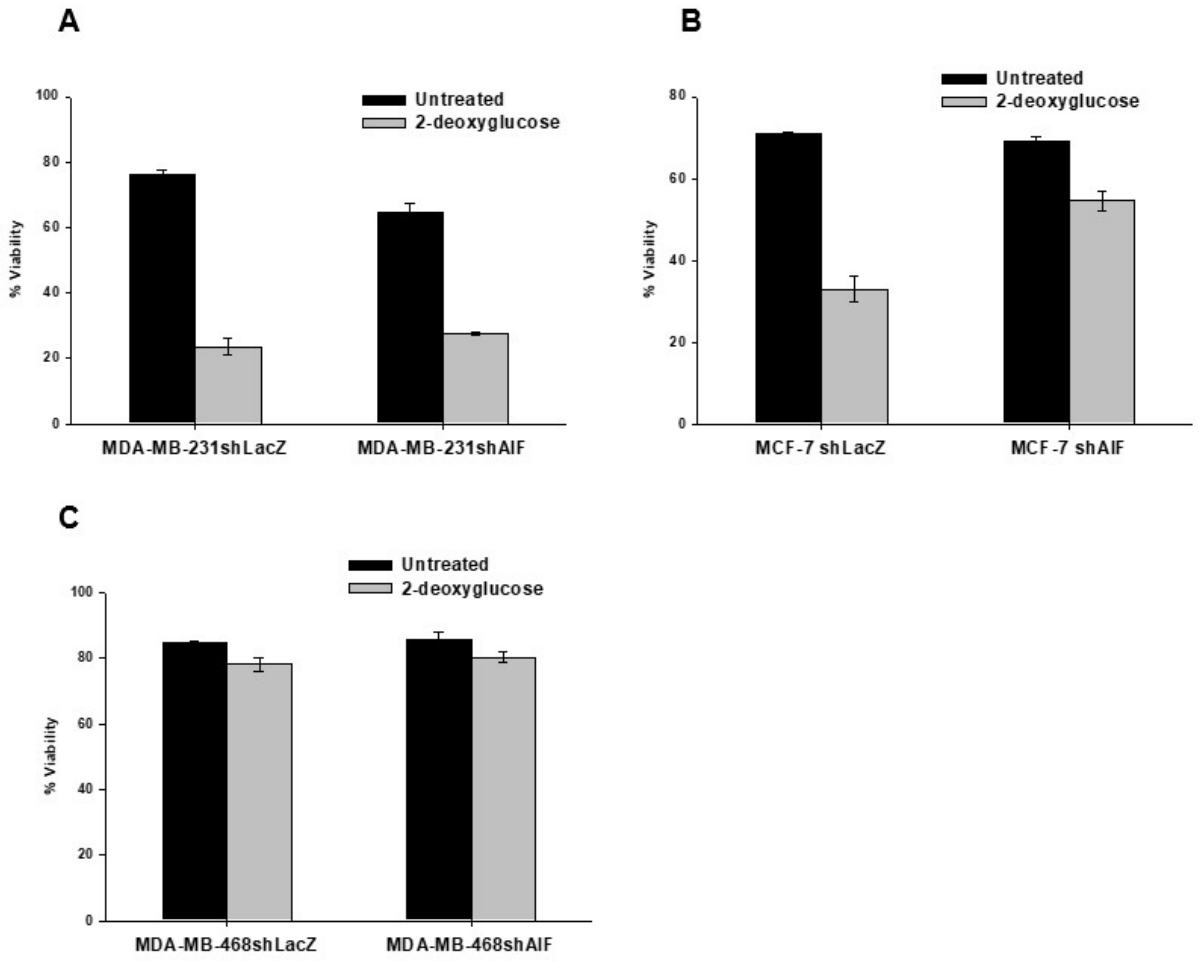

Figure 3.8: AIF-deficient breast cancer cells were not selective to glycolytic disruption. MDA-MB-231-derived **(A)**, MCF-7-derived **(B)**, and MDA-MB-468-derived **(C)** cell lines were seeded in equal densities and allowed to attach overnight before treatment with 50 mM 2-deoxyglucose. After 48 h cells were collected, and viability was determined by propidium iodide staining and flow cytometry. Data are shown as average ± standard deviation.

Figure 3.7B demonstrates how AIF ablation altered glucose consumption in MDA-MB-231 and MDA-MB-468. This alteration suggests that triple-negative breast cancer cell lines increased glucose uptake thus rendering them sensitive to AIF ablation. Therefore, we investigated

whether our panel of breast cancer cell lines is sensitized to glycolytic disruption. To test this hypothesis, we treated AIF deficient/proficient breast cancer cell lines with 2-deoxyglucose, a glycolysis inhibitor. In contrast to our previous findings, MDA-MB-468, whose basal metabolism relied on oxidative phosphorylation, was not sensitized to 2-deoxyglucose as shown in 3.8C. Also, MDA-MB-231, which has a predilection for glycolysis, was not sensitized further by AIF ablation. From Table 1, it can be suggested that MCF-7 can balance between glycolysis and oxidative phosphorylation and is flexible metabolically; thus, is most resistant to AIF ablation. Table 1 also demonstrates the metabolic flexibility of MDA-MB-468, which might contribute to bypassing metabolic hindrances caused by AIF ablation.

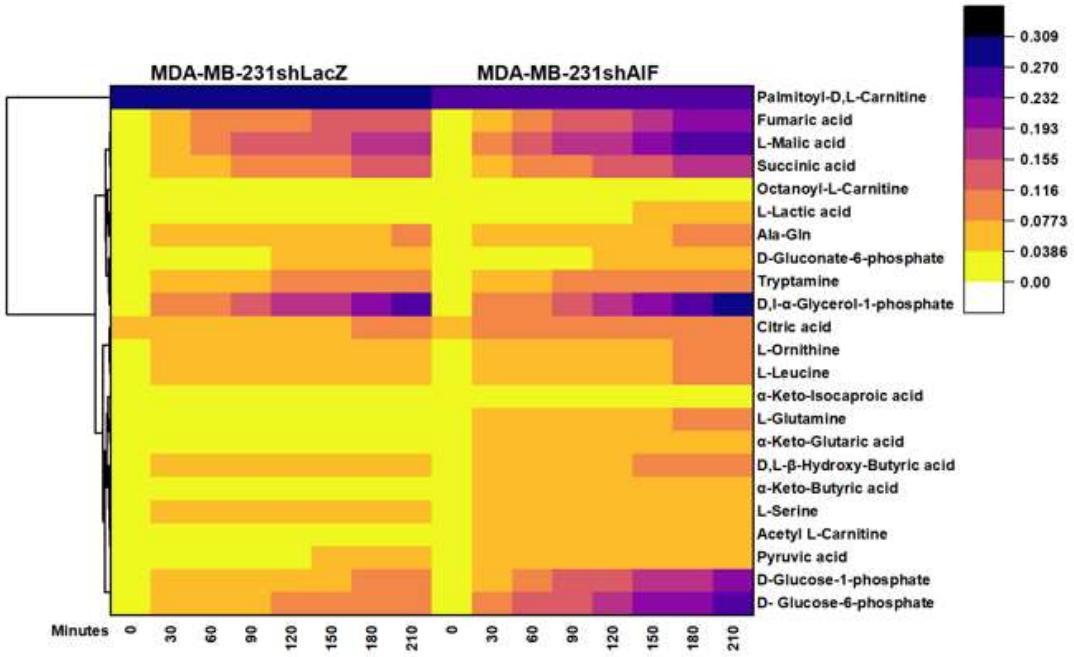

Figure 3.9: Metabolic alterations in AIF-deficient MDA-MB-231 breast cancer cells.
To assess the mitochondrial activities, the AIF-deficient/proficient MDA-MB-231 were transferred to a 96-well plate that also included a 100mM substrate, 6x tetrazolium-based dye and 2.4mg/ml saponin. The consumption rates of substrates were monitored by measuring the OD590 at the indicated time points (for 210 mins total). Unsupervised clustering of absorbance data was performed using OriginPro. The generated heat maps show metabolite clusters that are upregulated (blue) or downregulated (yellow) in the AIF-deficient group compared to the AIF-proficient control group. Each column represents a biological replicate from three-independent experiments; each row represents a metabolite. N=5.

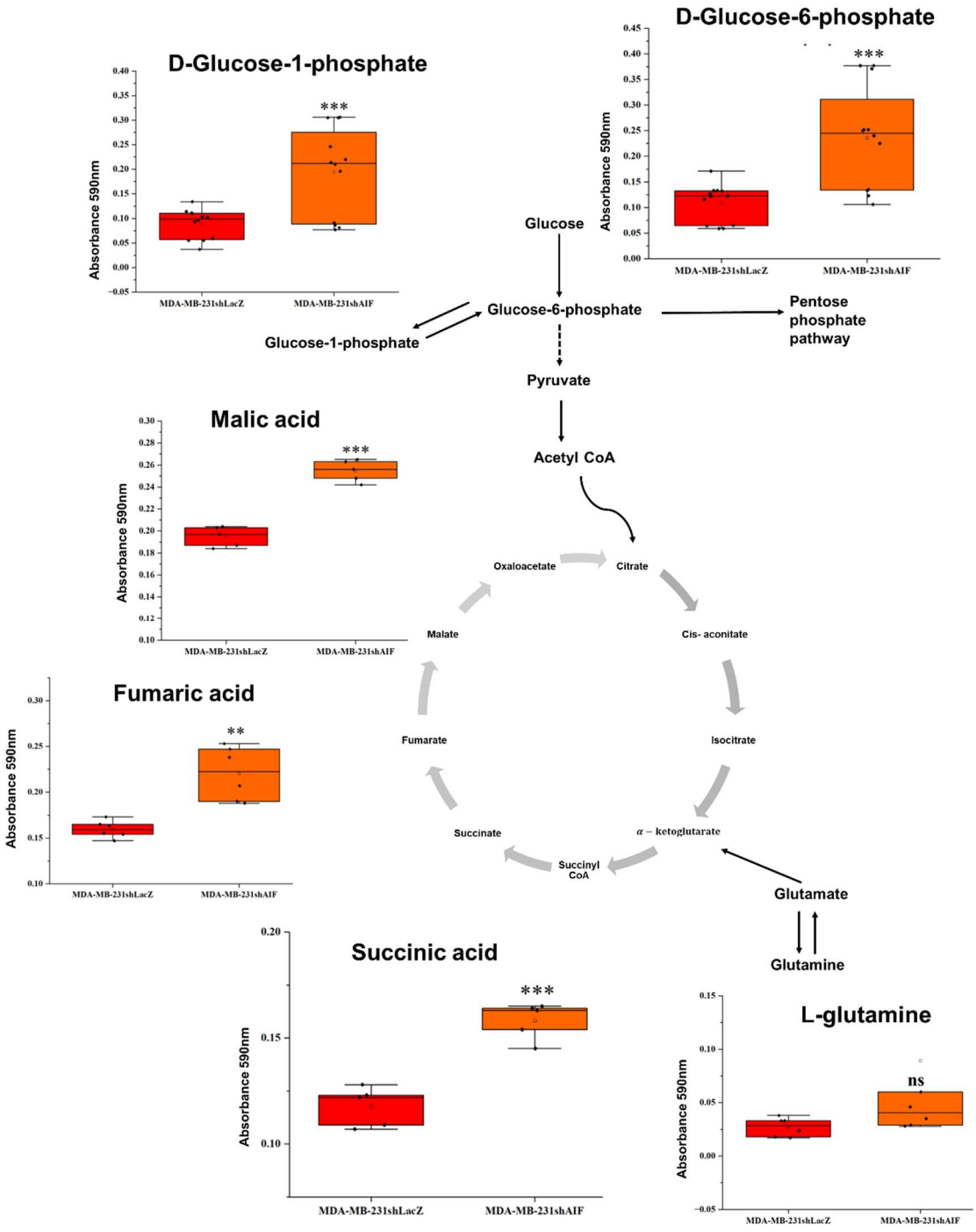

Figure 3.10: Representative boxplots of altered metabolites in AIF-deficient MDA-MB-231 breast cancer cells.

Representative boxplots show the metabolites: Malic acid, Fumaric acid, Succinic acid, D-Glucose-6-phosphate, D-Glucose-1-phosphate, and L-Glutamine that are altered in AIF-deficient cells compared to control cells. Statistical significance was assessed with Student's t test (*, $p < 0.05$; **, $p < 0.01$; ***, $p < 0.001$; ns, $p > 0.05$). N=5.

Therefore, we investigated if other substrates could be utilized for energy production in AIF-deficient/ proficient breast cancer cell lines. Here, we used a modified MitoPlate assay, which is a metabolic screening assay comprised of 23 substrates from glycolysis, the pentose phosphate pathway (PPP), TCA cycle, anaplerotic reactions, fatty acid transport/oxidation, and one-carbon metabolism. MDA-MB-231shAIF displayed a higher capacity to utilize intermediates of glycolysis (glucose-6-phosphate), glycogen synthesis(glucose-1-phosphate), and TCA cycle's intermediates (fumarate, succinate, malate) as shown in Figure 3.9. The PPP is tightly connected to glycolysis as they share intermediates, including glucose-6-phosphate (G-6-P). Additionally, AIF-deficient MDA-MB-231 has a modest capacity to utilize tryptamine, citric, glutamine, serine, and hydroxybutyric acid more than its controls. Several TCA intermediates (succinic acid, fumarate, malic acid) were utilized more by MDA-MB-468shAIF than MDA-MB-468shLacZ as shown in Figure 3.13. However, for MCF-7, glutamine and D-Gluconate-6-phosphate are modestly consumed more in AIF-deficient cells than their counterparts as shown in Figure 3.11. Here, the capacity of cells to alter the metabolite consumption when AIF is ablated is correlated to their basal metabolic requirements.

Control experiments were conducted to verify the accuracy of the MitoPlate assays, which revealed the increased consumption of specific substrates when AIF was ablated in breast cancer. Metabolic inhibitors such as lithium chloride and lonidamine were employed to validate the accuracy of the MitoPlate assay. Lithium chloride has demonstrated anticancer properties and is known to inhibit phosphoglucomutase, which catalyzes the interconversion of glucose-1-phosphate (G-1-P) to glucose-6-phosphate (G-6-P) ([188],[189]). Therefore, AIF-deficient cells consuming more glucose-6-phosphate and glucose-1-phosphate should give an absorbance reading similar to the control cells in the presence of lithium chloride.

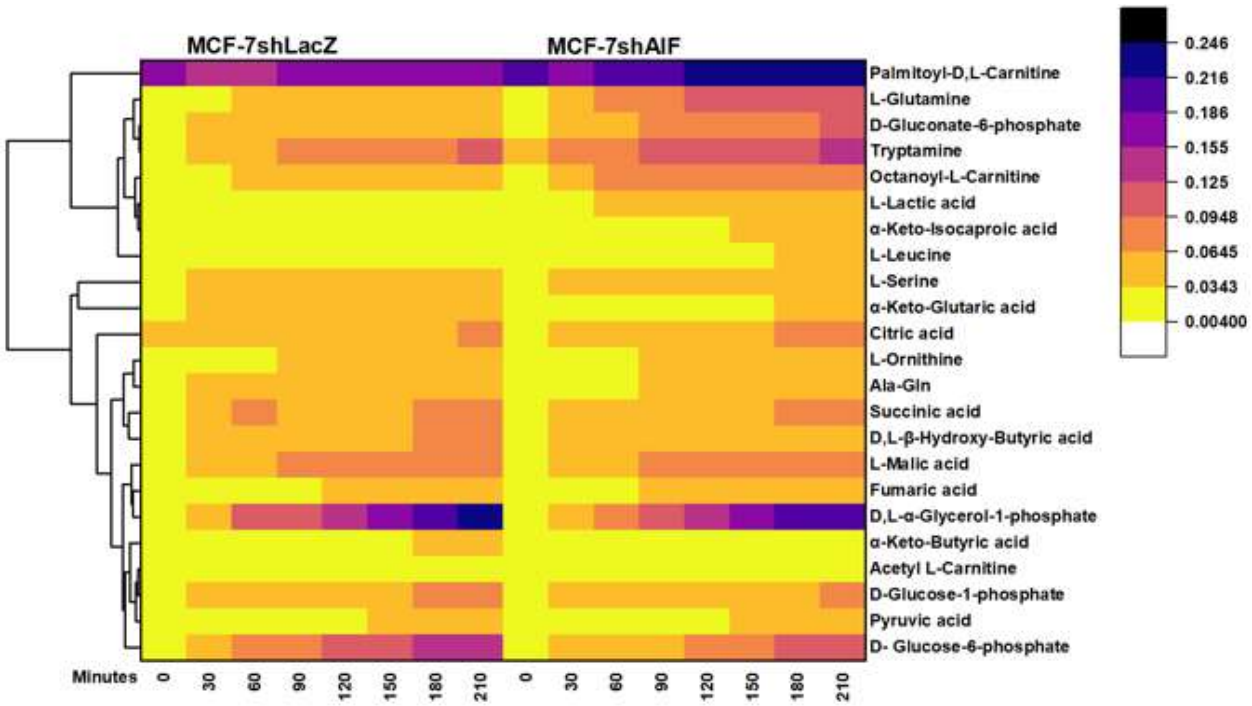

Figure 3.11: Metabolic alterations in AIF-deficient MCF-7 breast cancer cells.
To assess the mitochondrial activities, the AIF-deficient/proficient MCF-7 were transferred to a 96-well plate that also included a 100mM substrate, 6x tetrazolium-based dye and 2.4mg/ml saponin. The consumption rates of substrates were monitored by measuring the OD590 at the indicated time points (for 210 mins total). Unsupervised clustering of absorbance data was performed using OriginPro. The generated heat maps show metabolite clusters that are upregulated (blue) or downregulated (yellow) in the AIF-deficient group compared to the AIF-proficient control group. Each column represents a biological replicate from three-independent experiments; each row represents a metabolite. N=5

Lonidamine (LND) is a derivative of indazole-3-carboxylic acid and is known to inhibit mitochondrial hexokinase, inhibit the formation of fumarate and malate, and inhibit the succinate-ubiquinone reductase activity of respiratory complex II ([190],[191]). Therefore, AIF-deficient cells consuming more succinic acid should give an absorbance reading similar to the control cells in the presence of lithium chloride. From the figure 3.15(A-F), it can be observed that lithium chloride and lonidamine reverse the consumption of glucose-6-phosphate and succinic acid to the control levels, thus reinforcing our rationale and validating the efficacy of the MitoPlate assay.

To assess sensitivity to lithium chloride and lonidamine, cell viability was measured using MTT assay.

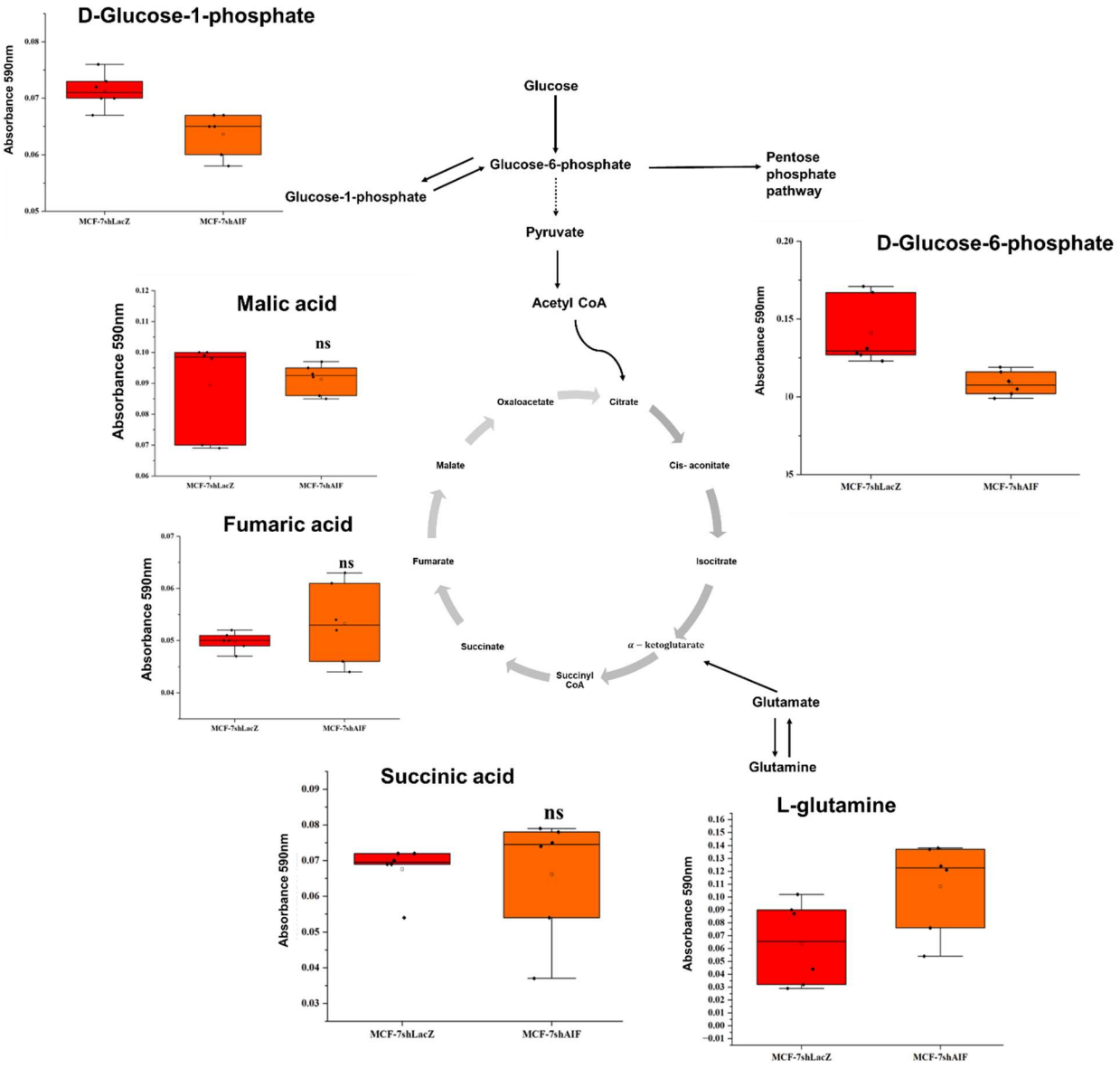

Figure 3.12: Representative boxplots of altered metabolites in AIF-deficient MCF-7 breast cancer cells.
Representative boxplots show the metabolites: Malic acid, Fumaric acid, Succinic acid, D-Glucose-6-phosphate, D-Glucose-1-phosphate, and L-Glutamine that are altered in AIF-deficient cells compared to control cells. Statistical significance was assessed with Student's t test (*, $p < 0.05$; **, $p < 0.01$; ***, $p < 0.001$; ns, $p > 0.05$). N=5.

Our results revealed that AIF-proficient MDA-MB-231 were resistant to lithium chloride, those that lack AIF displayed increased sensitivity with only 40% survival as shown in Figure 3.16A. However, both AIF-deficient/proficient MDA-MB-468 were affected after treatment with

lonidamine with AIF-deficient MDA-MB-468 exhibiting substantial sensitivity with only 30% survival as shown in Figure 3.16B. This lack of selectivity might be due to capability of lonidamine to inhibit broad range of energy-yielding processes, the selectivity and sensitivity to AIF-deficient cells can be refined by employing better formulations of metabolic inhibitors having enhanced specificity. Although we did not test a wide range of drugs; our results suggest that metabolic inhibitors can potentially increase the selectivity and sensitivity of AIF-deficient cells.

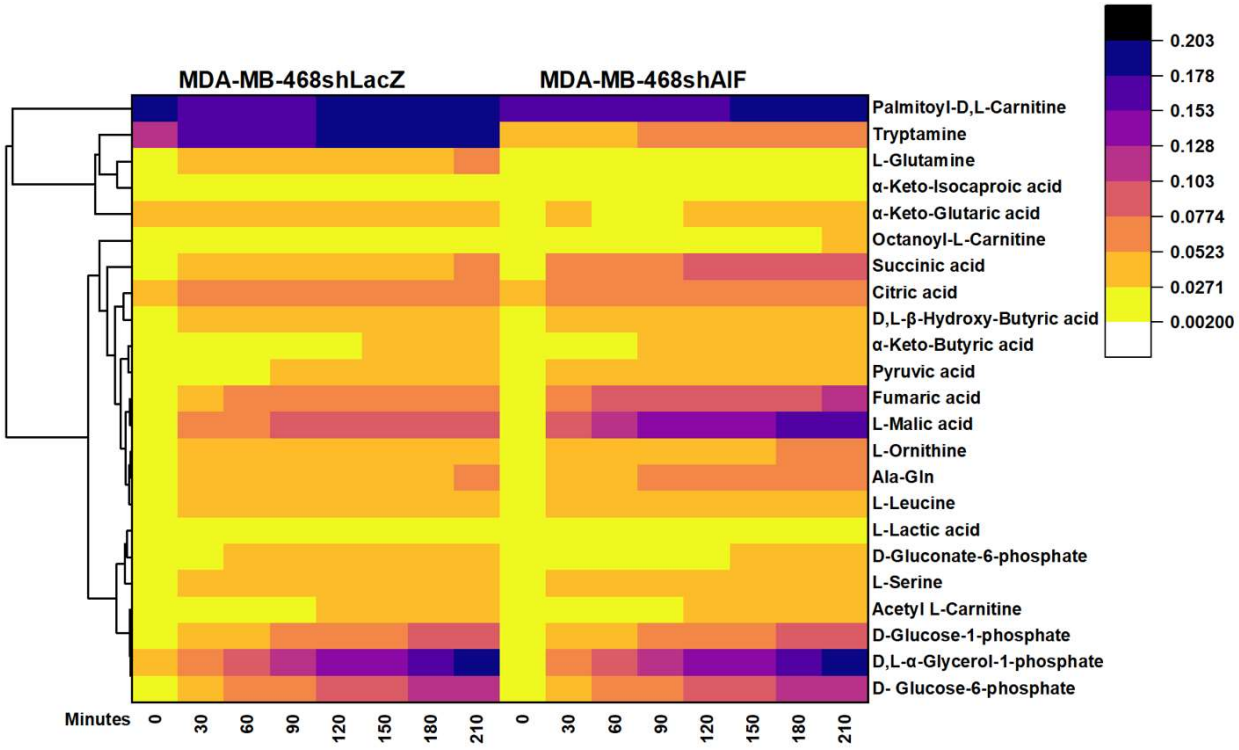

Figure 3.13: Metabolic alterations in AIF-deficient MDA-MB-468 breast cancer cells.
To assess the mitochondrial activities, AIF-deficient/proficient MDA-MB-468 were transferred to a 96-well plate that also included a 100mM substrate, 6x tetrazolium-based dye and 2.4mg/ml saponin. The consumption rates of substrates were monitored by measuring the OD590 at the indicated time points (for 210 mins total). Unsupervised clustering of absorbance data was performed using OriginPro. The generated heat maps show metabolite clusters that are upregulated (blue) or downregulated (yellow) in the AIF-deficient group compared to the AIF-proficient control group. Each column represents a biological replicate from three-independent experiments; each row represents a metabolite. N=5

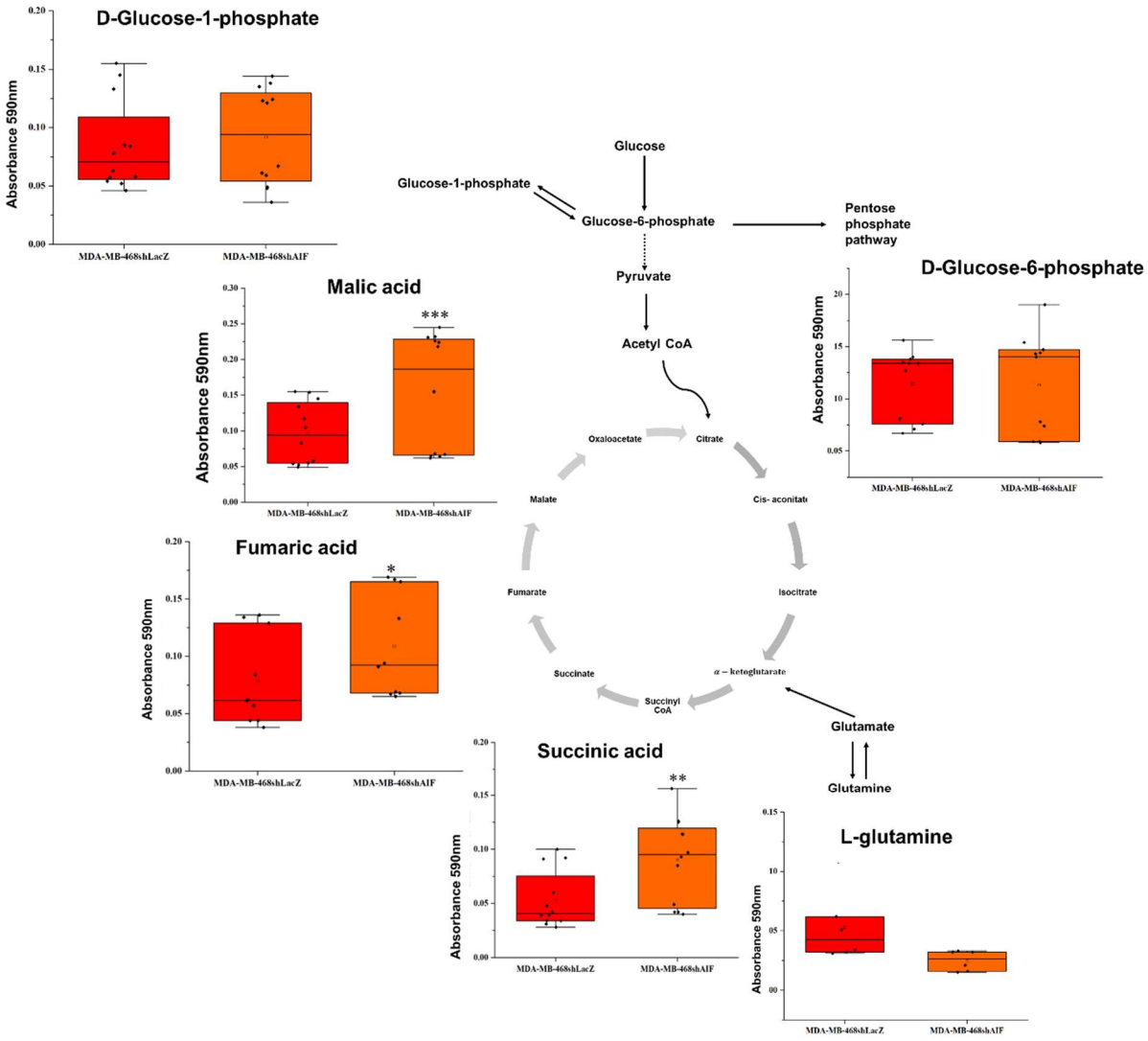

Figure 3.14: Representative boxplots of altered metabolites in AIF-deficient MDA-MB-468 breast cancer cells.
Representative boxplots show the metabolites: Malic acid, Fumaric acid, Succinic acid, D-Glucose-6-phosphate, D-Glucose-1-phosphate, and L-Glutamine that are altered in AIF-deficient cells compared to control cells. Statistical significance was assessed with Student's t test (*, $p < 0.05$; **, $p < 0.01$; ***, $p < 0.001$; ns, $p > 0.05$). N=5.

Discussion

The biological role of apoptosis-inducing factor (AIF) in inducing chromatin condensation, DNA fragmentation, and cell death in a caspase-independent manner grabbed the attention of researchers for more than two decades ([192],[60]). Studies conducted on harlequin mutant mice derived

from the inactivation of Aifm1 by proviral insertion in X-linked Aifm1 locus, showed that mice displayed higher oxidative stress and increased cerebellar degeneration ([87]). These observations implied that the apoptogenic function of AIF might be secondary and raised the possibility that its physiological functions might still be elusive. Previous studies on colorectal cancer demonstrated an elevated AIF expression and delineated the role of AIF in aiding tumor development via resisting chemical stress ([115]). In current studies, we demonstrated that AIF transcript levels are modestly elevated (less than 3-fold) in breast cancer tissues. The modest elevation of AIF expression in breast cancer cells is insufficient to trigger cell death, implying that the range of overexpression over which the increased AIF levels are either slightly advantageous or greater levels of AIF may become toxic.

An increased expression of AIF was observed in diverse cancer cell types (more than 2 fold), indicating that AIF might support tumor development contrary to its tumor-suppressive capabilities ([116],[114]). The studies have shown that AIF's enzymatic activity can regulate cellular redox signaling, which explains how overexpression of AIF in cancer might benefit cancer growth ([117],[118],[127],[124]). The catalytic activity of AIF in the JNK pathway is widespread, diverse, and dependent upon factors such as oncogene status and cellular metabolic activity; therefore, it might explain why AIF did not contribute to redox-mediated JNK activation in breast cancer as shown in Figure 3.3. From Table 1, it can be noted that our breast cancer panel is heterogeneous and differs in terms of histological grade and metabolic energy requirements. However, it was interesting to note that AIF leads to the activation of another redox-sensitive MAPK member, Extracellular signal-related kinase (ERK), in MCF-7, which is not reported in other cancer cell lines. Together this data suggests that in breast cancer, AIF-dependent redox activity might be correlated to the expression of the estrogen receptor.

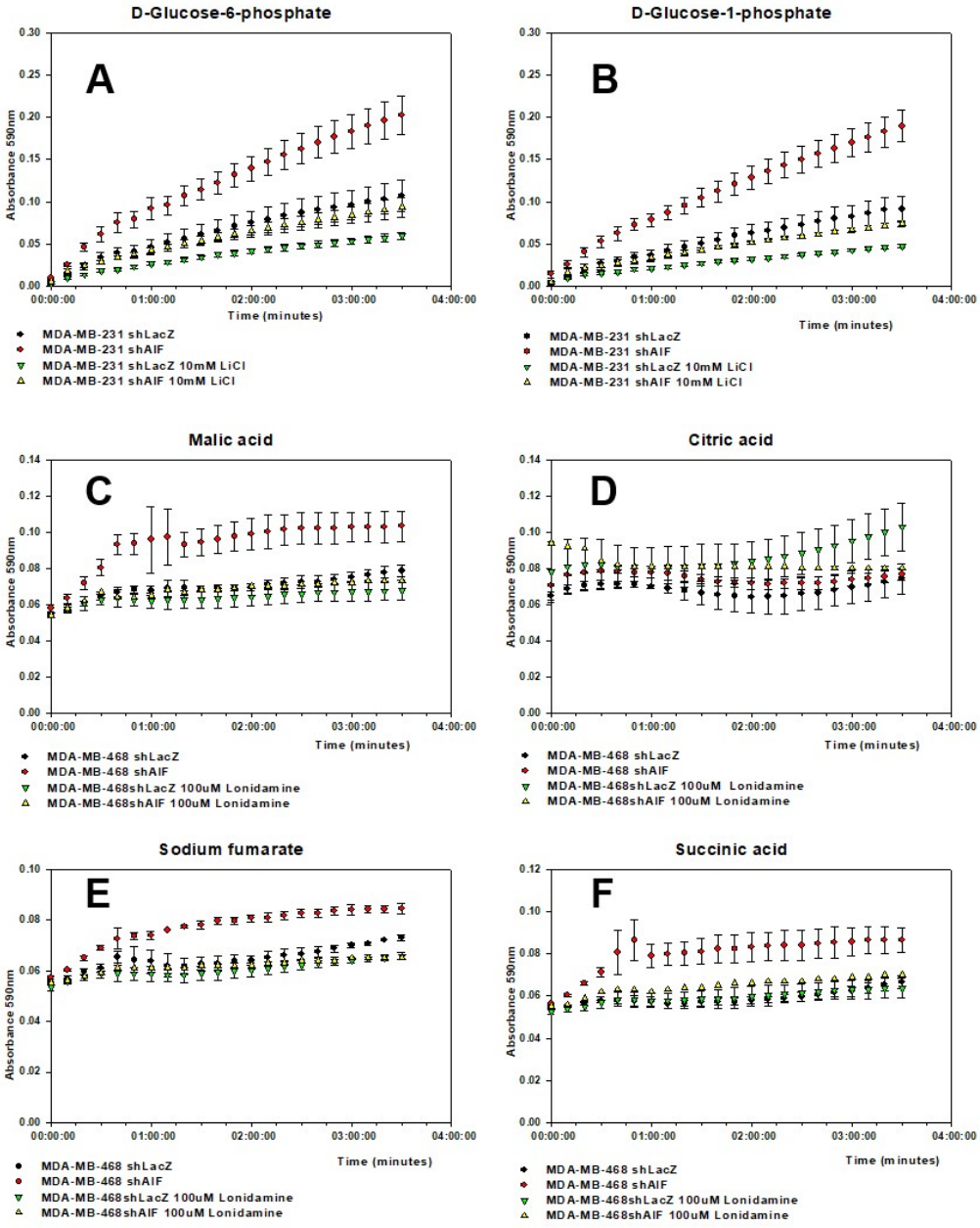

Figure 3.15: Control experiments verifying the sensitivity of AIF-deficient triple negative breast cancer cell lines to metabolic inhibitors.

The indicated cell lines were transferred to 96-well plate including the indicated substrates in presence of 10mM Lithium chloride or 100µM Lonidamine. The substrates consumption rates were measured with the modified MitoPlate assay for 210 minutes. Cells were seeded in equal densities and allowed to attach overnight before treatment with 10 mM Lithium chloride or 100µM Lonidamine. After 48-72 hours cells, viability was determined by MTT assay (Panel G-H). The data were pooled from three independent experiments. Data are shown as average ± s.e.m Statistical significance was assessed with Student's t test *, $p < 0.05$; **, $p < 0.01$; ***, $p < 0.001$; ns, $p > 0.05$). N=6.

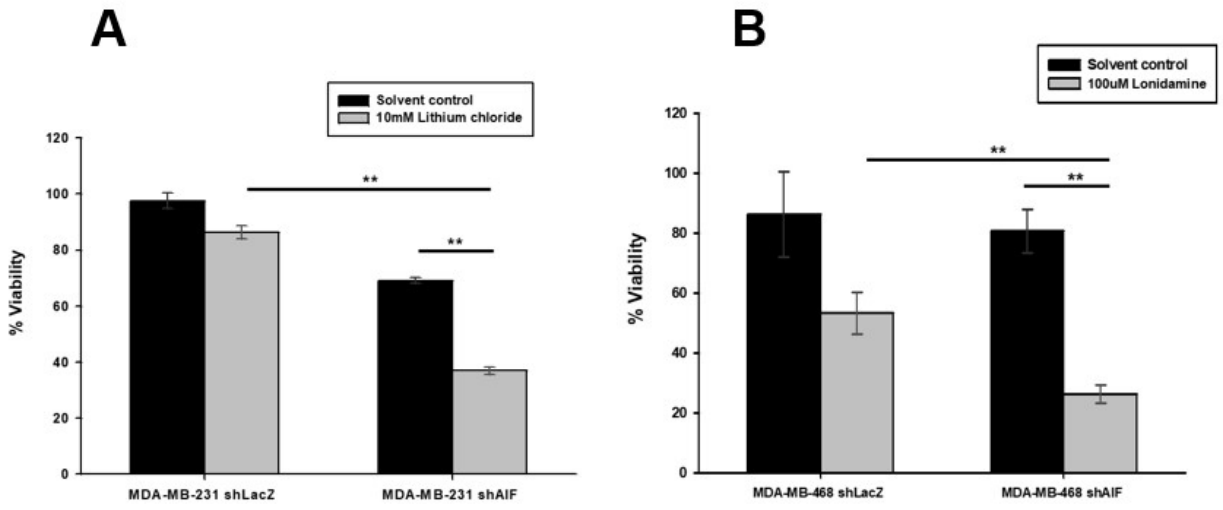

Figure 3.16: AIF-deficient triple negative breast cancer cell lines are sensitive to metabolic inhibitors.
Cells were seeded in equal densities and allowed to attach overnight before treatment with 10 mM Lithium chloride or 100µM Lonidamine. After 48-72 hours cells, viability was determined by MTT assay (Panel G-H). The data were pooled from three independent experiments. Data are shown as average ± s.e.m Statistical significance was assessed with Student's t test *, $p < 0.05$; **, $p < 0.01$; ***, $p < 0.001$; ns, $p > 0.05$). N=6.

Research on gene silencing of AIF in HeLa cells using small interfering RNA and genetic deletion of Aifm1 in mouse ES cells resulted in diminished oxygen consumption rate and increased lactate production ([88]). More studies in AIF deficient Saccharomyces cerevisiae and AIF-knockout Drosophila melanogaster displayed impaired OXPHOS due to loss of complex I and complex IV activities ([187]). Further studies implied that AIF interacts with IMS oxidoreductase CHCHD4 (coiled-coil-helix-coiled-coil-helix domain containing 4), which is the mammalian homolog of yeast Mia40. AIF interacts with the crucial component of the mitochondrial import machinery that provides oxidoreductase-mediated protein folding function along with the sulfhydryl oxidase GFER (ALR/Erv1) as a vital part of the disulfide relay system (DRS) within the mitochondrial IMS ([91],[92],[193],[93]). This line of evidence indicates that AIF indirectly assists in assembling the OXPHOS system, thus implying that dysfunctional OXPHOS impairs other mitochondrial

processes, apart from ATP synthesis ([194]). Our data show not only that AIF ablation leads to loss of complex I subunit expression but also that this loss is limited to triple-negative breast cancer. How this selectivity is achieved is unclear. Moreover, the mitochondrial status in our panel of breast cancer was affected by AIF ablation, which was undocumented in other cancer cell lines ([127]). Assessment of mitochondrial status by staining with tetramethylrhodamine ester (TMRM) and MitoTracker™ Red suggests that AIF ablation does dissipate the mitochondrial electrochemical gradient and mitochondrial abundance, which was undocumented in other cancer cell lines ([127]). Therefore, AIF likely controls complex I and might be critical for mitochondrial biogenesis restricted to triple-negative breast cancer cell lines.

The enzymatic activity of AIF is critical for the support and growth of prostate cancer and was more selective for advanced prostate cancer ([117]). In contrast, in pancreatic cancer cell lines, AIF selectively promotes the cancer progression directly related to cellular energy preferences ([118]). Presently, in breast cancer, the changes in growth rate in a nutrient-rich medium are correlated with changes in respiratory chain protein expression and concomitant alterations in glucose metabolism that were also selective for triple-negative breast cancer cell lines, an aggressive phenotype, but not based on its metabolic preferences. MDA-MB-468 cells relied on oxidative phosphorylation, demonstrating a decrease in complex I protein expression and elevated glucose consumption (approximately 6-fold) following an AIF ablation in agreement to our previous publication. MDA-MB-231 exhibits an elevated dependence on glycolysis compared to MDA-MB-468 and MCF-7 cells as shown in Table.1. In contrast to our previous publications, pancreatic cancer cell lines such as HPAF-II or MIA PaCa 2 cells addicted to glycolysis neither lost complex I subunits nor exhibited altered glucose consumption, but MDA-MB-231 displayed a reduction in all three subunits of complex I protein expression. A similar trend is observed that supports the

hypothesis that the role of AIF in maintaining efficient mitochondrial electron transport becomes more critical as cells become more aggressive.

AIF-deficient MDA-MB-231 and MDA-MB-468 displayed a metabolic phenotype of increased glucose consumption, but surprisingly, it was observed that AIF-deficient MDA-MB-231 and MDA-MB-468 cell lines were not selectively sensitized to glycolytic disruption with 2-deoxyglucose treatment as shown in Figure 3.8. Table 1 shows that MDA-MB-231 is already addicted to glycolysis; thus, AIF ablation would not aggravate the glycolytic disruption further. However, MDA-MB-468, which exhibits the greatest bias towards basal utilization of oxidative metabolism, did not demonstrate sensitivity to glycolytic disruption. The only possible explanation is that MDA-MB-468 cells exhibit the greatest metabolic flexibility, and thus, they can circumvent glycolytic disruption ([180]). Previously, we have shown that AIF plays a critical role in pancreatic cancer by inducing the cells to be reliant on glycolysis ([118]); however, AIF activity can be maximally exploited when a cell possessing a metabolic phenotype relies on a fuel source distinct from glucose. Therefore, we performed an experiment aimed at identifying additional metabolic substrates that are altered due to AIF ablation in our panel of breast cancer using a modified MitoPlate assay. Our Mitoplate assay shows that most of the consumption of Krebs cycle intermediate's such as succinate, malate, and fumarate was upregulated in AIF-deficient triple-negative breast cancer cells than their control cells. The increased mitochondrial metabolism in AIF-deficient cells can be attributed to the fact that cells with mitochondrial defects use bidirectional metabolism of the TCA cycle ([195]). The TCA cycle not only generates reducing equivalents for oxidative phosphorylation but also maintains pools of biosynthetic precursors that feed biosynthetic pathways to produce lipids, proteins, and nucleic acid ([196]). Increased consumption of succinic acid in AIF-deficient TNBCs can be due to the increased respiratory

capacity in order to compensate for complex I deficiency ([197]). Thus, succinic acid can provide reducing equivalents to complex II or replenish the pool of TCA cycle intermediate to bypass the complex I deficiency in both (OXPHOS-dependent) MDA-MB-468 and (glycolytic-dependent) MDA-MB-231. However, lonidamine, an inhibitor of succinate-ubiquinone reductase activity of respiratory Complex II, selectively inhibits AIF-deficient MDA-MB-468 but not MDA-MB-231 (data not shown) as MDA-MB-231 is glycolytic and lonidamine also targets hexokinase activity. The glycolytic phenotype in MDA-MB-231 can be due to the high preference to glycolysis rather than defects in mitochondrial function ([198]). In addition to TCA cycle intermediates, MDA-MB-231 consumes (more than 2-fold) glucose-6-phosphate and glucose-1-phosphate when AIF is ablated. However, it should be noted that glucose-6-phosphate can interconvert into glucose-1-phosphate. Both can act as a hub to metabolically connect glycolysis, the pentose phosphate pathway, glycogen synthesis, de novo lipogenesis, and the hexosamine pathway ([199],[200]). There has been increasing evidence of glycogen metabolism contributing to MDA-MB-231 growth, and oncogenic factors such as c-myc are likely upstream candidates to modulate glycogen metabolism ([201],[202],[203],[204],[205],[206],[207]). Lithium chloride is a potent inhibitor of phosphoglucomutase activity resulting in alterations in glucose-phosphate levels ([188],[189]). Therefore, lithium chloride inhibited AIF-deficient MDA-MB-231 more than their controls. The variations in substrate consumption in our panel of AIF-deficient breast cancer can potentially be correlated to their basal metabolic status, oncogenic status, or MAPK regulators. Additionally, we would like to emphasize that our study was conducted in an *in-vitro* 2D cell culture system; thus, our future goal is to conduct these experiments in a clinically relevant sample, such as patient-derived tissues or animal models, as their heterogeneity contributes to the metabolic reprogramming. Also, investigating the

involvement of the enzymatic activity of AIF in limiting metabolic flexibility can be another parameter to consider.

Based on our current data, we propose that AIF activity can be maximally exploited in aggressive breast cancer as it switches from metabolic plasticity to metabolic dependencies. At present, the molecular mechanism defining AIF's role in breast cancer remains to be investigated. However, our current and previous studies highlight how mitochondrial dynamics and ERK pathway might be involved in breast cancer in an AIF-dependent manner, which was undocumented in other cancers. Also, current studies provide a potential framework for how AIF-mediated therapy, in combination with an existing or new formulation of metabolic inhibitors, can increase the sensitivity and selectivity of hormone-independent breast tumors and can be exploited for neoadjuvant or adjuvant chemotherapy.

IV. SUMMARY, CONCLUDING REMARKS, AND FUTURE DIRECTIONS

The pro-survival activity of AIF benefits tumorigenesis

In 1996, Kroemer et al. first demonstrated the role of AIF in inducing cell death in a caspase-independent manner ([65]). However, contrary to its name and initial characterization, AIF does not function as a universal cell death effector. In contrast to apoptogenic activity, AIF also possesses intrinsic NADH oxidase activity that plays a critical role in maintaining the mitochondrial structure and function ([64]). In healthy cells, AIF is required to regulate mitochondrial bioenergetics through regulating ETC protein subunits, metabolic flux, and cellular redox state, as observed in knockout studies in mice and clinical mutations in humans ([121]).

Thus, the pro-survival activity of AIF in normal cells is poised to benefit cancer cell growth, survival, and mitochondrial homeostasis. An increased expression of AIF was observed in diverse cancer cell types, bolstering that AIF might support tumorigenesis contrary to its tumor-suppressive capabilities. Urbano *et al.* were the first to demonstrate that AIF promotes increased chemoresistance in colorectal cancer, suggesting that AIF might represent a novel drug target.

The work in our lab demonstrated the significance of the enzymatic activity of AIF for aggressiveness and metabolism of prostate cancer, but not early-stage prostate cancer cells, a prostate cancer that grows slowly and has not disseminated outside the prostate gland. When AIF was ablated, decreased levels of complex I, changes in growth rate, alteration in glucose metabolism, and lactate secretion were observed in advanced prostate cancer cells. Subsequent published data implicated that the enzymatic activity of AIF was required for the activation of JNK, a redox-sensitive MAPK. AIF also promoted the cadherin switch in PC3 by activating JNK1. Altogether, these data strongly suggest that AIF plays a critical role in advanced prostate cancer cell lines by mediating mitochondrial metabolism and AIF-mediated JNK signaling. Additional

publications from our lab demonstrated that AIF supports metabolically defined pancreatic cancer growth and survival. A spectrum of metabolic sensitivity to AIF ablation was observed in pancreatic cancer, which was not identified in prostate cancer. Overall, the basal energetic requirements of pancreatic cancer cells determine the ability of AIF to support metabolic plasticity that benefits growth and survival. AIF was regarded as a metabolic sensor, thus projecting it as a promising novel therapeutic target.

The physiological role of AIF in redox-signaling and mitochondrial metabolism unleashed the diverse possible functions of AIF but gives rise to more open-ended questions. Is AIF dependence associated with metabolic phenotype a unique feature of pancreatic cancer, or more cancer types? Further is the AIF-mediated signaling and metabolic activity relevant in a 3D cell culture model system? Therefore, the work presented in chapters 2 and 3 sought to answer the above questions and explore the potential of AIF as a therapeutic target.

AIF promotes a cadherin switch in 3D PDAC, unreported in the 2D monolayer

The enzymatic activity of AIF promotes the JNK1-mediated cadherin switch in the 2D monolayer culture of prostate cancer cells, PC3. We then questioned whether AIF-mediated cadherin switching was a unique feature of PC3 or whether a need to employ a different cell culture system was necessary

Pancreatic ductal adenocarcinoma (PDAC) is one of the most aggressive cancers and are difficult to treat as it metastasizes to distant sites. PANC1 and HPAC that differs in metabolic phenotype were employed to assess the significance of AIF in metastasis. However, the study was conducted in a 3D cell culture system as it is one of the best-characterized models to reflect the in vivo behavior of cells in tumor tissues as cells display nutrient and oxygen gradients, complex cell-cell and cell-extracellular matrix (ECM) contact interactions ([44],[142]).

Using methylcellulose as an additive in hanging drop proved to generate 3D spheroids of AIF-deficient/proficient PDAC cells as these cells are weak in self-aggregating. The characteristics of AIF-deficient PDAC were different from AIF-proficient PDAC in terms of viability, diameter size, and area of the spheroids. The diameter of 3D spheroids was also more than 400 μm, suggesting the presence of a hypoxia core. Immunoblot analysis demonstrated the involvement of AIF in promoting cadherin switch when PDACs were grown as 3D spheroids. The mechanism by which AIF might affect the downregulation of E-cadherin may be attributed to XIAP, one of the pro-survival binding partners of AIF. XIAP, an E3 ubiquitin ligase, ubiquitinates and induces E-cadherin endocytosis and promotes migration by activating TGF-β mediated EMT.([208]). Another speculation is the involvement of the ERK pathway in the regulation of the EMT. In chapter 3, we demonstrated AIF-mediated ROS-dependent ERK activation. And ERK is required to disassemble cell adherent's junctions and induce cell motility by TGF-β ([209]). Therefore, likely crosstalk between TGF-β signaling and AIF-mediated ERK signaling needs further investigation.

The EMT markers such as E-cadherin and N-cadherin were undetectable in 2D as 2D monolayer fails to exhibit strong cell-cell or cell-matrix interactions. The metabolic significance of AIF in 3D was revealed by increased glucose consumption in AIF-deficient PANC1 and HPAC cancer cell lines. However, the magnitude of increased glucose consumption was correlated to the metabolic phenotype of PDACs. Therefore, 3D spheroids of AIF-deficient PANC1 were more sensitized to glycolytic disruption as AIF-deficient spheroids lost their integrity and robustness after 2-deoxyglucose treatment. Altogether, these data demonstrated the metabolic significance of AIF and revealed a likely axis of AIF/E-cadherin/N-cadherin/ tumor size. The *in vivo* studies will better bolster the proposed axis of AIF supporting the growth of the tumor as shown in Figure 4.1.

Future studies can be extended to additional cancer cell lines in a more complex 3D system, such as a heterogenous 3D cell culture system or organoids, to understand the significance of AIF. The intricate architecture of the 3D cell culture model will provide a better understanding of AIF-mediated cellular signaling and AIF-mediated targeted therapy as it mimics the native ECM microenvironment. The metabolic function of AIF in 3D culture can further be expanded to identify additional substrates being altered in AIF-deficient cancer cell lines using MitoPlate and then employ appropriate metabolic inhibitors to inhibit cancer cells in an AIF-dependent manner.

Expanding the spectrum of AIF metabolic activity in breast cancer

The pro-survival activity and metabolic contribution of AIF increase with disease progression and are associated with an aggressive phenotype, as observed in prostate and pancreatic cancer ([117],[127]). Breast cancer is heterogenous and can be classified into clinical subtypes. TNBCs are considered the most aggressive breast cancer as they resist hormone-dependent therapy. Therefore, it was hypothesized that AIF might be well-positioned to influence TNBCs that critically rely on metabolic reprogramming for growth and survival.

The evaluation of AIF's role in breast cancer revealed an essential role for AIF-dependent metabolism in pancreatic tumorigenesis. The panel of breast cancer cell lines (MDA-MB-231, MCF-7, and MDA-MB-468) was selected to reflect diversity in metabolic requirements and clinical subtypes. A stable knockdown of AIF in breast cancer cell lines revealed a decrease in protein expression of complex I subunits, increased glucose consumption, and impaired cell growth. These observations were seen in TNBCs, considered an aggressive form of breast cancer, concurrent to our previous findings where AIF ablation affected the advanced prostate cancer cells. However, this spectrum of alterations was not correlated to metabolic sensitivity as observed in pancreatic cancer cells but based on its clinical subtype. Moreover, changes in membrane potential

and mitochondrial abundance were observed in AIF-deficient triple-negative breast cancer cell lines (MDA-MB 231 and MDA-MB-468), which were undocumented in other cancer cell types tested in our lab. Tissue-specific AIF knockout studies in mice demonstrated reduced activation of the PGC1α pathway ([210]). And peroxisome proliferator-activated receptor-gamma coactivator 1 alpha (PGC-1α) is the central regulator of mitochondrial biogenesis ([211]). Analysis of invasive breast cancer also revealed overexpression of Drp1, which has been implicated with the upregulation of mitochondrial biogenesis in breast cancer ([212]). The AIF ablation sensitivity in breast cancer was different than that observed in pancreatic or prostate cancer due to the heterogeneous characteristics of breast cancer. Relative to other cancer, breast cancer exhibits a complex overlap of clinical subtype and metabolic phenotype, which is not reported in pancreatic or prostate cancer. Additional factors such as oncogenic status (KRAS, PI3K, Akt, and c-MYC) and tumor suppressor genes (p53 and AMPK) in breast cancer might interact with cell signaling and epigenetic pathways orchestrating the network of metabolic adaptations, which in turn influence breast cancer progression ([3]).

In pancreatic cancer, AIF sensitivity was maximized when the cancer cells were dependent on OXPHOS; however, in the breast cancer cell lines, MDA-MB-468, regarded as OXPHOS-dependent, was insensitive to glycolytic disruption when AIF was ablated. This was attributed to the metabolic flexibility of MDA-MB-468 to circumvent the AIF deficiency. However, this data led to the exploration of additional metabolic substrates other than glucose that are altered due to AIF ablation in our panel of breast cancer using a modified MitoPlate assay. Mitoplate assay identified an upregulation in the consumption of intermediates of glycolysis (glucose-6-phosphate), glycogen synthesis(glucose-1-phosphate) in MDA-MB-231; TCA intermediates (fumarate, succinate, malate) in MDA-MB-468; and glutamine consumption was modestly

elevated in MCF-7 when AIF was ablated. These data gave a novel insight into employing metabolic inhibitors such as lonidamine and lithium chloride to inhibit triple-negative breast cancer in an AIF-dependent manner. The MitoPlate assay highlights the identification of oncometabolite and provides potential therapeutic opportunities for targeting the TCA cycle intermediates in cancer cells. To date, fumarate and succinate have been characterized as bona fide oncometabolites ([213]). The TCA cycle intermediates qualify more than the ordinary intermediate as the intermediates can act as effector molecules to activate or inhibit signaling pathways or assume cytokine-like or chemokine-like roles ([214]). Overall, these suggest that AIF exerts its pro-tumorigenic role by modulating oncometabolite abundance. Altogether, the data conveys that AIF activity can be maximally exploited in aggressive breast cancer as it switches from metabolic plasticity to metabolic dependencies.

Future experiments should focus on investigating the molecular mechanism defining the role of AIF in breast cancer and also define the enzymatic activity of AIF in breast cancer progression. The present study observed AIF-mediated ROS-dependent ERK activation in MCF-7, a non-invasive breast cancer, which was undocumented in other cancers. Therefore, identifying downstream or upstream effectors in AIF-mediated ERK activation will draw a detailed picture of AIF in MAPK signaling. We also questioned the ability of AIF to influence other redox sensitive pathways that needs further investigation. Moreover, the Mitoplate assay allowed the identification of substrates involved in myriad biochemical pathways that can be extended to additional cancer, including prostate and pancreatic cancer. Also, current studies provide a potential framework to employ a combination of existing or new formulations of metabolic inhibitors to increase the sensitivity and selectivity of a tumor in an AIF-dependent manner that can be exploited for neoadjuvant or adjuvant chemotherapy. Cell-targeted delivery such as liposome-based, gold-, and

magnetic-nanoparticle-based delivery systems can reduce the overall toxicity of cytotoxic drugs and increase their effectiveness and selectivity.

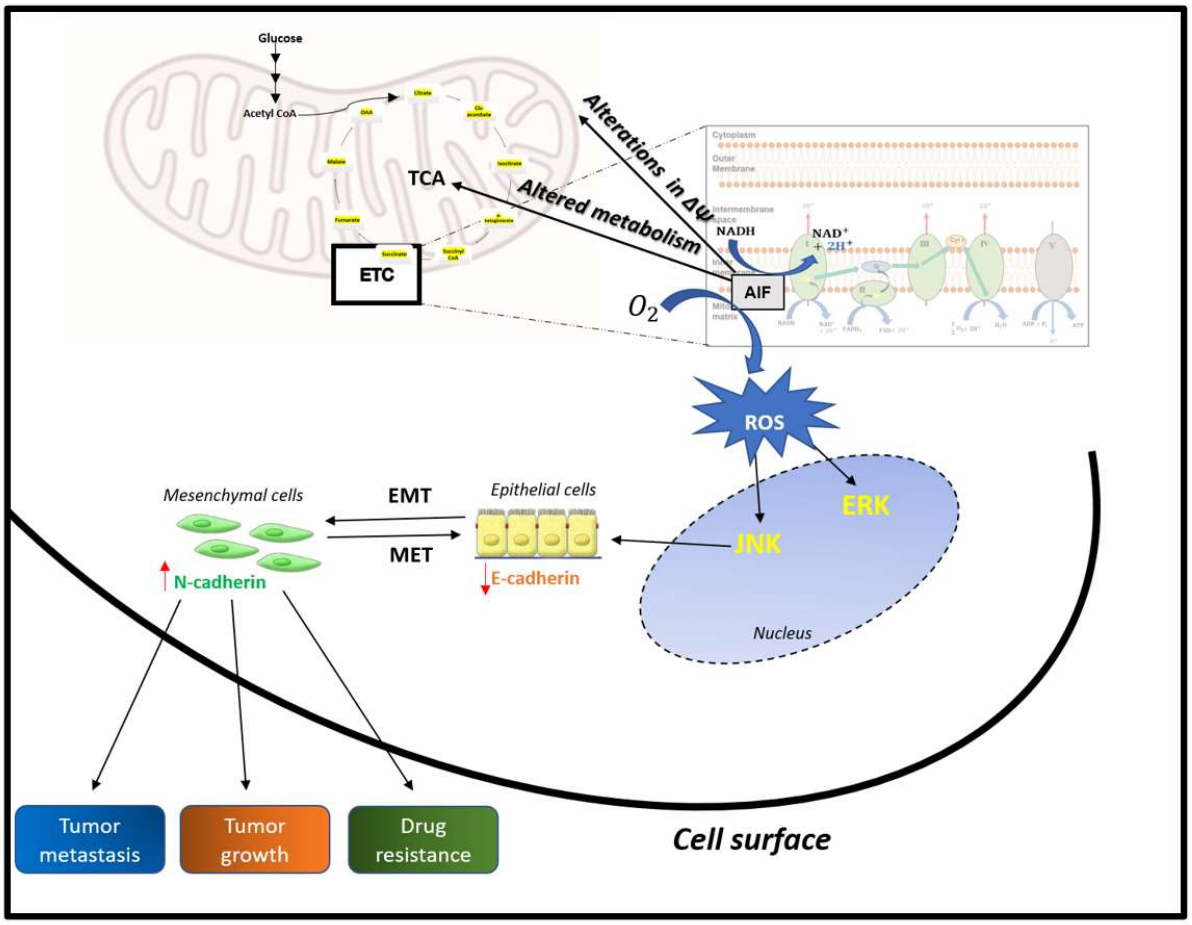

Figure 4.1: Proposed mechanism of AIF-mediated control of metabolism, mitochondrial dynamics, and redox-signaling observed in various cancers.
AIF activity promotes redox-signaling regulating EMT. AIF regulates metabolism by modulating the TCA cycle's intermediates. AIF activity mediates the control of membrane potential. AIF activity mediated ROS-dependent ERK and JNK activation. (Note: The spectrum of AIF-mediated regulation can be cancer-specific).

Conclusions

Altogether, the present study underscores the pleiotropic role of AIF in mediating a balance among different hallmarks of cancer, notably 1) resists cell death, 2) activates metastasis, 3) sustains proliferative signaling, and 4) deregulates cellular metabolism as proposed in Figure 4.1. The significance of AIF in a complex 3D environment reinforces the impact of AIF on cadherin switch and metabolic function. The metabolic function of AIF modulates cellular activities, including metabolism, ERK signaling, and mitochondrial biogenesis in breast cancer as shown in Figure 4.1. The current study highlighted AIF activity in modulating TCA cycle metabolites, especially succinic acid and fumarate, a bonafide oncometabolite. These provide a fresh insight into cancer metabolism, which was predisposed by the Warburg effect. Overall, AIF plays a pivotal role in identifying metabolic vulnerabilities for therapeutic interventions, eventually bringing targeted metabolomics to fruition.

REFERENCES

(1) Glück, S.; Ross, J. S.; Royce, M.; McKenna, E. F., Jr.; Perou, C. M.; Avisar, E.; Wu, L. TP53 genomics predict higher clinical and pathologic tumor response in operable early-stage breast cancer treated with docetaxel-capecitabine ± trastuzumab. *Breast Cancer Res Treat* **2012**, *132* (3), 781-791. DOI: 10.1007/s10549-011-1412-7.

(2) Richardson, A. L.; Wang, Z. C.; De Nicolo, A.; Lu, X.; Brown, M.; Miron, A.; Liao, X.; Iglehart, J. D.; Livingston, D. M.; Ganesan, S. X chromosomal abnormalities in basal-like human breast cancer. *Cancer Cell* **2006**, *9* (2), 121-132. DOI: 10.1016/j.ccr.2006.01.013

(3) Ripoll, C.; Roldan, M.; Ruedas-Rama, M. J.; Orte, A.; Martin, M. Breast Cancer Cell Subtypes Display Different Metabolic Phenotypes That Correlate with Their Clinical Classification. *Biology (Basel)* **2021**, *10* (12). DOI: 10.3390/biology10121267.

(4) Rhodes, D. R.; Yu, J.; Shanker, K.; Deshpande, N.; Varambally, R.; Ghosh, D.; Barrette, T.; Pandey, A.; Chinnaiyan, A. M. ONCOMINE: a cancer microarray database and integrated data-mining platform. *Neoplasia* **2004**, *6* (1), 1-6. DOI: 10.1016/s1476-5586(04)80047-2.

(5) Kühlbrandt, W. Structure and function of mitochondrial membrane protein complexes. *BMC Biol* **2015**, *13*, 89. DOI: 10.1186/s12915-015-0201-x.

(6) Rizzuto, R.; De Stefani, D.; Raffaello, A.; Mammucari, C. Mitochondria as sensors and regulators of calcium signalling. *Nat Rev Mol Cell Biol* **2012**, *13* (9), 566-578. DOI: 10.1038/nrm3412 .

(7) Pellegrino, M. W.; Haynes, C. M. Mitophagy and the mitochondrial unfolded protein response in neurodegeneration and bacterial infection. *BMC Biol* **2015**, *13*, 22. DOI: 10.1186/s12915-015-0129-1

(8) Chandel, N. S. Mitochondria as signaling organelles. *BMC Biol* **2014**, *12*, 34. DOI: 10.1186/1741-7007-12-34

(9) McCarron, J. G.; Wilson, C.; Sandison, M. E.; Olson, M. L.; Girkin, J. M.; Saunter, C.; Chalmers, S. From structure to function: mitochondrial morphology, motion and shaping in vascular smooth muscle. *J Vasc Res* **2013**, *50* (5), 357-371. DOI: 10.1159/000353883

(10) Shami, G. J.; Cheng, D.; Verhaegh, P.; Koek, G.; Wisse, E.; Braet, F. Three-dimensional ultrastructure of giant mitochondria in human non-alcoholic fatty liver disease. *Sci Rep* **2021**, *11* (1), 3319. DOI: 10.1038/s41598-021-82884-z

(11) Jaipargas, E. A.; Barton, K. A.; Mathur, N.; Mathur, J. Mitochondrial pleomorphy in plant cells is driven by contiguous ER dynamics. *Front Plant Sci* **2015**, *6*, 783. DOI: 10.3389/fpls.2015.00783

(12) Wu, Z.; Ho, W. S.; Lu, R. Targeting Mitochondrial Oxidative Phosphorylation in Glioblastoma Therapy. *Neuromolecular Med* **2022**, *24* (1), 18-22. DOI: 10.1007/s12017-021-08678-8

(13) Zorov, D. B.; Juhaszova, M.; Sollott, S. J. Mitochondrial reactive oxygen species (ROS) and ROS-induced ROS release. *Physiol Rev* **2014**, *94* (3), 909-950. DOI: 10.1152/physrev.00026.2013

(14) Sena, L. A.; Chandel, N. S. Physiological roles of mitochondrial reactive oxygen species. *Mol Cell* **2012**, *48* (2), 158-167. DOI: 10.1016/j.molcel.2012.09.025

(15) Comhair, S. A.; Erzurum, S. C. Redox control of asthma: molecular mechanisms and therapeutic opportunities. *Antioxid Redox Signal* **2010**, *12* (1), 93-124. DOI: 10.1089/ars.2008.2425

(16) Kim, Y. W.; Byzova, T. V. Oxidative stress in angiogenesis and vascular disease. *Blood* **2014**, *123* (5), 625-631. DOI: 10.1182/blood-2013-09-512749

(17) Liu, Z.; Ren, Z.; Zhang, J.; Chuang, C. C.; Kandaswamy, E.; Zhou, T.; Zuo, L. Role of ROS and Nutritional Antioxidants in Human Diseases. *Front Physiol* **2018**, *9*, 477. DOI: 10.3389/fphys.2018.00477

(18) Di Meo, S.; Reed, T. T.; Venditti, P.; Victor, V. M. Role of ROS and RNS Sources in Physiological and Pathological Conditions. *Oxid Med Cell Longev* **2016**, *2016*, 1245049. DOI: 10.1155/2016/1245049

(19) Yadav, D. K.; Kumar, S.; Choi, E. H.; Chaudhary, S.; Kim, M. H. Molecular dynamic simulations of oxidized skin lipid bilayer and permeability of reactive oxygen species. *Sci Rep* **2019**, *9* (1), 4496. DOI: 10.1038/s41598-019-40913-y

(20) Nguyen, G. T.; Green, E. R.; Mecsas, J. Neutrophils to the ROScue: Mechanisms of NADPH Oxidase Activation and Bacterial Resistance. *Front Cell Infect Microbiol* **2017**, *7*, 373. DOI: 10.3389/fcimb.2017.00373

(21) Chance, B.; Sies, H.; Boveris, A. Hydroperoxide metabolism in mammalian organs. *Physiol Rev* **1979**, *59* (3), 527-605. DOI: 10.1152/physrev.1979.59.3.527

(22) Zorov, D. B.; Bannikova, S. Y.; Belousov, V. V.; Vyssokikh, M. Y.; Zorova, L. D.; Isaev, N. K.; Krasnikov, B. F.; Plotnikov, E. Y. Reactive oxygen and nitrogen species: friends or foes? *Biochemistry (Mosc)* **2005**, *70* (2), 215-221. DOI: 10.1007/s10541-005-0103-6

(23) Runkel, E. D.; Baumeister, R.; Schulze, E. Mitochondrial stress: balancing friend and foe. *Exp Gerontol* **2014**, *56*, 194-201. DOI: 10.1016/j.exger.2014.02.013

(24) Verbon, E. H.; Post, J. A.; Boonstra, J. The influence of reactive oxygen species on cell cycle progression in mammalian cells. *Gene* **2012**, *511* (1), 1-6. DOI: 10.1016/j.gene.2012.08.038

(25) Juhaszova, M.; Rabuel, C.; Zorov, D. B.; Lakatta, E. G.; Sollott, S. J. Protection in the aged heart: preventing the heart-break of old age? *Cardiovasc Res* **2005**, *66* (2), 233-244. DOI: 10.1016/j.cardiores.2004.12.020

(26) Rovini, A.; Heslop, K.; Hunt, E. G.; Morris, M. E.; Fang, D.; Gooz, M.; Gerencser, A. A.; Maldonado, E. N. Quantitative analysis of mitochondrial membrane potential heterogeneity in unsynchronized and synchronized cancer cells. *Faseb j* **2021**, *35* (1), e21148. DOI: 10.1096/fj.202001693R

(27) Nicholls, D. G.; Budd, S. L. Mitochondria and neuronal survival. *Physiol Rev* **2000**, *80* (1), 315-360. DOI: 10.1152/physrev.2000.80.1.315

(28) Zorova, L. D.; Popkov, V. A.; Plotnikov, E. Y.; Silachev, D. N.; Pevzner, I. B.; Jankauskas, S. S.; Babenko, V. A.; Zorov, S. D.; Balakireva, A. V.; Juhaszova, M.; et al. Mitochondrial membrane potential. *Analytical Biochemistry* **2018**, *552*, 50-59.

(29) Korshunov, S. S.; Skulachev, V. P.; Starkov, A. A. High protonic potential actuates a mechanism of production of reactive oxygen species in mitochondria. *FEBS Lett* **1997**, *416* (1), 15-18. DOI: 10.1016/s0014-5793(97)01159-9

(30) Jin, S. M.; Lazarou, M.; Wang, C.; Kane, L. A.; Narendra, D. P.; Youle, R. J. Mitochondrial membrane potential regulates PINK1 import and proteolytic destabilization by PARL. *J Cell Biol* **2010**, *191* (5), 933-942. DOI: 10.1083/jcb.201008084

(31) Ma, K.; Chen, G.; Li, W.; Kepp, O.; Zhu, Y.; Chen, Q. Mitophagy, Mitochondrial Homeostasis, and Cell Fate. *Front Cell Dev Biol* **2020**, *8*, 467. DOI: 10.3389/fcell.2020.00467

(32) Michel, S.; Wanet, A.; De Pauw, A.; Rommelaere, G.; Arnould, T.; Renard, P. Crosstalk between mitochondrial (dys)function and mitochondrial abundance. *J Cell Physiol* **2012**, *227* (6), 2297-2310. DOI: 10.1002/jcp.23021

(33) Yamamori, T.; Sasagawa, T.; Ichii, O.; Hiyoshi, M.; Bo, T.; Yasui, H.; Kon, Y.; Inanami, O. Analysis of the mechanism of radiation-induced upregulation of mitochondrial abundance in mouse fibroblasts. *J Radiat Res* **2017**, *58* (3), 292-301. DOI: 10.1093/jrr/rrw113

(34) Swerdlow, R. H. Role and treatment of mitochondrial DNA-related mitochondrial dysfunction in sporadic neurodegenerative diseases. *Curr Pharm Des* **2011**, *17* (31), 3356-3373. DOI: 10.2174/138161211798072535

(35) van Loo, G.; Saelens, X.; van Gurp, M.; MacFarlane, M.; Martin, S. J.; Vandenabeele, P. The role of mitochondrial factors in apoptosis: a Russian roulette with more than one bullet. *Cell Death Differ* **2002**, *9* (10), 1031-1042. DOI: 10.1038/sj.cdd.4401088

(36) Green, D. R.; Llambi, F. Cell Death Signaling. *Cold Spring Harb Perspect Biol* **2015**, *7* (12). DOI: 10.1101/cshperspect.a006080

(37) Chen, Y.; Hua, Y.; Li, X.; Arslan, I. M.; Zhang, W.; Meng, G. Distinct Types of Cell Death and the Implication in Diabetic Cardiomyopathy. *Front Pharmacol* **2020**, *11*, 42. DOI: 10.3389/fphar.2020.00042

(38) Jeong, S. Y.; Seol, D. W. The role of mitochondria in apoptosis. *BMB Rep* **2008**, *41* (1), 11-22. DOI: 10.5483/bmbrep.2008.41.1.011

(39) Wong, R. S. Apoptosis in cancer: from pathogenesis to treatment. *J Exp Clin Cancer Res* **2011**, *30* (1), 87. DOI: 10.1186/1756-9966-30-87

(40) Fink, S. L.; Cookson, B. T. Apoptosis, pyroptosis, and necrosis: mechanistic description of dead and dying eukaryotic cells. *Infect Immun* **2005**, *73* (4), 1907-1916. DOI: 10.1128/iai.73.4.1907-1916.2005

(41) Elmore, S. Apoptosis: a review of programmed cell death. *Toxicol Pathol* **2007**, *35* (4), 495-516. DOI: 10.1080/01926230701320337

(42) Ferreira, L. P.; Gaspar, V. M.; Mano, J. F. Design of spherically structured 3D in vitro tumor models -Advances and prospects. *Acta Biomater* **2018**, *75*, 11-34. DOI: 10.1016/j.actbio.2018.05.034

(43) Ingber, D. E. Human organs-on-chips for disease modelling, drug development and personalized medicine. *Nat Rev Genet* **2022**, *23* (8), 467-491. DOI: 10.1038/s41576-022-00466-9

(44) Lv, D.; Hu, Z.; Lu, L.; Lu, H.; Xu, X. Three-dimensional cell culture: A powerful tool in tumor research and drug discovery. *Oncol Lett* **2017**, *14* (6), 6999-7010. DOI: 10.3892/ol.2017.7134

(45) Langhans, S. A. Three-Dimensional in Vitro Cell Culture Models in Drug Discovery and Drug Repositioning. *Front Pharmacol* **2018**, *9*, 6. DOI: 10.3389/fphar.2018.00006

(46) Rozario, T.; DeSimone, D. W. The extracellular matrix in development and morphogenesis: a dynamic view. *Dev Biol* **2010**, *341* (1), 126-140. DOI: 10.1016/j.ydbio.2009.10.026

(47) Holle, A. W.; Young, J. L.; Spatz, J. P. In vitro cancer cell-ECM interactions inform in vivo cancer treatment. *Adv Drug Deliv Rev* **2016**, *97*, 270-279. DOI: 10.1016/j.addr.2015.10.007

(48) Egeblad, M.; Nakasone, E. S.; Werb, Z. Tumors as organs: complex tissues that interface with the entire organism. *Dev Cell* **2010**, *18* (6), 884-901. DOI: 10.1016/j.devcel.2010.05.012

(49) Jones, V. S.; Huang, R. Y.; Chen, L. P.; Chen, Z. S.; Fu, L.; Huang, R. P. Cytokines in cancer drug resistance: Cues to new therapeutic strategies. *Biochim Biophys Acta* **2016**, *1865* (2), 255-265. DOI: 10.1016/j.bbcan.2016.03.005

(50) Prieto-Vila, M.; Takahashi, R. U.; Usuba, W.; Kohama, I.; Ochiya, T. Drug Resistance Driven by Cancer Stem Cells and Their Niche. *Int J Mol Sci* **2017**, *18* (12). DOI: 10.3390/ijms18122574

(51) Han, S. J.; Kwon, S.; Kim, K. S. Challenges of applying multicellular tumor spheroids in preclinical phase. *Cancer Cell Int* **2021**, *21* (1), 152. DOI: 10.1186/s12935-021-01853-8

(52) Shamir, E. R.; Ewald, A. J. Three-dimensional organotypic culture: experimental models of mammalian biology and disease. *Nat Rev Mol Cell Biol* **2014**, *15* (10), 647-664. DOI: 10.1038/nrm3873

(53) Bidarra, S. J.; Oliveira, P.; Rocha, S.; Saraiva, D. P.; Oliveira, C.; Barrias, C. C. A 3D in vitro model to explore the inter-conversion between epithelial and mesenchymal states during EMT and its reversion. *Sci Rep* **2016**, *6*, 27072. DOI: 10.1038/srep27072

(54) Kalluri, R.; Weinberg, R. A. The basics of epithelial-mesenchymal transition. *J Clin Invest* **2009**, *119* (6), 1420-1428. DOI: 10.1172/jci39104

(55) Nelson, W. J.; Nusse, R. Convergence of Wnt, beta-catenin, and cadherin pathways. *Science* **2004**, *303* (5663), 1483-1487. DOI: 10.1126/science.1094291

(56) Gagliano, N.; Celesti, G.; Tacchini, L.; Pluchino, S.; Sforza, C.; Rasile, M.; Valerio, V.; Laghi, L.; Conte, V.; Procacci, P. Epithelial-to-mesenchymal transition in pancreatic

ductal adenocarcinoma: Characterization in a 3D-cell culture model. *World J Gastroenterol* **2016**, *22* (18), 4466-4483. DOI: 10.3748/wjg.v22.i18.4466 .

(57) Al Ameri, W.; Ahmed, I.; Al-Dasim, F. M.; Ali Mohamoud, Y.; Al-Azwani, I. K.; Malek, J. A.; Karedath, T. Cell Type-Specific TGF-β Mediated EMT in 3D and 2D Models and Its Reversal by TGF-β Receptor Kinase Inhibitor in Ovarian Cancer Cell Lines. *Int J Mol Sci* **2019**, *20* (14). DOI: 10.3390/ijms20143568

(58) Jechlinger, M.; Grünert, S.; Beug, H. Mechanisms in epithelial plasticity and metastasis: insights from 3D cultures and expression profiling. *J Mammary Gland Biol Neoplasia* **2002**, *7* (4), 415-432. DOI: 10.1023/a:1024090116451

(59) Tse, J. C.; Kalluri, R. Mechanisms of metastasis: epithelial-to-mesenchymal transition and contribution of tumor microenvironment. *J Cell Biochem* **2007**, *101* (4), 816-829. DOI: 10.1002/jcb.21215

(60) Lorenzo, H. K.; Susin, S. A.; Penninger, J.; Kroemer, G. Apoptosis inducing factor (AIF): a phylogenetically old, caspase-independent effector of cell death. *Cell Death Differ* **1999**, *6* (6), 516-524. DOI: 10.1038/sj.cdd.4400527

(61) Daugas, E.; Nochy, D.; Ravagnan, L.; Loeffler, M.; Susin, S. A.; Zamzami, N.; Kroemer, G. Apoptosis-inducing factor (AIF): a ubiquitous mitochondrial oxidoreductase involved in apoptosis. *FEBS Lett* **2000**, *476* (3), 118-123. DOI: 10.1016/s0014-5793(00)01731-2 .

(62) Elguindy, M. M.; Nakamaru-Ogiso, E. Apoptosis-inducing Factor (AIF) and Its Family Member Protein, AMID, Are Rotenone-sensitive NADH:Ubiquinone Oxidoreductases (NDH-2). *J Biol Chem* **2015**, *290* (34), 20815-20826. DOI: 10.1074/jbc.M115.641498

(63) Candé, C.; Cecconi, F.; Dessen, P.; Kroemer, G. Apoptosis-inducing factor (AIF): key to the conserved caspase-independent pathways of cell death? *J Cell Sci* **2002**, *115* (Pt 24), 4727-4734. DOI: 10.1242/jcs.00210

(64) Sevrioukova, I. F. Apoptosis-inducing factor: structure, function, and redox regulation. *Antioxidants & redox signaling* **2011**, *14* (12), 2545-2579. DOI: 10.1089/ars.2010.3445 PubMed.

(65) Susin, S. A.; Zamzami, N.; Castedo, M.; Hirsch, T.; Marchetti, P.; Macho, A.; Daugas, E.; Geuskens, M.; Kroemer, G. Bcl-2 inhibits the mitochondrial release of an apoptogenic protease. *J Exp Med* **1996**, *184* (4), 1331-1341. DOI: 10.1084/jem.184.4.1331

(66) Susin, S. A.; Lorenzo, H. K.; Zamzami, N.; Marzo, I.; Brenner, C.; Larochette, N.; Prévost, M. C.; Alzari, P. M.; Kroemer, G. Mitochondrial release of caspase-2 and -9 during the apoptotic process. *J Exp Med* **1999**, *189* (2), 381-394. DOI: 10.1084/jem.189.2.381

(67) Susin, S. A.; Lorenzo, H. K.; Zamzami, N.; Marzo, I.; Snow, B. E.; Brothers, G. M.; Mangion, J.; Jacotot, E.; Costantini, P.; Loeffler, M.; et al. Molecular characterization of mitochondrial apoptosis-inducing factor. *Nature* **1999**, *397* (6718), 441-446. DOI: 10.1038/17135

(68) Cregan, S. P.; Dawson, V. L.; Slack, R. S. Role of AIF in caspase-dependent and caspase-independent cell death. *Oncogene* **2004**, *23* (16), 2785-2796. DOI: 10.1038/sj.onc.1207517

(69) Arnoult, D.; Gaume, B.; Karbowski, M.; Sharpe, J. C.; Cecconi, F.; Youle, R. J. Mitochondrial release of AIF and EndoG requires caspase activation downstream of Bax/Bak-mediated permeabilization. *Embo j* **2003**, *22* (17), 4385-4399. DOI: 10.1093/emboj/cdg423

(70) Susin, S. A.; Daugas, E.; Ravagnan, L.; Samejima, K.; Zamzami, N.; Loeffler, M.; Costantini, P.; Ferri, K. F.; Irinopoulou, T.; Prévost, M. C.; et al. Two distinct pathways leading to nuclear apoptosis. *J Exp Med* **2000**, *192* (4), 571-580. DOI: 10.1084/jem.192.4.571

(71) Zhu, C.; Wang, X.; Deinum, J.; Huang, Z.; Gao, J.; Modjtahedi, N.; Neagu, M. R.; Nilsson, M.; Eriksson, P. S.; Hagberg, H.; et al. Cyclophilin A participates in the nuclear translocation of apoptosis-inducing factor in neurons after cerebral hypoxia-ischemia. *J Exp Med* **2007**, *204* (8), 1741-1748. DOI: 10.1084/jem.20070193

(72) Widlak, P.; Garrard, W. T. Discovery, regulation, and action of the major apoptotic nucleases DFF40/CAD and endonuclease G. *J Cell Biochem* **2005**, *94* (6), 1078-1087. DOI: 10.1002/jcb.20409

(73) Artus, C.; Boujrad, H.; Bouharrour, A.; Brunelle, M. N.; Hoos, S.; Yuste, V. J.; Lenormand, P.; Rousselle, J. C.; Namane, A.; England, P.; et al. AIF promotes chromatinolysis and caspase-independent programmed necrosis by interacting with histone H2AX. *Embo j* **2010**, *29* (9), 1585-1599. DOI: 10.1038/emboj.2010.43

(74) Yu, S. W.; Wang, H.; Poitras, M. F.; Coombs, C.; Bowers, W. J.; Federoff, H. J.; Poirier, G. G.; Dawson, T. M.; Dawson, V. L. Mediation of poly(ADP-ribose) polymerase-1-dependent cell death by apoptosis-inducing factor. *Science* **2002**, *297* (5579), 259-263. DOI: 10.1126/science.1072221

(75) Cregan, S. P.; Fortin, A.; MacLaurin, J. G.; Callaghan, S. M.; Cecconi, F.; Yu, S. W.; Dawson, T. M.; Dawson, V. L.; Park, D. S.; Kroemer, G.; et al. Apoptosis-inducing factor is involved in the regulation of caspase-independent neuronal cell death. *J Cell Biol* **2002**, *158* (3), 507-517. DOI: 10.1083/jcb.200202130

(76) Wang, Y.; An, R.; Umanah, G. K.; Park, H.; Nambiar, K.; Eacker, S. M.; Kim, B.; Bao, L.; Harraz, M. M.; Chang, C.; et al. A nuclease that mediates cell death induced by DNA damage and poly(ADP-ribose) polymerase-1. *Science* **2016**, *354* (6308). DOI: 10.1126/science.aad6872

(77) Lenhausen, A. M.; Wilkinson, A. S.; Lewis, E. M.; Dailey, K. M.; Scott, A. J.; Khan, S.; Wilkinson, J. C. Apoptosis Inducing Factor Binding Protein PGAM5 Triggers Mitophagic Cell Death That Is Inhibited by the Ubiquitin Ligase Activity of X-Linked Inhibitor of Apoptosis. *Biochemistry* **2016**, *55* (23), 3285-3302. DOI: 10.1021/acs.biochem.6b00306

(78) Ravagnan, L.; Gurbuxani, S.; Susin, S. A.; Maisse, C.; Daugas, E.; Zamzami, N.; Mak, T.; Jäättelä, M.; Penninger, J. M.; Garrido, C.; et al. Heat-shock protein 70 antagonizes apoptosis-inducing factor. *Nat Cell Biol* **2001**, *3* (9), 839-843. DOI: 10.1038/ncb0901-839

(79) Huang, H.; Joazeiro, C. A.; Bonfoco, E.; Kamada, S.; Leverson, J. D.; Hunter, T. The inhibitor of apoptosis, cIAP2, functions as a ubiquitin-protein ligase and promotes in vitro monoubiquitination of caspases 3 and 7. *J Biol Chem* **2000**, *275* (35), 26661-26664. DOI: 10.1074/jbc.C000199200

(80) Moskowitz, M. A.; Lo, E. H.; Iadecola, C. The science of stroke: mechanisms in search of treatments. *Neuron* **2010**, *67* (2), 181-198. DOI: 10.1016/j.neuron.2010.07.002

(81) Curcio, M.; Salazar, I. L.; Mele, M.; Canzoniero, L. M.; Duarte, C. B. Calpains and neuronal damage in the ischemic brain: The swiss knife in synaptic injury. *Prog Neurobiol* **2016**, *143*, 1-35. DOI: 10.1016/j.pneurobio.2016.06.001

(82) Berliocchi, L.; Bano, D.; Nicotera, P. Ca2+ signals and death programmes in neurons. *Philos Trans R Soc Lond B Biol Sci* **2005**, *360* (1464), 2255-2258. DOI: 10.1098/rstb.2005.1765

(83) Bano, D.; Ankarcrona, M. Beyond the critical point: An overview of excitotoxicity, calcium overload and the downstream consequences. *Neurosci Lett* **2018**, *663*, 79-85. DOI: 10.1016/j.neulet.2017.08.048

(84) Lai, T. W.; Zhang, S.; Wang, Y. T. Excitotoxicity and stroke: identifying novel targets for neuroprotection. *Prog Neurobiol* **2014**, *115*, 157-188. DOI: 10.1016/j.pneurobio.2013.11.006

(85) Miramar, M. D.; Costantini, P.; Ravagnan, L.; Saraiva, L. M.; Haouzi, D.; Brothers, G.; Penninger, J. M.; Peleato, M. L.; Kroemer, G.; Susin, S. A. NADH oxidase activity of mitochondrial apoptosis-inducing factor. *J Biol Chem* **2001**, *276* (19), 16391-16398. DOI: 10.1074/jbc.M010498200

(86) Joza, N.; Susin, S. A.; Daugas, E.; Stanford, W. L.; Cho, S. K.; Li, C. Y.; Sasaki, T.; Elia, A. J.; Cheng, H. Y.; Ravagnan, L.; et al. Essential role of the mitochondrial apoptosis-inducing factor in programmed cell death. *Nature* **2001**, *410* (6828), 549-554. DOI: 10.1038/35069004

(87) Klein, J. A.; Longo-Guess, C. M.; Rossmann, M. P.; Seburn, K. L.; Hurd, R. E.; Frankel, W. N.; Bronson, R. T.; Ackerman, S. L. The harlequin mouse mutation downregulates apoptosis-inducing factor. *Nature* **2002**, *419* (6905), 367-374. DOI: 10.1038/nature01034

(88) Vahsen, N.; Candé, C.; Brière, J.-J.; Bénit, P.; Joza, N.; Larochette, N.; Mastroberardino, P. G.; Pequignot, M. O.; Casares, N.; Lazar, V.; et al. AIF deficiency compromises

oxidative phosphorylation. *The EMBO journal* **2004**, *23* (23), 4679-4689. DOI: 10.1038/sj.emboj.7600461 PubMed.

(89) Cheung, E. C.; Joza, N.; Steenaart, N. A.; McClellan, K. A.; Neuspiel, M.; McNamara, S.; MacLaurin, J. G.; Rippstein, P.; Park, D. S.; Shore, G. C.; et al. Dissociating the dual roles of apoptosis-inducing factor in maintaining mitochondrial structure and apoptosis. *Embo j* **2006**, *25* (17), 4061-4073. DOI: 10.1038/sj.emboj.7601276

(90) Joza, N.; Oudit, G. Y.; Brown, D.; Bénit, P.; Kassiri, Z.; Vahsen, N.; Benoit, L.; Patel, M. M.; Nowikovsky, K.; Vassault, A.; et al. Muscle-specific loss of apoptosis-inducing factor leads to mitochondrial dysfunction, skeletal muscle atrophy, and dilated cardiomyopathy. *Mol Cell Biol* **2005**, *25* (23), 10261-10272. DOI: 10.1128/mcb.25.23.10261-10272.2005

(91) Hangen, E.; Féraud, O.; Lachkar, S.; Mou, H.; Doti, N.; Fimia, G. M.; Lam, N. V.; Zhu, C.; Godin, I.; Muller, K.; et al. Interaction between AIF and CHCHD4 Regulates Respiratory Chain Biogenesis. *Mol Cell* **2015**, *58* (6), 1001-1014. DOI: 10.1016/j.molcel.2015.04.020

(92) Meyer, K.; Buettner, S.; Ghezzi, D.; Zeviani, M.; Bano, D.; Nicotera, P. Loss of apoptosis-inducing factor critically affects MIA40 function. *Cell Death Dis* **2015**, *6* (7), e1814. DOI: 10.1038/cddis.2015.170

(93) Banci, L.; Bertini, I.; Cefaro, C.; Ciofi-Baffoni, S.; Gallo, A.; Martinelli, M.; Sideris, D. P.; Katrakili, N.; Tokatlidis, K. MIA40 is an oxidoreductase that catalyzes oxidative protein folding in mitochondria. *Nat Struct Mol Biol* **2009**, *16* (2), 198-206. DOI: 10.1038/nsmb.1553

(94) Kim, J. T.; Kim, K. D.; Song, E. Y.; Lee, H. G.; Kim, J. W.; Chae, S. K.; Kim, E.; Lee, M. S.; Yang, Y.; Lim, J. S. Apoptosis-inducing factor (AIF) inhibits protein synthesis by

interacting with the eukaryotic translation initiation factor 3 subunit p44 (eIF3g). *FEBS Lett* **2006**, *580* (27), 6375-6383. DOI: 10.1016/j.febslet.2006.10.049

(95) Shen, S. M.; Guo, M.; Xiong, Z.; Yu, Y.; Zhao, X. Y.; Zhang, F. F.; Chen, G. Q. AIF inhibits tumor metastasis by protecting PTEN from oxidation. *EMBO Rep* **2015**, *16* (11), 1563-1580. DOI: 10.15252/embr.201540536

(96) Morton, S. U.; Prabhu, S. P.; Lidov, H. G. W.; Shi, J.; Anselm, I.; Brownstein, C. A.; Bainbridge, M. N.; Beggs, A. H.; Vargas, S. O.; Agrawal, P. B. AIFM1 mutation presenting with fatal encephalomyopathy and mitochondrial disease in an infant. *Cold Spring Harb Mol Case Stud* **2017**, *3* (2), a001560. DOI: 10.1101/mcs.a001560 .

(97) Diodato, D.; Tasca, G.; Verrigni, D.; D'Amico, A.; Rizza, T.; Tozzi, G.; Martinelli, D.; Verardo, M.; Invernizzi, F.; Nasca, A.; et al. A novel AIFM1 mutation expands the phenotype to an infantile motor neuron disease. *Eur J Hum Genet* **2016**, *24* (3), 463-466. DOI: 10.1038/ejhg.2015.141

(98) Rinaldi, C.; Grunseich, C.; Sevrioukova, I. F.; Schindler, A.; Horkayne-Szakaly, I.; Lamperti, C.; Landouré, G.; Kennerson, M. L.; Burnett, B. G.; Bönnemann, C.; et al. Cowchock syndrome is associated with a mutation in apoptosis-inducing factor. *Am J Hum Genet* **2012**, *91* (6), 1095-1102. DOI: 10.1016/j.ajhg.2012.10.008

(99) Miyake, N.; Wolf, N. I.; Cayami, F. K.; Crawford, J.; Bley, A.; Bulas, D.; Conant, A.; Bent, S. J.; Gripp, K. W.; Hahn, A.; et al. X-linked hypomyelination with spondylometaphyseal dysplasia (H-SMD) associated with mutations in AIFM1. *Neurogenetics* **2017**, *18* (4), 185-194. DOI: 10.1007/s10048-017-0520-x

(100) Warburg, O. The metabolism of carcinoma cells. *The Journal of Cancer Research* **1925**, *9* (1), 148-163.

(101) Warburg, O. On the origin of cancer cells. *Science* **1956**, *123* (3191), 309-314. DOI: 10.1126/science.123.3191.309

(102) Koppenol, W. H.; Bounds, P. L.; Dang, C. V. Otto Warburg's contributions to current concepts of cancer metabolism. *Nat Rev Cancer* **2011**, *11* (5), 325-337. DOI: 10.1038/nrc3038

(103) Tran, Q.; Lee, H.; Kim, C.; Kong, G.; Gong, N.; Kwon, S. H.; Park, J.; Kim, S. H. Revisiting the Warburg Effect: Diet-Based Strategies for Cancer Prevention. *Biomed Res Int* **2020**, *2020*, 8105735. DOI: 10.1155/2020/8105735

(104) Cassim, S.; Vučetić, M.; Ždralević, M.; Pouyssegur, J. Warburg and Beyond: The Power of Mitochondrial Metabolism to Collaborate or Replace Fermentative Glycolysis in Cancer. *Cancers (Basel)* **2020**, *12* (5). DOI: 10.3390/cancers12051119

(105) Boerner, P.; Resnick, R. J.; Racker, E. Stimulation of glycolysis and amino acid uptake in NRK-49F cells by transforming growth factor beta and epidermal growth factor. *Proc Natl Acad Sci U S A* **1985**, *82* (5), 1350-1353. DOI: 10.1073/pnas.82.5.1350

(106) Hiraki, Y.; Rosen, O.; Birnbaum, M. Growth factors rapidly induce expression of the glucose transporter gene. *Journal of Biological Chemistry* **1988**, *263* (27), 13655-13662.

(107) Hamanaka, R. B.; Chandel, N. S. Cell biology. Warburg effect and redox balance. *Science* **2011**, *334* (6060), 1219-1220. DOI: 10.1126/science.1215637

(108) Zhang, J.; Wang, X.; Vikash, V.; Ye, Q.; Wu, D.; Liu, Y.; Dong, W. ROS and ROS-Mediated Cellular Signaling. *Oxid Med Cell Longev* **2016**, *2016*, 4350965. DOI: 10.1155/2016/4350965

(109) Liberti, M. V.; Locasale, J. W. The Warburg Effect: How Does it Benefit Cancer Cells? *Trends Biochem Sci* **2016**, *41* (3), 211-218. DOI: 10.1016/j.tibs.2015.12.001

(110) Junttila, M. R.; Li, S. P.; Westermarck, J. Phosphatase-mediated crosstalk between MAPK signaling pathways in the regulation of cell survival. *Faseb j* **2008**, *22* (4), 954-965. DOI: 10.1096/fj.06-7859rev

(111) Ravingerová, T.; Barancík, M.; Strnisková, M. Mitogen-activated protein kinases: a new therapeutic target in cardiac pathology. *Mol Cell Biochem* **2003**, *247* (1-2), 127-138. DOI: 10.1023/a:1024119224033

(112) Guo, Y. J.; Pan, W. W.; Liu, S. B.; Shen, Z. F.; Xu, Y.; Hu, L. L. ERK/MAPK signalling pathway and tumorigenesis. *Exp Ther Med* **2020**, *19* (3), 1997-2007. DOI: 10.3892/etm.2020.8454

(113) Tournier, C. The 2 Faces of JNK Signaling in Cancer. *Genes Cancer* **2013**, *4* (9-10), 397-400. DOI: 10.1177/1947601913486349

(114) Skyrlas, A.; Hantschke, M.; Passa, V.; Gaitanis, G.; Malamou-Mitsi, V.; Bassukas, I. D. Expression of apoptosis-inducing factor (AIF) in keratoacanthomas and squamous cell carcinomas of the skin. *Exp Dermatol* **2011**, *20* (8), 674-676. DOI: 10.1111/j.1600-0625.2011.01249.x

(115) Jeong, E. G.; Lee, J. W.; Soung, Y. H.; Nam, S. W.; Kim, S. H.; Lee, J. Y.; Yoo, N. J.; Lee, S. H. Immunohistochemical and mutational analysis of apoptosis-inducing factor (AIF) in colorectal carcinomas. *Apmis* **2006**, *114* (12), 867-873. DOI: 10.1111/j.1600-0463.2006.apm_502.x

(116) Fan, T.; Tian, F.; Yi, S.; Ke, Y.; Han, S.; Zhang, L.; Liu, H. Implications of Bit1 and AIF overexpressions in esophageal squamous cell carcinoma. *Tumour Biol* **2014**, *35* (1), 519-527. DOI: 10.1007/s13277-013-1073-8

(117) Lewis, E. M.; Wilkinson, A. S.; Jackson, J. S.; Mehra, R.; Varambally, S.; Chinnaiyan, A. M.; Wilkinson, J. C. The enzymatic activity of apoptosis-inducing factor supports energy metabolism benefiting the growth and invasiveness of advanced prostate cancer cells. *The Journal of biological chemistry* **2012**, *287* (52), 43862-43875. DOI: 10.1074/jbc.M112.407650 PubMed.

(118) Scott, A. J.; Wilkinson, A. S.; Wilkinson, J. C. Basal metabolic state governs AIF-dependent growth support in pancreatic cancer cells. *BMC Cancer* **2016**, *16* (1), 286. DOI: 10.1186/s12885-016-2320-3.

(119) Lee, J. W.; Jeong, E. G.; Soung, Y. H.; Kim, S. Y.; Nam, S. W.; Kim, S. H.; Lee, J. Y.; Yoo, N. J.; Lee, S. H. Immunohistochemical analysis of apoptosis-inducing factor (AIF) expression in gastric carcinomas. *Pathol Res Pract* **2006**, *202* (7), 497-501. DOI: 10.1016/j.prp.2006.03.004

(120) Wilkinson, J. C.; Wilkinson, A. S.; Galbán, S.; Csomos, R. A.; Duckett, C. S. Apoptosis-inducing factor is a target for ubiquitination through interaction with XIAP. *Mol Cell Biol* **2008**, *28* (1), 237-247. DOI: 10.1128/mcb.01065-07

(121) Bano, D.; Prehn, J. H. M. Apoptosis-Inducing Factor (AIF) in Physiology and Disease: The Tale of a Repented Natural Born Killer. *EBioMedicine* **2018**, *30*, 29-37. DOI: 10.1016/j.ebiom.2018.03.016 PubMed.

(122) Hsu, C. C.; Tseng, L. M.; Lee, H. C. Role of mitochondrial dysfunction in cancer progression. *Exp Biol Med (Maywood)* **2016**, *241* (12), 1281-1295. DOI: 10.1177/1535370216641787

(123) Liou, G. Y.; Storz, P. Reactive oxygen species in cancer. *Free Radic Res* **2010**, *44* (5), 479-496. DOI: 10.3109/10715761003667554

(124) Urbano, A.; Lakshmanan, U.; Choo, P. H.; Kwan, J. C.; Ng, P. Y.; Guo, K.; Dhakshinamoorthy, S.; Porter, A. AIF suppresses chemical stress-induced apoptosis and maintains the transformed state of tumor cells. *Embo j* **2005**, *24* (15), 2815-2826. DOI: 10.1038/sj.emboj.7600746

(125) Li, J.; Yen, C.; Liaw, D.; Podsypanina, K.; Bose, S.; Wang, S. I.; Puc, J.; Miliaresis, C.; Rodgers, L.; McCombie, R.; et al. PTEN, a putative protein tyrosine phosphatase gene mutated in human brain, breast, and prostate cancer. *Science* **1997**, *275* (5308), 1943-1947. DOI: 10.1126/science.275.5308.1943

(126) Wang, S.; Gao, J.; Lei, Q.; Rozengurt, N.; Pritchard, C.; Jiao, J.; Thomas, G. V.; Li, G.; Roy-Burman, P.; Nelson, P. S.; et al. Prostate-specific deletion of the murine Pten tumor suppressor gene leads to metastatic prostate cancer. *Cancer Cell* **2003**, *4* (3), 209-221. DOI: 10.1016/s1535-6108(03)00215-0

(127) Scott, A. J.; Walker, S. A.; Krank, J. J.; Wilkinson, A. S.; Johnson, K. M.; Lewis, E. M.; Wilkinson, J. C. AIF promotes a JNK1-mediated cadherin switch independently of respiratory chain stabilization. *Journal of Biological Chemistry* **2018**. DOI: 10.1074/jbc.RA118.004022.

(128) Imhoff, B. R.; Hansen, J. M. Tert-butylhydroquinone induces mitochondrial oxidative stress causing Nrf2 activation. *Cell Biol Toxicol* **2010**, *26* (6), 541-551. DOI: 10.1007/s10565-010-9162-6

(129) Bode, A. M.; Dong, Z. The functional contrariety of JNK. *Mol Carcinog* **2007**, *46* (8), 591-598. DOI: 10.1002/mc.20348

(130) Davis, R. J. Signal transduction by the JNK group of MAP kinases. *Cell* **2000**, *103* (2), 239-252. DOI: 10.1016/s0092-8674(00)00116-1

(131) Lamouille, S.; Xu, J.; Derynck, R. Molecular mechanisms of epithelial-mesenchymal transition. *Nat Rev Mol Cell Biol* **2014**, *15* (3), 178-196. DOI: 10.1038/nrm3758

(132) Hazan, R. B.; Qiao, R.; Keren, R.; Badano, I.; Suyama, K. Cadherin switch in tumor progression. *Ann N Y Acad Sci* **2004**, *1014*, 155-163. DOI: 10.1196/annals.1294.016

(133) Sousa, C. M.; Kimmelman, A. C. The complex landscape of pancreatic cancer metabolism. *Carcinogenesis* **2014**, *35* (7), 1441-1450. DOI: 10.1093/carcin/bgu097

(134) Espiau-Romera, P.; Courtois, S.; Parejo-Alonso, B.; Sancho, P. Molecular and Metabolic Subtypes Correspondence for Pancreatic Ductal Adenocarcinoma Classification. *J Clin Med* **2020**, *9* (12). DOI: 10.3390/jcm9124128

(135) Baliu-Piqué, M.; Pandiella, A.; Ocana, A. Breast Cancer Heterogeneity and Response to Novel Therapeutics. *Cancers (Basel)* **2020**, *12* (11). DOI: 10.3390/cancers12113271

(136) Wang, Z.; Jiang, Q.; Dong, C. Metabolic reprogramming in triple-negative breast cancer. *Cancer Biol Med* **2020**, *17* (1), 44-59. DOI: 10.20892/j.issn.2095-3941.2019.0210

(137) Sarantis, P.; Koustas, E.; Papadimitropoulou, A.; Papavassiliou, A. G.; Karamouzis, M. V. Pancreatic ductal adenocarcinoma: Treatment hurdles, tumor microenvironment and immunotherapy. *World J Gastrointest Oncol* **2020**, *12* (2), 173-181. DOI: 10.4251/wjgo.v12.i2.173

(138) Principe, D. R.; Underwood, P. W.; Korc, M.; Trevino, J. G.; Munshi, H. G.; Rana, A. The Current Treatment Paradigm for Pancreatic Ductal Adenocarcinoma and Barriers to Therapeutic Efficacy. *Front Oncol* **2021**, *11*, 688377. DOI: 10.3389/fonc.2021.688377

(139) Kleeff, J.; Korc, M.; Apte, M.; La Vecchia, C.; Johnson, C. D.; Biankin, A. V.; Neale, R. E.; Tempero, M.; Tuveson, D. A.; Hruban, R. H.; et al. Pancreatic cancer. *Nat Rev Dis Primers* **2016**, *2*, 16022. DOI: 10.1038/nrdp.2016.22

(140) Rahib, L.; Wehner, M. R.; Matrisian, L. M.; Nead, K. T. Estimated Projection of US Cancer Incidence and Death to 2040. *JAMA Netw Open* **2021**, *4* (4), e214708. DOI: 10.1001/jamanetworkopen.2021.4708

(141) Rhim, A. D.; Mirek, E. T.; Aiello, N. M.; Maitra, A.; Bailey, J. M.; McAllister, F.; Reichert, M.; Beatty, G. L.; Rustgi, A. K.; Vonderheide, R. H.; et al. EMT and dissemination precede pancreatic tumor formation. *Cell* **2012**, *148* (1-2), 349-361. DOI: 10.1016/j.cell.2011.11.025

(142) Nath, S.; Devi, G. R. Three-dimensional culture systems in cancer research: Focus on tumor spheroid model. *Pharmacol Ther* **2016**, *163*, 94-108. DOI: 10.1016/j.pharmthera.2016.03.013

(143) Nunes, A. S.; Barros, A. S.; Costa, E. C.; Moreira, A. F.; Correia, I. J. 3D tumor spheroids as in vitro models to mimic in vivo human solid tumors resistance to therapeutic drugs. *Biotechnology and Bioengineering* **2019**, *116* (1), 206-226. DOI: 10.1002/bit.26845.

(144) Ware, M. J.; Colbert, K.; Keshishian, V.; Ho, J.; Corr, S. J.; Curley, S. A.; Godin, B. Generation of Homogenous Three-Dimensional Pancreatic Cancer Cell Spheroids Using an Improved Hanging Drop Technique. *Tissue engineering. Part C, Methods* **2016**, *22* (4), 312-321. DOI: 10.1089/ten.TEC.2015.0280 PubMed.

(145) Nasatto, P. L.; Pignon, F.; Silveira, J. L. M.; Duarte, M. E. R.; Noseda, M. D.; Rinaudo, M. Methylcellulose, a Cellulose Derivative with Original Physical Properties and Extended Applications. *Polymers* **2015**, *7* (5), 777-803.

(146) Goldblum, S.; Bae, Y. K.; Hink, W. F.; Chalmers, J. Protective effect of methylcellulose and other polymers on insect cells subjected to laminar shear stress. *Biotechnol Prog* **1990**, *6* (5), 383-390. DOI: 10.1021/bp00005a011

(147) Galbán, S.; Hwang, C.; Rumble, J. M.; Oetjen, K. A.; Wright, C. W.; Boudreault, A.; Durkin, J.; Gillard, J. W.; Jaquith, J. B.; Morris, S. J.; et al. Cytoprotective effects of IAPs revealed by a small molecule antagonist. *The Biochemical journal* **2009**, *417* (3), 765-771. DOI: 10.1042/BJ20081677 PubMed.

(148) Qin, X.-F.; An, D. S.; Chen, I. S. Y.; Baltimore, D. Inhibiting HIV-1 infection in human T cells by lentiviral-mediated delivery of small interfering RNA against CCR5. *Proceedings of the National Academy of Sciences of the United States of America* **2003**, *100* (1), 183-188. DOI: 10.1073/pnas.232688199 PubMed.

(149) Sarbassov, D. D.; Guertin, D. A.; Ali, S. M.; Sabatini, D. M. Phosphorylation and regulation of Akt/PKB by the rictor-mTOR complex. *Science* **2005**, *307* (5712), 1098-1101. DOI: 10.1126/science.1106148

(150) Onder, T. T.; Gupta, P. B.; Mani, S. A.; Yang, J.; Lander, E. S.; Weinberg, R. A. Loss of E-cadherin promotes metastasis via multiple downstream transcriptional pathways. *Cancer Res* **2008**, *68* (10), 3645-3654. DOI: 10.1158/0008-5472.can-07-2938

(151) Shihan, M. H.; Novo, S. G.; Le Marchand, S. J.; Wang, Y.; Duncan, M. K. A simple method for quantitating confocal fluorescent images. *Biochem Biophys Rep* **2021**, *25*, 100916. DOI: 10.1016/j.bbrep.2021.100916

(152) Liang, C. C.; Park, A. Y.; Guan, J. L. In vitro scratch assay: a convenient and inexpensive method for analysis of cell migration in vitro. *Nat Protoc* **2007**, *2* (2), 329-333. DOI: 10.1038/nprot.2007.30

(153) Sobel, R. E.; Sadar, M. D. Cell lines used in prostate cancer research: a compendium of old and new lines--part 1. *J Urol* **2005**, *173* (2), 342-359. DOI: 10.1097/01.ju.0000141580.30910.57

(154) Edmondson, R.; Broglie, J. J.; Adcock, A. F.; Yang, L. Three-dimensional cell culture systems and their applications in drug discovery and cell-based biosensors. *Assay and drug development technologies* **2014**, *12* (4), 207-218. DOI: 10.1089/adt.2014.573 PubMed.

(155) Gagliano, N.; Celesti, G.; Tacchini, L.; Pluchino, S.; Sforza, C.; Rasile, M.; Valerio, V.; Laghi, L.; Conte, V.; Procacci, P. Epithelial-to-mesenchymal transition in pancreatic ductal adenocarcinoma: Characterization in a 3D-cell culture model. *World journal of gastroenterology* **2016**, *22* (18), 4466-4483. DOI: 10.3748/wjg.v22.i18.4466 PubMed.

(156) Yeon, S. E.; No da, Y.; Lee, S. H.; Nam, S. W.; Oh, I. H.; Lee, J.; Kuh, H. J. Application of concave microwells to pancreatic tumor spheroids enabling anticancer drug evaluation in a clinically relevant drug resistance model. *PLoS One* **2013**, *8* (9), e73345. DOI: 10.1371/journal.pone.0073345

(157) Deer, E. L.; González-Hernández, J.; Coursen, J. D.; Shea, J. E.; Ngatia, J.; Scaife, C. L.; Firpo, M. A.; Mulvihill, S. J. Phenotype and genotype of pancreatic cancer cell lines. *Pancreas* **2010**, *39* (4), 425-435. DOI: 10.1097/MPA.0b013e3181c15963

(158) Subramani, R.; Lopez-Valdez, R.; Salcido, A.; Boopalan, T.; Arumugam, A.; Nandy, S.; Lakshmanaswamy, R. Growth hormone receptor inhibition decreases the growth and metastasis of pancreatic ductal adenocarcinoma. *Exp Mol Med* **2014**, *46* (10), e117. DOI: 10.1038/emm.2014.61

(159) Nakajima, S.; Doi, R.; Toyoda, E.; Tsuji, S.; Wada, M.; Koizumi, M.; Tulachan, S. S.; Ito, D.; Kami, K.; Mori, T.; et al. N-cadherin expression and epithelial-mesenchymal transition in pancreatic carcinoma. *Clin Cancer Res* **2004**, *10* (12 Pt 1), 4125-4133. DOI: 10.1158/1078-0432.ccr-0578-03

(160) Roche, J. The Epithelial-to-Mesenchymal Transition in Cancer. *Cancers* **2018**, *10* (2), 52. DOI: 10.3390/cancers10020052 PubMed.

(161) Melissaridou, S.; Wiechec, E.; Magan, M.; Jain, M. V.; Chung, M. K.; Farnebo, L.; Roberg, K. The effect of 2D and 3D cell cultures on treatment response, EMT profile and stem cell features in head and neck cancer. *Cancer Cell Int* **2019**, *19*, 16. DOI: 10.1186/s12935-019-0733-1

(162) Daemen, A.; Peterson, D.; Sahu, N.; McCord, R.; Du, X.; Liu, B.; Kowanetz, K.; Hong, R.; Moffat, J.; Gao, M.; et al. Metabolite profiling stratifies pancreatic ductal adenocarcinomas into subtypes with distinct sensitivities to metabolic inhibitors. *Proc Natl Acad Sci U S A* **2015**, *112* (32), E4410-4417. DOI: 10.1073/pnas.1501605112

(163) Milone, M. C.; O'Doherty, U. Clinical use of lentiviral vectors. *Leukemia* **2018**, *32* (7), 1529-1541. DOI: 10.1038/s41375-018-0106-0

(164) Zanoni, M.; Piccinini, F.; Arienti, C.; Zamagni, A.; Santi, S.; Polico, R.; Bevilacqua, A.; Tesei, A. 3D tumor spheroid models for in vitro therapeutic screening: a systematic approach to enhance the biological relevance of data obtained. *Sci Rep* **2016**, *6*, 19103. DOI: 10.1038/srep19103

(165) Riffle, S.; Hegde, R. S. Modeling tumor cell adaptations to hypoxia in multicellular tumor spheroids. *J Exp Clin Cancer Res* **2017**, *36* (1), 102. DOI: 10.1186/s13046-017-0570-9

(166) Silvestris, N.; Gnoni, A.; Brunetti, A. E.; Vincenti, L.; Santini, D.; Tonini, G.; Merchionne, F.; Maiello, E.; Lorusso, V.; Nardulli, P.; et al. Target therapies in pancreatic carcinoma. *Curr Med Chem* **2014**, *21* (8), 948-965. DOI: 10.2174/09298673113209990238

(167) Miyake, T.; Honma, Y.; Urano, T.; Kato, N.; Suzumiya, J. Combined treatment with tamoxifen and a fusicoccin derivative (ISIR-042) to overcome resistance to therapy and

to enhance the antitumor activity of 5-fluorouracil and gemcitabine in pancreatic cancer cells. *Int J Oncol* **2015**, *47* (1), 315-324. DOI: 10.3892/ijo.2015.2979

(168) Fujita, Y.; Krause, G.; Scheffner, M.; Zechner, D.; Leddy, H. E.; Behrens, J.; Sommer, T.; Birchmeier, W. Hakai, a c-Cbl-like protein, ubiquitinates and induces endocytosis of the E-cadherin complex. *Nat Cell Biol* **2002**, *4* (3), 222-231. DOI: 10.1038/ncb758

(169) Zhao, H.; Liang, Y.; Xu, Z.; Wang, L.; Zhou, F.; Li, Z.; Jin, J.; Yang, Y.; Fang, Z.; Hu, Y.; et al. N-glycosylation affects the adhesive function of E-Cadherin through modifying the composition of adherens junctions (AJs) in human breast carcinoma cell line MDA-MB-435. *J Cell Biochem* **2008**, *104* (1), 162-175. DOI: 10.1002/jcb.21608

(170) Zheng, J. Energy metabolism of cancer: Glycolysis versus oxidative phosphorylation (Review). *Oncol Lett* **2012**, *4* (6), 1151-1157. DOI: 10.3892/ol.2012.928 . Scott, D. A.; Richardson, A. D.; Filipp, F. V.; Knutzen, C. A.; Chiang, G. G.; Ronai, Z. A.; Osterman, A. L.; Smith, J. W. Comparative metabolic flux profiling of melanoma cell lines: beyond the Warburg effect. *J Biol Chem* **2011**, *286* (49), 42626-42634. DOI: 10.1074/jbc.M111.282046

(171) Rhodes, D. R.; Kalyana-Sundaram, S.; Mahavisno, V.; Varambally, R.; Yu, J.; Briggs, B. B.; Barrette, T. R.; Anstet, M. J.; Kincead-Beal, C.; Kulkarni, P.; et al. Oncomine 3.0: genes, pathways, and networks in a collection of 18,000 cancer gene expression profiles. *Neoplasia* **2007**, *9* (2), 166-180. DOI: 10.1593/neo.07112

(172) Qin, X. F.; An, D. S.; Chen, I. S.; Baltimore, D. Inhibiting HIV-1 infection in human T cells by lentiviral-mediated delivery of small interfering RNA against CCR5. *Proc Natl Acad Sci U S A* **2003**, *100* (1), 183-188. DOI: 10.1073/pnas.232688199

(173) Dull, T.; Zufferey, R.; Kelly, M.; Mandel, R. J.; Nguyen, M.; Trono, D.; Naldini, L. A third-generation lentivirus vector with a conditional packaging system. *J Virol* **1998**, *72* (11), 8463-8471. DOI: 10.1128/jvi.72.11.8463-8471.1998

(174) Yee, J. K.; Friedmann, T.; Burns, J. C. Generation of high-titer pseudotyped retroviral vectors with very broad host range. *Methods Cell Biol* **1994**, *43 Pt A*, 99-112. DOI: 10.1016/s0091-679x(08)60600-7 .

(175) Wilkinson, J. C.; Cepero, E.; Boise, L. H.; Duckett, C. S. Upstream regulatory role for XIAP in receptor-mediated apoptosis. *Mol Cell Biol* **2004**, *24* (16), 7003-7014. DOI: 10.1128/mcb.24.16.7003-7014.2004

(176) Karki, P.; Angardi, V.; Mier, J. C.; Orman, M. A. A Transient Metabolic State in Melanoma Persister Cells Mediated by Chemotherapeutic Treatments. *Front Mol Biosci* **2021**, *8*, 780192. DOI: 10.3389/fmolb.2021.780192

(177) Curtis, C.; Shah, S. P.; Chin, S. F.; Turashvili, G.; Rueda, O. M.; Dunning, M. J.; Speed, D.; Lynch, A. G.; Samarajiwa, S.; Yuan, Y.; et al. The genomic and transcriptomic architecture of 2,000 breast tumours reveals novel subgroups. *Nature* **2012**, *486* (7403), 346-352. DOI: 10.1038/nature10983

(178) Lanning, N. J.; Castle, J. P.; Singh, S. J.; Leon, A. N.; Tovar, E. A.; Sanghera, A.; MacKeigan, J. P.; Filipp, F. V.; Graveel, C. R. Metabolic profiling of triple-negative breast cancer cells reveals metabolic vulnerabilities. *Cancer Metab* **2017**, *5*, 6. DOI: 10.1186/s40170-017-0168-x

(179) Avagliano, A.; Ruocco, M. R.; Aliotta, F.; Belviso, I.; Accurso, A.; Masone, S.; Montagnani, S.; Arcucci, A. Mitochondrial Flexibility of Breast Cancers: A Growth Advantage and a Therapeutic Opportunity. *Cells* **2019**, *8* (5). DOI: 10.3390/cells8050401

(180) Louie, M. C.; Ton, J.; Brady, M. L.; Le, D. T.; Mar, J. N.; Lerner, C. A.; Gerencser, A. A.; Mookerjee, S. A. Total Cellular ATP Production Changes With Primary Substrate in MCF7 Breast Cancer Cells. *Front Oncol* **2020**, *10*, 1703. DOI: 10.3389/fonc.2020.01703

(181) Lehmann, B. D.; Jovanović, B.; Chen, X.; Estrada, M. V.; Johnson, K. N.; Shyr, Y.; Moses, H. L.; Sanders, M. E.; Pietenpol, J. A. Refinement of Triple-Negative Breast Cancer Molecular Subtypes: Implications for Neoadjuvant Chemotherapy Selection. *PLoS One* **2016**, *11* (6), e0157368. DOI: 10.1371/journal.pone.0157368

(182) Allison, K. H. Molecular pathology of breast cancer: what a pathologist needs to know. *Am J Clin Pathol* **2012**, *138* (6), 770-780. DOI: 10.1309/ajcpiv9iq1mrqmoo

(183) Chavez, K. J.; Garimella, S. V.; Lipkowitz, S. Triple negative breast cancer cell lines: one tool in the search for better treatment of triple negative breast cancer. *Breast Dis* **2010**, *32* (1-2), 35-48. DOI: 10.3233/bd-2010-0307

(184) Comşa, Ş.; Cîmpean, A. M.; Raica, M. The Story of MCF-7 Breast Cancer Cell Line: 40 years of Experience in Research. *Anticancer Res* **2015**, *35* (6), 3147-3154. .

(185) McBride, H. M.; Neuspiel, M.; Wasiak, S. Mitochondria: More Than Just a Powerhouse. *Current Biology* **2006**, *16* (14), R551-R560. DOI: https://doi.org/10.1016/j.cub.2006.06.054.

(186) Brand, M. D.; Orr, A. L.; Perevoshchikova, I. V.; Quinlan, C. L. The role of mitochondrial function and cellular bioenergetics in ageing and disease. *Br J Dermatol* **2013**, *169 Suppl 2* (0 2), 1-8. DOI: 10.1111/bjd.12208

(187) Joza, N.; Galindo, K.; Pospisilik, J. A.; Benit, P.; Rangachari, M.; Kanitz, E. E.; Nakashima, Y.; Neely, G. G.; Rustin, P.; Abrams, J. M.; et al. The molecular archaeology

of a mitochondrial death effector: AIF in Drosophila. *Cell Death Differ* **2008**, *15* (6), 1009-1018. DOI: 10.1038/cdd.2008.24

(188) Csutora, P.; Karsai, A.; Nagy, T.; Vas, B.; G, L. K.; Rideg, O.; Bogner, P.; Miseta, A. Lithium induces phosphoglucomutase activity in various tissues of rats and in bipolar patients. *Int J Neuropsychopharmacol* **2006**, *9* (5), 613-619. DOI: 10.1017/s146114570500622x

(189) Souza Ade, A.; da Silva, G. S.; Velez, B. S.; Santoro, A. B.; Montero-Lomelí, M. Glycogen synthesis in brain and astrocytes is inhibited by chronic lithium treatment. *Neurosci Lett* **2010**, *482* (2), 128-132. DOI: 10.1016/j.neulet.2010.07.016

(190) Nath, K.; Guo, L.; Nancolas, B.; Nelson, D. S.; Shestov, A. A.; Lee, S. C.; Roman, J.; Zhou, R.; Leeper, D. B.; Halestrap, A. P.; et al. Mechanism of antineoplastic activity of lonidamine. *Biochim Biophys Acta* **2016**, *1866* (2), 151-162. DOI: 10.1016/j.bbcan.2016.08.001

(191) Guo, L.; Shestov, A. A.; Worth, A. J.; Nath, K.; Nelson, D. S.; Leeper, D. B.; Glickson, J. D.; Blair, I. A. Inhibition of Mitochondrial Complex II by the Anticancer Agent Lonidamine. *J Biol Chem* **2016**, *291* (1), 42-57. DOI: 10.1074/jbc.M115.697516

(192) Zhang, X.; Chen, J.; Graham, S. H.; Du, L.; Kochanek, P. M.; Draviam, R.; Guo, F.; Nathaniel, P. D.; Szabó, C.; Watkins, S. C.; et al. Intranuclear localization of apoptosis-inducing factor (AIF) and large scale DNA fragmentation after traumatic brain injury in rats and in neuronal cultures exposed to peroxynitrite. *J Neurochem* **2002**, *82* (1), 181-191. DOI: 10.1046/j.1471-4159.2002.00975.x

(193) Sideris, D. P.; Tokatlidis, K. Oxidative protein folding in the mitochondrial intermembrane space. *Antioxid Redox Signal* **2010**, *13* (8), 1189-1204. DOI: 10.1089/ars.2010.3157

(194) Madreiter-Sokolowski, C. T.; Ramadani-Muja, J.; Ziomek, G.; Burgstaller, S.; Bischof, H.; Koshenov, Z.; Gottschalk, B.; Malli, R.; Graier, W. F. Tracking intra- and inter-organelle signaling of mitochondria. *Febs j* **2019**, *286* (22), 4378-4401. DOI: 10.1111/febs.15103

(195) Mullen, A. R.; Hu, Z.; Shi, X.; Jiang, L.; Boroughs, L. K.; Kovacs, Z.; Boriack, R.; Rakheja, D.; Sullivan, L. B.; Linehan, W. M.; et al. Oxidation of alpha-ketoglutarate is required for reductive carboxylation in cancer cells with mitochondrial defects. *Cell Rep* **2014**, *7* (5), 1679-1690. DOI: 10.1016/j.celrep.2014.04.037

(196) Al-Masri, M.; Paliotti, K.; Tran, R.; Halaoui, R.; Lelarge, V.; Chatterjee, S.; Wang, L. T.; Moraes, C.; McCaffrey, L. Architectural control of metabolic plasticity in epithelial cancer cells. *Commun Biol* **2021**, *4* (1), 371. DOI: 10.1038/s42003-021-01899-4

(197) Ehinger, J. K.; Piel, S.; Ford, R.; Karlsson, M.; Sjövall, F.; Frostner, E.; Morota, S.; Taylor, R. W.; Turnbull, D. M.; Cornell, C.; et al. Cell-permeable succinate prodrugs bypass mitochondrial complex I deficiency. *Nat Commun* **2016**, *7*, 12317. DOI: 10.1038/ncomms12317

(198) Fantin, V. R.; St-Pierre, J.; Leder, P. Attenuation of LDH-A expression uncovers a link between glycolysis, mitochondrial physiology, and tumor maintenance. *Cancer Cell* **2006**, *9* (6), 425-434. DOI: 10.1016/j.ccr.2006.04.023

(199) Rajas, F.; Gautier-Stein, A.; Mithieux, G. Glucose-6 Phosphate, A Central Hub for Liver Carbohydrate Metabolism. *Metabolites* **2019**, *9* (12). DOI: 10.3390/metabo9120282

(200) Zois, C. E.; Harris, A. L. Glycogen metabolism has a key role in the cancer microenvironment and provides new targets for cancer therapy. *J Mol Med (Berl)* **2016**, *94* (2), 137-154. DOI: 10.1007/s00109-015-1377-9

(201) Altemus, M. A.; Goo, L. E.; Little, A. C.; Yates, J. A.; Cheriyan, H. G.; Wu, Z. F.; Merajver, S. D. Breast cancers utilize hypoxic glycogen stores via PYGB, the brain isoform of glycogen phosphorylase, to promote metastatic phenotypes. *PLoS One* **2019**, *14* (9), e0220973. DOI: 10.1371/journal.pone.0220973

(202) Rousset, M.; Zweibaum, A.; Fogh, J. Presence of glycogen and growth-related variations in 58 cultured human tumor cell lines of various tissue origins. *Cancer Res* **1981**, *41* (3), 1165-1170.

(203) Sato, A.; Kawasaki, T.; Kashiwaba, M.; Ishida, K.; Nagashima, Y.; Moritani, S.; Ichihara, S.; Sugai, T. Glycogen-rich clear cell carcinoma of the breast showing carcinomatous lymphangiosis and extremely aggressive clinical behavior. *Pathol Int* **2015**, *65* (12), 674-676. DOI: 10.1111/pin.12321

(204) Oh, S. S.; Park, S.; Lee, K. W.; Madhi, H.; Park, S. G.; Lee, H. G.; Cho, Y. Y.; Yoo, J.; Dong Kim, K. Extracellular cystatin SN and cathepsin B prevent cellular senescence by inhibiting abnormal glycogen accumulation. *Cell Death Dis* **2017**, *8* (4), e2729. DOI: 10.1038/cddis.2017.153

(205) Chen, J.; Lee, H. J.; Wu, X.; Huo, L.; Kim, S. J.; Xu, L.; Wang, Y.; He, J.; Bollu, L. R.; Gao, G.; et al. Gain of glucose-independent growth upon metastasis of breast cancer cells to the brain. *Cancer Res* **2015**, *75* (3), 554-565. DOI: 10.1158/0008-5472.can-14-2268

(206) Gupta, N.; Jung, K.; Wu, C.; Alshareef, A.; Alqahtani, H.; Damaraju, S.; Mackey, J. R.; Ghosh, S.; Sabri, S.; Abdulkarim, B. S.; et al. High Myc expression and transcription activity underlies intra-tumoral heterogeneity in triple-negative breast cancer. *Oncotarget* **2017**, *8* (17), 28101-28115. DOI: 10.18632/oncotarget.15891

(207) Ji, W.; Zhang, W.; Wang, X.; Shi, Y.; Yang, F.; Xie, H.; Zhou, W.; Wang, S.; Guan, X. c-myc regulates the sensitivity of breast cancer cells to palbociclib via c-myc/miR-29b-3p/CDK6 axis. *Cell Death Dis* **2020**, *11* (9), 760. DOI: 10.1038/s41419-020-02980-2

(208) Jin, Y.; Lu, X.; Wang, M.; Zhao, X.; Xue, L. X-linked inhibitor of apoptosis protein accelerates migration by inducing epithelial-mesenchymal transition through TGF-β signaling pathway in esophageal cancer cells. *Cell Biosci* **2019**, *9*, 76. DOI: 10.1186/s13578-019-0338-3

(209) Olea-Flores, M.; Zuñiga-Eulogio, M. D.; Mendoza-Catalán, M. A.; Rodríguez-Ruiz, H. A.; Castañeda-Saucedo, E.; Ortuño-Pineda, C.; Padilla-Benavides, T.; Navarro-Tito, N. Extracellular-Signal Regulated Kinase: A Central Molecule Driving Epithelial-Mesenchymal Transition in Cancer. *Int J Mol Sci* **2019**, *20* (12). DOI: 10.3390/ijms20122885

(210) Pospisilik, J. A.; Knauf, C.; Joza, N.; Benit, P.; Orthofer, M.; Cani, P. D.; Ebersberger, I.; Nakashima, T.; Sarao, R.; Neely, G.; et al. Targeted deletion of AIF decreases mitochondrial oxidative phosphorylation and protects from obesity and diabetes. *Cell* **2007**, *131* (3), 476-491. DOI: 10.1016/j.cell.2007.08.047

(211) Puigserver, P.; Spiegelman, B. M. Peroxisome proliferator-activated receptor-gamma coactivator 1 alpha (PGC-1 alpha): transcriptional coactivator and metabolic regulator. *Endocr Rev* **2003**, *24* (1), 78-90. DOI: 10.1210/er.2002-0012

(212) Zou, P.; Liu, L.; Zheng, L. D.; Payne, K. K.; Manjili, M. H.; Idowu, M. O.; Zhang, J.; Schmelz, E. M.; Cheng, Z. Coordinated Upregulation of Mitochondrial Biogenesis and Autophagy in Breast Cancer Cells: The Role of Dynamin Related Protein-1 and

Implication for Breast Cancer Treatment. *Oxid Med Cell Longev* **2016**, *2016*, 4085727. DOI: 10.1155/2016/4085727

(213) Yong, C.; Stewart, G. D.; Frezza, C. Oncometabolites in renal cancer. *Nat Rev Nephrol* **2020**, *16* (3), 156-172. DOI: 10.1038/s41581-019-0210-z

(214) Eniafe, J.; Jiang, S. The functional roles of TCA cycle metabolites in cancer. *Oncogene* **2021**, *40* (19), 3351-3363. DOI: 10.1038/s41388-020-01639-8